Journal of Materials Chemistry A

ROYAL SOCIETY OF CHEMISTRY

REVIEW

View Article Online
View Journal | View Issue

Cite this: J. Mater. Chem. A, 2025, 13, 24185

Lignocellulosic biomass and its main structural polymers as sustainable materials for (bio)sensing applications

Arnaud Kamdem Tamo, *[abc] Ingo Doench, [ab] Gullit Deffo, [d] Sherman Lesly Zambou Jiokeng,[e] Giscard Doungmo,[f] Cyrille Ghislain Fotsop, [g] Ranil Clément Tonleu Temgoua, [h] Alexandra Montembault, [c] Anatoli Serghei,[c] Evangéline Njanja,[i] Ignas Kenfack Tonle [i] and Anayancy Osorio-Madrazo *[ab]

(Bio)sensors are integral to various aspects of daily life, contributing to safety, monitoring, and awareness. In modern sensor devices, polymers play an important role, with increasing interest in bio-based materials. Biopolymers, unlike their synthetic counterparts, are abundant in nature and exhibit interesting functional properties that make them highly suitable as biomaterials for sensor technologies. Enhancing sensor performance to achieve a rapid response to stimuli is a key objective in sensor development. Lignocellulosic biomass (LCB) from plants holds promise in meeting such requirements due to its high surface area, tunable surface characteristics (including diverse pore sizes and morphologies), flexibility, printability, low density, and favorable physicochemical and thermal properties. Growing research in recent decades has focused on lignocellulosic composite materials due to their functional and environmentally friendly attributes. This review focuses on the valorization of lignocellulosic biomass and its three main biopolymer constituents (cellulose, hemicellulose, and lignin) for the development of electrochemical (bio)sensors. It also explores the macromolecular structure, sources, and inherent properties of LCB, with emphasis on the three main biopolymers and their applications in sensor technologies. Recent advances in the use of LCB and its structural biopolymers as materials for (bio) sensing applications are described and reviewed. The challenges associated with using these biomaterials in electroanalytical applications are also discussed, along with the exploration of their future potential for developing high-performance sensing technologies.

Received 12th April 2025
Accepted 11th June 2025

DOI: 10.1039/d5ta02900g

rsc.li/materials-a

1. Introduction

Sensors serve as ubiquitous analytical platforms used across diverse environments to detect events or changes with high precision.[1–3] These platforms commonly integrate an active device, known as a transducer, which can record a physical quantity and converts it into a signal suitable for subsequent processing. Sensors are widely employed to measure a broad range of physicochemical and biological parameters.[3–7] The pivotal characteristics of (bio)sensors include their sensitivity to input changes and their selectivity in distinguishing specific targets from adjacent inputs. Enhancements in sensor performance are continuously pursued through the integration of biological receptors or additional materials that amplify the transducer response.[3,8,9] These receptors must exhibit excellent target recognition capabilities and efficient interaction to ensure effective signal transduction to the output system.[10,11] Accordingly, sensor technologies leverage novel materials to streamline processes and enhance key attributes, including sensitivity, specificity, and reproducibility.[3,8,12,13] A wide variety of (bio)sensors, including analytical,[7,14,15] humidity,[16,17] strain[18–20] and gas sensors[21,22] are documented in the literature for diverse applications. Sensor technology offers myriad benefits, such as predictive and preventive maintenance, facilitating faster transmission of measurement data, enhancing accuracy, improving process control, and bolstering asset

[a]Laboratory for Organ Printing, University of Bayreuth, 95447 Bayreuth, Germany. E-mail: arnaud.kamdem-tamo@uni-bayreuth.de; anayancy.osorio-madrazo@uni-bayreuth.de
[b]Laboratory for Bioinspired Materials for Biomedical Engineering, Department of Microsystems Engineering IMTEK, University of Freiburg, 79110 Freiburg, Germany
[c]Ingénierie des Matériaux Polymères (IMP) UMR CNRS, 5223, Université Claude Bernard Lyon 1, 69622 Villeurbanne Cedex, France
[d]Faculty of Chemistry and Mineralogy, University of Leipzig, 04103 Leipzig, Germany
[e]Institute of Analytical and Bioanalytical Chemistry, University of Ulm, 89081 Ulm, Germany
[f]Institute for Inorganic Chemistry, University of Kiel, 24118 Kiel, Germany
[g]Chemical Institute Industrial Chemistry, University of Magdeburg, 39106 Magdeburg, Germany
[h]Federal Institute for Materials Research and Testing BAM, 12489 Berlin, Germany
[i]Electrochemistry and Chemistry of Materials, Department of Chemistry, University of Dschang, P. O. Box 67, Dschang, Cameroon

health.[3,23] Moreover, the development of efficient sensors for sensitive determination of target element levels in various environments holds significant importance. Sensors offer numerous advantages, including ease of operation, high reliability, simplicity, selectivity, sensitivity, time and cost efficiency, portability, and direct applicability in point-of-care assays. These attributes highlight the importance of sensor technology in modern analytical and environmental monitoring endeavors.[24,25] For instance, electrochemical sensors are analytical devices that detect and quantify specific chemical species by converting chemical interactions into measurable electrical signals through redox reactions occurring at the electrode interface, which results in changes in current, voltage, or impedance.[26,27] In recent advancements, lignocellulosic biomass and their main structural biopolymers have emerged as promising sources of electrode materials for sensing applications. These biopolymers offer distinct properties, such as high surface area, structural stability, porosity, and diverse functional groups.[6,7,28,29] While these biomaterials typically exhibit low electrical conductivity in their natural state, their conductivity can be enhanced through processes such as carbonization, doping with metal nanoparticles, and functionalization with electrically conductive polymers. These modifications result in composites with improved conductivity, making them highly suitable for enhancing electron transfer processes in electrochemical reactions.[6,15,30–33] By incorporating lignocellulosic biomass and their composites into sensor design, it is possible to create sustainable, cost-effective, and highly sensitive electrode materials for a wide range of applications.[15,17,30,32]

The development of new sensors has primarily focused on novel materials for electrode modification.[34–38] Traditionally, materials used for supporting surfaces or electrodes exhibit inert characteristics, meaning they lack electroactive species while maintaining conductivity across a broad potential range.[11,27,39] Carbon-based materials have emerged as key components for enhancing the electroanalytical performance of sensors, particularly in terms of sensitivity and selectivity. Lignocellulosic biomass, primarily composed of carbon-rich biopolymers, has gained increasing attention as a surface modifier to improve the sensitivity and selectivity of sensors.[14,15,40–42] These bio-based materials offer numerous advantageous properties, including high surface area, porosity, hierarchical structure, permselective coating capabilities, and suitability for use as immobilization matrices and diffusion-limiting membranes.[43,44] As a major constituent of plant cell walls, LCB is abundantly available in nature and serves as the primary source of the most prevalent biopolymer worldwide, namely cellulose. Consequently, LCB is regarded as a promising renewable resource, characterized by high availability and non-toxicity, for the development of sustainable materials and technologies. Its constituent biopolymers exhibit diverse chemical functionalities, including aliphatic and aromatic hydroxyl groups, carboxyl, acetal, hemiacetal, amine, and amide groups, enabling self-assembly, chemical or physical binding of various molecules and biological entities, and even the formation of chelates with metal ions.[45,46] The interesting mechanical, thermal, and physicochemical properties of LCB, coupled with its eco-friendly attributes including renewability, biocompatibility, and biodegradability position its major components (cellulose, hemicellulose, and lignin) as key candidates for replacing conventional materials in sensing and biosensing technologies.[16,47,48] The significant annual production of biomass waste, estimated at approximately 140 Gtons globally, presents a major management challenge due to its potential environmental impact.[49] Biomass waste is often incinerated by local populations for heating purposes, leading to CO_2 emissions and contributing to global warming. However, numerous pathways for biomass and by-product valorization have been reported across various fields, including renewable energy production, construction, furniture manufacturing, biofuel synthesis, and the chemical industry.[49,50] Concurrently, an increasing number of research efforts are focused on the valorization of these bio-based polymers in sensor and biosensor technologies.[6,51–54]

Lignocellulosic biomass undergoes a biorefinery process to yield value-added products with numerous applications in (bio) sensing. Cellulose, lignin, and hemicellulose serve as versatile byproducts, yielding sugars, ethanol, and various chemicals.[55,56] Despite the abundance and low cost of LCB, the primary challenge lies in achieving high selectivity and yield in the production of value-added chemicals at an economically viable scale.[57] This review focuses on recent advances in the utilization of LCB in sensor applications. It presents recent research showcasing the use of LCB and its major biopolymeric constituents in sensing technologies. The review is structured into different sections. First, a comprehensive description of the intricate and complex macromolecular structure of LCB is provided, along with insights into their sources, properties, and biodiversity. Next, the fractionation process is examined, detailing various pretreatment methods used to isolate its three primary biopolymers: cellulose, hemicellulose, and lignin. This section includes an in-depth discussion of the properties and characteristics of each byproduct obtained through fractionation, highlighting their potential applications in (bio)sensor technologies. Finally, recent research studies highlighting the applications of LCB, cellulose, hemicellulose, and lignin in sensing technologies are reviewed and discussed. The challenges associated with these biomaterials in sensing applications are also addressed, along with their potential to contribute to the future development of high-performance (bio)sensing devices.

2. From the hierarchical structure of lignocellulosic biomass to its application in the development of (bio) sensor technologies

2.1. Lignocellulosic biomass and its potential as bio-based materials

Lignocellulosic biomass can be collected from various plant sources, including agricultural residues such as rice straw, rice husk, coconut shells, wheat straw, and sugarcane bagasse.[56,58–61]

Additionally, woody waste residues like wood chips, branches, and sawdust from sawmills and paper mills contribute to this biomass pool. These materials are often considered low-value byproducts of industrial sectors, including forestry. Furthermore, energy crops such as miscanthus, energycane, and grasses are cultivated specifically for their high yield of LCB, which serves as a crucial raw material for the production of second-generation biofuels.[62,63] The structure and composition of LCB vary depending on factors such as plant species, soil composition, and climate. However, there are common aspects across these materials.[64] Lignocellulosic biomass typically comprises approximately 90% organic macromolecules (cellulose, hemicellulose, and lignin) which form the structural backbone of plant cell walls. In addition to these macromolecules, LCB contains 2–10% low molecular weight compounds referred to as extractives, along with mineral components.[57,65] Isikgora and Remzi Becer[57] reported on various types of biomass, emphasizing the diversity in cellulose, hemicellulose, and lignin content across different plants. Lignocellulosic biomass can show diverse chemical compositions, particularly in terms of relative contents of cellulose, hemicellulose and lignin.[57] Hardwood species such as poplar, oak, and eucalyptus have relatively high cellulose levels (40–54%), with oak also displaying very high hemicellulose content (36%), but lower lignin percentages compared to softwoods. Softwood varieties like pine and Douglas fir typically exhibit moderate cellulose (40–50%) and high lignin content (20–28%), reflecting their sturdier structure. Agricultural wastes, including wheat straw, barley hulls, and rice husks, exhibit more variability in composition.[57] For instance, wheat straw and barley straw have moderate cellulose content (35–43%), while their hemicellulose content can be as high as 36%, although lignin remains lower (6–19%). Rice husks show a wider range of hemicellulose (12–29%) and lignin (15–20%), indicative of structural differences in these wastes. Grasses, including switchgrass, generally have moderate cellulose content (25–40%) and a wide range of hemicellulose (25–50%) and lignin (10–30%). This variability in composition among biomass types is key to determining their suitability for biofuel production and other industrial applications, with lignin content particularly influencing biomass recalcitrance and conversion efficiency.[57]

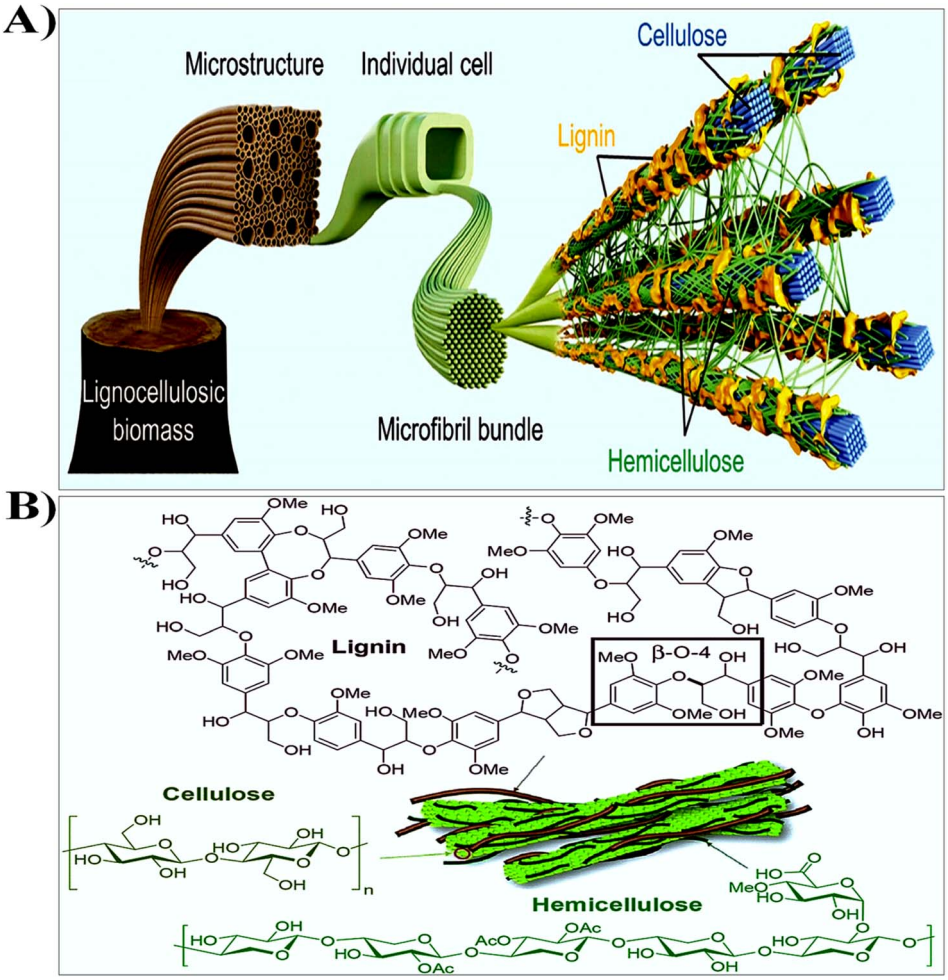

Fig. 1 (A) Scheme of main macromolecular components and their arrangement in the LCB. Reproduced with permission from ref. 81, copyright © 2022 Elsevier. (B) Typical chemical structures of the primary biopolymers that compose LCB. Reproduced with permission from ref. 67, copyright © 2022 Royal Society of Chemistry.

Cellulose, hemicellulose and lignin are abundant in the secondary cell wall of plants. Lignocellulosic biomass is characterized by a complex and fibrous structure that contributes to its high porosity, making it an excellent candidate for applications requiring lightweight and permeable materials.[66,67] The cellulose provides structural strength, hemicellulose acts as a matrix that binds cellulose fibers, and lignin offers rigidity and resistance to microbial degradation (Fig. 1A and B). The diverse composition of organic compounds in the plant cell walls holds promise as a sustainable alternative to traditional polymer materials derived from fossil fuels.[66–68] With growing concerns over environmental sustainability and the finite nature of fossil resources, the exploration and utilization of LCB represent a pivotal avenue in the quest for greener and more sustainable material solutions.

At the forefront of this exploration is cellulose, a polysaccharide polymer consisting of glucose units interconnected through β-1,4-glycosidic bonds, forming long, unbranched chains.[56,59] These chains aggregate into microfibrils, creating a crystalline structure that imparts high tensile strength and stability to the LCB. The hydrogen bonding between cellulose molecules contributes to its rigidity and resistance to degradation.[56] As the most abundant organic compound on Earth, cellulose serves as the primary structural component in plant cell walls, providing stiffness, strength, and resilience. The inherent properties of cellulose, including biodegradability, low toxicity, and exceptional mechanical strength, render it an attractive candidate for a wide range of applications.[69] Hemicellulose is a key component of LCB, acting as a matrix that surrounds and binds cellulose fibers, thereby contributing to the overall structural integrity of plant cell walls. Hemicellulose offers complementary properties that further enhance the versatility of LCB.[70–72] Unlike cellulose, which consists of long chains of glucose molecules, hemicellulose is made up of a variety of sugar monomers, including xylose, mannose, galactose, rhamnose, and arabinose, forming shorter and more branched structures. This branching allows hemicellulose to act as a flexible matrix that binds tightly to cellulose microfibrils, providing structural support and connecting them to lignin.[70,72] This diversity lends hemicellulose its amorphous nature and water-soluble characteristics, making it suitable for applications requiring adhesion, film and/or hydrogel formation.[72] Additionally, hemicellulose is involved in maintaining the porosity and permeability of the cell wall, allowing for the diffusion of water and nutrients while contributing to the resistance of the walls to microbial degradation. The role of hemicellulose in cross-linking cellulose microfibrils also facilitates the overall mechanical properties of biomass, impacting its strength and durability.[73,74] In terms of biochemical functions, hemicellulose serves as a reservoir of fermentable sugars, which are valuable in biofuel production processes. It is also involved in the plant response to environmental stresses, contributing to its ability to adapt to changes in water availability and mechanical pressure.[70,72,74] Lignin, although often regarded as a byproduct of biomass processing, plays a vital role in providing structural support and hydrophobicity to plant cell walls.[75,76] The hydrophobic nature of lignin helps reduce water absorption and permeability, contributing to water transport regulation and protection from excessive moisture loss. It also enhances the resistance of plants to environmental stress, such as pathogens, extreme weather, and ultraviolet (UV) radiation. As a complex polyphenolic compound composed of phenylpropanoid units, lignin confers rigidity and impermeability to plant tissues, contributing to their resistance against microbial degradation and environmental stresses.[67,75–77] The three-dimensional structure of lignin is composed of various phenolic compounds, making it highly resistant to microbial attack and enzymatic degradation, which enhances the durability and longevity of plant material. This resistance also acts as a protective barrier against pathogens and environmental stressors, safeguarding the more easily degradable cellulose and hemicellulose within the cell walls.[75,77–79] Despite its inherent complexity and challenges associated with its extraction and processing, lignin exhibits immense potential as a renewable feedstock for the synthesis of value-added products, including adhesives, thermoplastics, and carbon fibers.[76,80] Celluloses and hemicelluloses are carbohydrates which are tightly linked to the lignin through covalent and hydrogen bonds, making the structure highly complex and robust (Fig. 1A and B).[57,66,81]

The use of LCB extends beyond its traditional applications in the pulp and paper industry. With progress in biorefinery technologies and interdisciplinary research, novel approaches have emerged for the valorization of biomass-derived compounds.[82,83] Through processes such as enzymatic hydrolysis, fermentation, and thermochemical conversion, lignocellulosic feedstocks can be transformed into biofuels, biochemicals, and biomaterials, thereby reducing reliance on fossil resources and mitigating the environmental impacts associated with conventional manufacturing processes.[84,85] Lignocellulosic materials can exhibit tailored properties through modification and blending, allowing customization to meet specific application requirements across sectors such as building, automotive, packaging, and biomedical engineering.[85] Furthermore, the abundance and renewability of lignocellulosic feedstocks provide a reliable and cost-effective source of raw materials, mitigating supply chain risks and promoting economic resilience in a rapidly evolving global landscape.[86] Despite the considerable progress in harnessing the potential of LCB, several challenges remain in realizing its full potential viability. Issues such as feedstock variability, pretreatment efficiency, and product diversification require continued research and development efforts to optimize processes and overcome technical barriers.[64,86]

The complex and densely intertwined structure of LCB presents a significant challenge due to its limited chemical accessibility, which inhibits the digestibility of biomass and the extraction of its constituent components.[87] To overcome this challenge, effective enhancement strategies often involve pretreatment steps aimed at facilitating the degradation or release of these components, thereby improving both chemical and biological accessibility. Pretreatment is crucial for unlocking the full potential of LCB in various applications.[87,88] Following pretreatment, LCB undergoes a series of

transformations, ultimately resulting in the extraction of lignin, hemicellulose, and cellulose, which leads to the production of simpler components. This process significantly enhances the versatility and applicability of LCB-derived biopolymers across a wide range of industries and fields.[55,87] A wide range of pretreatment methods is employed for LCB processing, including physical techniques like milling, grinding, and irradiation; mechanical methods such as steam explosion, extrusion, and cavitation; chemical treatments like acid hydrolysis, alkaline hydrolysis, organosolv, oxidative pretreatments, ionic liquid-mediated processes; biological methods such as enzymatic hydrolysis and microbial fermentation; and combinations of these techniques.[89,90] Table 1 provides an overview of pretreatment methods, categorized into physical,[91,92] chemical,[93–95] physico-chemical,[96,97] and biological[96,98] approaches. The advantages and limitations of each technique are discussed, offering insights into their effectiveness and environmental impact. Physical pretreatment methods typically rely on mechanical forces or thermal treatments to disrupt the biomass structure, reducing particle size and increasing the surface area of the biomass for further enzymatic or chemical treatments. However, while effective in disrupting biomass, these methods can be energy-intensive and offer limited specificity.[91,92] Chemical methods, including acid or alkali treatments, modify the lignocellulosic structure through chemicals that break down lignin and hemicellulose, thereby improving cellulose accessibility. Acid treatments, typically using sulfuric acid, often hydrolyze hemicellulose into fermentable sugars, while alkali treatments, commonly using sodium hydroxide, disrupt lignin structure and enhance cellulose accessibility.[57,93–95] These chemical methods are highly effective in improving the yield of biopolymers; however, they can lead to the formation of toxic by-products and require careful disposal strategies. The use of strong acids and alkalis also raises environmental concerns, as these chemicals can cause significant damage to ecosystems if not handled properly. Furthermore, the post-treatment recovery of these chemicals can be costly and energy-intensive.[93–95] In addition, biological pretreatments have garnered attention due to their environmentally friendly nature and high specificity. Using ligninolytic, cellulolytic, or hemicellulolytic microorganisms and enzymes to degrade specific biomass components allows for selective breakdown, leading to milder processing conditions.[76,96,98–100] The advantage of these biological treatments lies in their ability to function under mild conditions, minimizing energy input and avoiding the need for harsh chemicals, which can be detrimental to the environment. Additionally, biological pretreatments have shown promise in reducing the formation of toxic by-products and enhancing the overall sustainability of biomass conversion.[96,99,100] However, the main limitation of biological methods lies in their slower rate of action and the need for precise control over microbial or enzymatic activity. The challenge of scaling up these methods to industrial levels remains a significant hurdle, particularly when considering the relatively long timeframes required for biological processes compared to the rapid nature of physical and chemical methods.[101,102] Moreover, the integration of physical and chemical methods, known as physico-chemical pretreatments, combines the benefits of both approaches, utilizing the mechanical breakdown of the biomass structure while chemically altering its composition to enhance biopolymer extraction.[97,103] For example, steam explosion coupled with acid or alkaline treatment has been shown to increase cellulose accessibility and improve the overall efficiency of the extraction process. This synergy leads to better disruption of the lignocellulosic matrix, but the combined environmental impact and energy consumption must be carefully considered, as they may offset the benefits of enhanced efficiency.[104–106] Similarly, integrating biological treatments with physico-chemical approaches can combine the high specificity and environmental friendliness of biological methods with the efficiency of physico-chemical treatments.[107,108] One promising approach for the biomass conversion is the use of enzymatic treatments in conjunction with physical or chemical pretreatments. Cellulolytic enzymes can hydrolyze cellulose into fermentable sugars, but their action is often hindered by the recalcitrance of lignin in the biomass and the crystalline structure of cellulose.[109,110] Physico-chemical pretreatments can be used to partially break down the lignin and disrupt the cellulose structure, making it more accessible to the action of enzymes and microorganisms.[111] This process enhances the efficiency of subsequent enzymatic hydrolysis and microbial degradation by increasing the surface area and reducing the protective barrier that lignin poses, thereby improving the overall conversion of biomass into fermentable sugars and other valuable products. In this hybrid approach, the physico-chemical method creates a more favorable structure for enzymatic action, while the biological method ensures a more selective degradation of biomass, without the harsh conditions that could result in the loss of valuable sugars.[111,112] Another interesting concept is the use of microbial consortia capable of producing both enzymes and metabolites that assist in breaking down complex lignocellulosic matrices. These microbial populations can be applied alongside or after physico-chemical pretreatments, further improving the overall process.[113,114]

2.2. Properties and (bio)sensing applications of lignocellulosic biomass

The physical properties of lignocellulosic biomass, such as particle size, density, grindability, moisture sorption, and thermal properties, play a crucial role in determining its functional attributes.[44] Biomass particles typically exhibit irregular shapes, making it challenging to accurately measure their length, width, and thickness. Experimental investigations by Guo *et al.*[159] revealed the anisotropic nature of biomass particles, meaning their optical, physical, and mechanical properties show directional dependence. This anisotropy results in biomass particles having a needle-like shape and a high aspect ratio.[159] Moreover, the aspect ratio of biomass particles varies significantly with particle size, with larger particles exhibiting distinct aspect ratios. The particle size distributions of LCB show linear dependence on different sizes of biomass particles, which, in turn, are linked to variations in the mechanisms

Table 1 Overview of pretreatment methods for biopolymer extraction from lignocellulosic biomass: principles, advantages, and limitations

Category	Pretreatment methods	Working principle	Advantages	Limitations	Ref.
Physical methods	Pyrolysis	Thermal decomposition at high temperatures (300–900 °C) in the absence of oxygen, leading to the breakdown of biomass	- Produces biochar, bio-oil, and syngas - Reduces biomass volume - Can be used as a preliminary step for polymer extraction - Can improve energy recovery through syngas and bio-oil	- High energy consumption - Complex product separation and process control - May lead to incomplete decomposition - Requires further treatment to obtain desired polymers - Potential formation of tar and char residues	92 and 115
	Milling	Mechanical size reduction by using grinding mills to break down biomass into smaller particles, increasing the surface area for further processing	- Breaks down biomass into smaller particles, increasing surface area for easier enzymatic or chemical processing - Smaller particle sizes improve the reactivity of materials for further treatment or extraction - Does not require chemicals - Milling is relatively straightforward and easy to operate	- Can requires significant energy input to break down biomass, especially for hard or dense materials - Wear and tear of milling equipment - Achieving uniform particle sizes can be challenging, affecting the consistency of the pretreatment	116 and 117
	Grinding	Similar to milling, it involves mechanical force to reduce particle size, but typically refers to more aggressive size reduction	- Increases surface area of biomass, improving accessibility for further chemical or enzymatic treatments - Can be applied to various feedstocks such as agricultural residues, wood, and other biomass - Simple and scalable	- Grinding can be energy-intensive, especially for tougher or denser materials - May not sufficiently disrupt lignocellulose structure - Can cause excessive dust generation	118 and 119
	Ultrasonication	Application of high-frequency sound waves to create cavitation bubbles that disrupt the biomass structure, facilitating polymer extraction	- High-intensity sound waves break down biomass, improving the accessibility of cellulose, hemicellulose, and other components - Can be combined with other treatments - Reduces the need for chemicals, making it an environmentally friendly method	- Limited to small-scale applications - Requires specialized equipment - Ultrasonic devices can be expensive, especially for large-scale applications - The process requires careful control of parameters (*e.g.*, frequency, power, time) to avoid negative impacts on the feedstock	120–123
	Chipping	Cutting large biomass into small chips, facilitating easier handling and increasing the surface area for subsequent treatments	- Simple process - Low-cost method for reducing biomass size - Reduces biomass size for easier transport and handling	- Does not significantly alter biomass structure - Limited effect on lignin disruption - Not effective alone for polymer extraction	124 and 125
	Pelletization	Compressing biomass into pellets, increasing its density, and improving the handling and storage efficiency	- Improves biomass density - Facilitates transport and storage	- Pelletizing biomass requires significant energy input, especially for tougher or denser feedstocks - Mainly useful for logistic purposes	91 and 126

Table 1 (*Contd.*)

Category	Pretreatment methods	Working principle	Advantages	Limitations	Ref.
			- Produces consistent pellets, which ensures more predictable processing in subsequent steps - Pellets have better flow characteristics, making them easier to feed into processing systems	- Does not alter biomass structure significantly, which may require additional pretreatment for extraction	
	Torrefaction	Mild pyrolysis (200–300 °C) in the absence of oxygen, leading to partial decomposition and removal of moisture and volatiles, making the biomass more brittle and easier to grind	- Lowers the moisture content of biomass, improving its handling and storage characteristics - Torrefied biomass is easier to grind and process compared to untreated biomass, facilitating downstream operations - Makes biomass more resistant to water absorption, which can improve its long-term storage and processing - Improves the carbon content, which increases the overall calorific value	- Can release volatile organic compounds and other gases, potentially contributing to air pollution if not managed properly - Requires significant energy to heat biomass to high temperatures (200–300 °C), which increases operational costs - The setup for torrefaction involves specialized equipment, which can be expensive to install and maintain	127–130
	Microwave-assisted pretreatment	Application of microwave radiation to rapidly heat the biomass, causing thermal and chemical disruption of the cell wall structure	- Microwaves heat biomass quickly and uniformly, reducing pretreatment time - Increases the porosity of biomass, making it more accessible for subsequent enzymatic or chemical processes - Often requires fewer or no chemicals, making it a more sustainable and eco-friendly method	- Requires specialized equipment - Uneven heating can occur - If not carefully controlled, microwaves can cause overheating or degradation of sensitive compounds in biomass, reducing yield or quality - Scaling the process for large biomass volumes can be challenging and costly	131 and 132
	Extrusion pretreatment	Forcing biomass through a screw orifice at high temperature and pressure, causing shear and friction that break down the biomass structure	- The process is relatively fast and continuous, making it suitable for large-scale operations - Increases the surface area and disrupts the structure, making cellulose and hemicellulose more accessible for extraction - Reduces particle size and disrupts lignocellulosic structure	- High energy consumption - Equipment wear and tear - Requires optimization of operating conditions - The high temperatures and pressures during extrusion can cause degradation of heat-sensitive compounds like sugars or proteins	133 and 134
Chemical methods	Alkali pretreatment	Use of alkaline substances (*e.g.*, NaOH, KOH) to break down lignin, making cellulose more accessible	- Effective lignin removal - Improves cellulose accessibility - Relatively mild conditions	- Can result in chemical waste - Requires neutralization post-treatment - High chemical consumption - Potential environmental issues with waste disposal	93, 135 and 136

Table 1 (*Contd.*)

Category	Pretreatment methods	Working principle	Advantages	Limitations	Ref.
			- Alkali pretreatment generally requires lower temperatures compared to thermal methods - It can be easily scaled up for industrial applications with relatively simple equipment and operational processes	- Can lead to cellulose degradation if not controlled - Alkali solutions are corrosive, requiring specialized equipment to handle and process safely	
	Acid pretreatment	Use of dilute or concentrated acids (e_4, HCl) to break down hemicellulose and disrupt the lignocellulosic structure, making cellulose more accessible for enzymatic hydrolysis	- Highly effective at breaking down hemicellulose - Increases the digestibility of lignocellulosic biomass, enhancing the extraction of cellulose and hemicellulose - Increases the rate of conversion of biomass into valuable products - Acid hydrolysis produces a high yield of sugars (*e.g.*, glucose, xylose), which can be used in biofuel production or fermentation processes	- Strong acids can be highly corrosive, requiring specialized equipment and safety precautions - Acid recovery and neutralization after the process can be complex and costly, posing environmental and operational challenges - Overuse or prolonged exposure to acid can degrade cellulose and reduce the yield of valuable biopolymers	137–139
	Organosolv pretreatment	Use of organic solvents (*e.g.*, ethanol, methanol) often in combination with water and acid catalysts to solubilize lignin	- Organosolv treatment is highly effective in breaking down and solubilizing lignin, enhancing the accessibility of cellulose and hemicellulose - Uses organic alcohol solvents, which are more environmentally friendly compared to harsh chemicals like strong acids or alkalis - Alcohol solvents used in organosolv can be recovered and reused - Typically operates at lower temperatures and pressures compared to some other methods, reducing energy consumption	- Requires complex solvent recovery systems - The effectiveness of organosolv pretreatment can vary depending on biomass type, solvent concentration, and process conditions, leading to inconsistent outcomes - Scaling up the organosolv process from lab to industrial scale can be challenging - The choice of solvent and its concentration can vary depending on the feedstock, requiring careful optimization to achieve desired results	140–142
	Ionic liquids (ILs)	Use of ILs to break down lignin and disrupt the crystalline structure of cellulose, making it more accessible for subsequent enzymatic hydrolysis	- High efficiency in lignin removal - ILs can operate under relatively mild temperatures and pressures, reducing the need for high-energy input - ILs can be tailored to selectively dissolve specific components of biomass,	- High cost of ILs - Potential environmental impact if not recovered - Some ILs may be toxic or harmful to the environment if not handled properly,	123, 125 and 143–145

Table 1 (*Contd.*)

Category	Pretreatment methods	Working principle	Advantages	Limitations	Ref.
			enhancing the efficiency of further extraction	requiring careful disposal and management	
	Oxidative pretreatment	Use of oxidative agents (*e.g.*, H_2O_2, O_3, CH_3CO_3H) to break down lignin and other components by oxidation, enhancing cellulose accessibility	- Effective lignin removal - Can be combined with other treatments - By weakening the lignocellulosic structure, oxidative pretreatment increases the digestibility of biomass - It typically operates under moderate conditions (low to moderate temperatures and pressures), reducing the need for energy–intensive processes	- Potential formation of inhibitory by-products - Requires safe handling of oxidants - Oxidative pretreatment may produce compounds (like organic acids or aldehydes) that can inhibit subsequent fermentation or enzymatic processes	146 and 147
Physico-chemical methods	Steam explosion	Rapid heating of biomass with high-pressure steam followed by sudden decompression, causing the biomass to rupture and disrupt its structure	- Disrupts lignin-carbohydrate complex - Effective hemicellulose removal when combined with other methods - High-pressure steam breaks down the lignocellulosic structure, making cellulose and hemicellulose more accessible for enzymatic hydrolysis	- The high temperatures and pressures can degrade hemicellulose-derived sugars, leading to the formation of inhibitory compounds like furfural and hydroxymethylfurfural - Requires specialized high-pressure reactors, making it expensive to set up - Requires high energy for steam generation - Requires careful control of temperature, pressure and residence time to maximize sugar yield while minimizing degradation	148 and 149
	Supercritical CO_2 ($scCO_2$) treatment	Use of CO_2 above its critical point (31 °C, 7.4 MPa) to penetrate and disrupt the biomass structure, often combined with co-solvents for enhanced effect	- Non-toxic, recyclable solvent - Mild operating conditions - Can selectively extract certain components - $scCO_2$ requires no harsh chemicals, which lowers environmental impact and handling concerns - $scCO_2$ can selectively extract valuable compounds (*e.g.*, lipids, aromatic compounds) without damaging the cellulose structure	- High-pressure equipment required - Limited lignin disruption alone - The process requires energy-intensive compression of CO_2 to supercritical conditions, which can increase operational costs - Scaling the process for large biomass quantities is technically challenging, and achieving uniform treatment can be difficult	150–152
	Ammonia fiber explosion (AFEX)	Treatment of biomass with liquid ammonia under high pressure, followed by rapid release of	- This process increases the porosity and surface area of biomass, making biopolymer more accessible to enzymes for hydrolysis	- High cost and recovery of ammonia	153 and 154

Table 1 (*Contd.*)

Category	Pretreatment methods	Working principle	Advantages	Limitations	Ref.
		pressure, causing the biomass to swell and disrupt its structure	- AFEX efficiently breaks down the physical structure of biomass by using high-pressure ammonia, which disrupts lignin-carbohydrate bonds - A significant portion of the ammonia used in AFEX can be recovered and recycled - AFEX does not require extreme pH adjustments before or after treatment, unlike acid or alkali pretreatment, simplifying downstream processing	- Ammonia is a hazardous and toxic chemical that requires strict safety measures for handling, storage, and transport - Leakage or exposure can pose health risks to workers and requires specialized containment systems - AFEX requires high-pressure reactors, ammonia recovery units, and specialized storage tanks, increasing capital investment and maintenance costs - AFEX is particularly effective for herbaceous biomass, such as grasses or agricultural residues, but less so for woody biomass (*e.g.*, hardwoods, softwoods)	
Biological methods	Bacterial treatment	Use of bacteria (*e.g.*, cellulolytic bacteria) to degrade lignin and hemicellulose, leaving cellulose accessible for polymer extraction	- Uses naturally occurring bacteria to break down lignocellulosic biomass, making it an environmentally friendly alternative to chemical or thermal pretreatments - Bacterial pretreatment can be combined with physical or chemical methods to enhance biomass degradation efficiency - Bacterial treatment occurs at ambient or mild temperatures, reducing the energy input compared to physical and chemical pretreatment methods	- Bacterial degradation is much slower than chemical or thermal methods, often requiring days or weeks to achieve significant biomass breakdown - Requires careful optimization of bacterial strains, temperature, pH, oxygen levels, and nutrient supply to ensure efficient biomass degradation - Unwanted microbial growth can compete with the desired bacteria, reducing pretreatment efficiency and complicating process control - Large-scale bacterial pretreatment requires specialized bioreactors and controlled conditions, increasing capital costs and complexity	100 and 155
	Enzymatic treatment	Use of specific enzymes (*e.g.*, cellulases, hemicellulases) to break down cellulose and hemicellulose into fermentable sugars for polymer extraction	- High specificity, enzymes specifically target cellulose, hemicellulose, or lignin, minimizing unwanted degradation and preserving valuable sugar yields - Works under relatively low temperatures (30–60 °C), reducing energy consumption compared to thermal or chemical methods - Can be combined with mechanical, chemical, or microbial methods to enhance overall biomass digestibility	- Enzymes can be expensive to produce and require optimization for cost-effective large-scale use - Enzyme activity can be affected by temperature, pH, and the presence of inhibitors, requiring strict process control - Enzymes may lose activity over time or in harsh process conditions, requiring regular replenishment - Enzymatic hydrolysis can be slow, often requiring extended periods (from hours to days) to break down biomass	100, 146, 156 and 157

Table 1 (*Contd.*)

Category	Pretreatment methods	Working principle	Advantages	Limitations	Ref.
	Fungi pretreatment	Use of ligninolytic fungi (*e.g.*, white-rot fungi) to selectively degrade lignin, enhancing the accessibility of cellulose for polymer extraction	- It is an eco-friendly process - Can improve the efficiency of subsequent enzymatic treatments - Fungi are selective in their degradation, mainly breaking down lignin and some hemicellulose, while preserving the structure of cellulose - Since fungal pretreatment does not rely on harsh chemicals, it minimizes the formation of inhibitory compounds	effectively, which may limit its commercial scalability - Slow process - Requires precise environmental control (*e.g.*, temperature, moisture) - Maintaining a pure fungal culture in large-scale operations can be challenging, as unwanted microorganisms may interfere with the process - Growing fungi for pretreatment can require additional resources (*e.g.*, nutrients, time) and infrastructure for maintaining fungal cultures, making it a resource-intensive method compared to other pretreatment technologies	98 and 158

governing particle break-up, primarily influenced by the structural characteristics of the material.[159] According to Gera *et al.*,[160] the aspect ratio of biomass particles significantly impacts heat transfer during their thermal conversion processes. Similarly, Wang *et al.*[161] demonstrated that an increase in particle size resulted in a greater weight loss of biomass particles during torrefaction. Additionally, biomass particle size plays an important role in biomass conversion yield and energy consumption, influencing mass and heat transfer processes and directly affecting the rate of enzymatic bioconversion of biomass particles.[162] In literature, two types of density are commonly discussed in relation to LCB particles: bulk density and particle density (also known as true density). Bulk density is defined as the mass of a collection of biomass particles divided by the total volume they occupy, including voids between particles. In contrast, particle density refers to the mass per unit volume of the individual particles themselves, excluding the volume of pore spaces or voids.[163] Bulk density is an important physical property that influences the design of logistical systems for biomass handling. Several factors, such as size, shape, moisture content, individual particle density, and surface characteristics, affect bulk density.[164] Studies conducted by Rezaei *et al.*[165] have highlighted the significance of particle size, shape, and density in biomass transportation, fluidization, drying rates, and thermal decomposition. Pelleting of wood particles has been shown to increase particle density and reduce variability in physical properties among biomass particles, which in turn enhances the bulk density of LCB and improves energy production.[165] Liu *et al.*[166] found that incorporating 40% pine particles into bamboo pellets increased their bulk density from 0.54 g cm^{-3} to 0.60 g cm^{-3}, improving energy production efficiency. Moreover, significant interactions were observed between bulk density, inorganic ash content, net calorific value, combustion rate, and heat release rate.[166]

In addition, the physical and mechanical pretreatment of LCB includes processes such as particle size reduction, which is closely associated with energy consumption and a key physical property known as grindability. Grindability, commonly quantified by the Hardgrove Grindability Index (HGI), plays a significant role in determining both grinding efficiency and combustion performance.[167] Biomass presents challenges during grinding due to its fibrous and resilient nature, making uniform particle size reduction difficult and consequently reducing combustion efficiency.[128] Grinding and torrefaction processes applied to LCB lead to a reduction in material toughness and stiffness, mainly due to the breakdown of the hemicellulose matrix and the depolymerization of cellulose. This transformation alters the aspect ratio of the resulting fibers. During grinding operations, both the particle size and length decrease, while the thickness of the material is also reduced.[129,168] Notably, torrefied biomass chips have been observed to consume approximately 90% less energy compared to non-torrefied wood chips during grinding.[130] Moreover, moisture sorption is another important parameter when assessing the characteristics and properties of biomass. This parameter can be mathematically estimated at equilibrium by examining the relationship between water content and

equilibrium relative humidity of a material. This relationship is often graphically represented by a curve known as a moisture sorption isotherm, which provides insight into the water content of biomass at specific temperatures. Various mathematical models have been developed to describe these sorption isotherms.[169] The quality of lignocellulosic feedstock depends on factors such as moisture content and uptake, which are directly correlated with intrinsic properties of the biomass, including porosity, surface area, and surface chemistry. The sorption or desorption of moisture by LCB is influenced by the vapor pressure of water within the material and its surrounding environment.[170]

The mechanical properties of LCB, which are crucial for various applications, are significantly influenced by its hierarchical structure and chemical composition. Cellulose, the primary load-bearing component, plays a central role in determining stiffness and tensile strength. The highly ordered cellulose fibrils provide structural integrity, resisting tensile forces, while the crystalline regions contribute to high tensile strength, helping to prevent deformation or failure.[56,171,172] Hemicellulose, being more amorphous and surrounding the cellulose fibrils, adds flexibility and toughness to the structure. It absorbs energy and dampens mechanical stresses, which enhances the overall toughness of the material.[70,72] Despite its minor weight, lignin significantly enhances the mechanical properties of LCB by acting as a binder. Its amorphous, cross-linked structure reinforces the cellulose-hemicellulose matrix, improving compression strength and impact resistance. The presence of lignin reduces the susceptibility of biomass to deformation under compressive loads and increases its ability to absorb energy during impact events.[98,173,174]

The thermal properties of LCB, including thermal conductivity and specific heat, are critical for understanding biomass combustion behavior and for modeling large-scale power generation.[170] Mason *et al.*[175] conducted evaluations on various biomass types, finding that wood pellets exhibited thermal conductivity values ranging from 0.11 to 0.12 W m^{-1} K^{-1}, while miscanthus and willow had slightly lower values, approximately 0.11 and 0.10 W m^{-1} K^{-1}, respectively. In contrast, wheat straw and rape straw exhibited significantly lower thermal conductivity values, potentially as low as 0.05 W m^{-1} K^{-1}. Specific heat refers to the amount of heat required to raise the temperature of a substance by one degree Celsius per unit mass. It is essential for understanding heat transport in biomass particles and the size-related implications for their processing and utilization.[115]

Regarding the chemical characteristics of LCB, proximate and ultimate analyses are commonly employed to chemically characterize the material.[176] Proximate analysis provides a snapshot of biomass composition, focusing on easily measured parameters. This analysis typically quantifies volatile matter, ash content, moisture content, and fixed carbon content, utilizing standardized methods.[127] Volatile matter refers to the gaseous phase formed during thermal degradation, consisting of both condensable and non-condensable vapors released upon heating.[127] Ash content is the residue left after combustion and generally consists of primary components like silica, calcium, and iron oxides.[177] Moisture content indicates the water present in the biomass sample and is representative of the mineralized aqueous solution containing various ions or species.[178] Fixed carbon is the carbon remaining after the volatiles have been expelled and is calculated by subtracting the moisture and ash content from the total mass.[179] In contrast, ultimate (or elemental) analysis provides a breakdown of the elemental composition of biomass, determining the contents of carbon, hydrogen, oxygen, nitrogen, and sulfur in the organic coal substance.[180] This analysis is typically conducted using specialized equipment like carbon, hydrogen, nitrogen, sulfur (CHNS) analyzers.[180] Additionally, the macromolecular content of biomass can be assessed using biomass parietal composition analysis, often performed with the Van Soest protocol. This method involves sequential partitioning of cell walls and extracting soluble components with various solvents to evaluate the parietal polymer content.[181] Moreover, LCB and its derivatives possess a wide range of intriguing properties, including high surface area, diverse chemical functionalities, complex macromolecular structure, biodegradability, high porosity, ultrafine network structure, favorable mechanical properties, tunable biocompatibility, and suitability for permselective coatings and immobilization matrices. These materials also exhibit high adsorption capacity and contain numerous surface-active functional groups such as hydroxyl (OH), ether (C–O–C), carbonyl (C=O), and carboxyl (COOH) groups.[7,60,182–184] Furthermore, LCB exhibit diverse chemical properties that influence their reactivity and susceptibility to degradation. Cellulose, the dominant structural component, resists chemical attack due to its crystalline structure and strong intermolecular hydrogen bonding. In contrast, hemicellulose, though also a polysaccharide like cellulose, is more susceptible to hydrolysis due to its amorphous nature and more accessible glycosidic bonds.[16,56,70] Lignin, a complex aromatic polymer, presents challenges due to its highly cross-linked structure and intricate chemical composition. Specialized processes, such as alkaline delignification or enzymatic breakdown, are necessary to effectively depolymerize and extract lignin from LCB.[77,185]

2.2.1 Lignocellulosic biomass for (bio)sensor applications. Lignocellulosic biomass sourced from plants, derived from plants and primarily composed of cellulose, hemicellulose, and lignin, holds significant potential for (bio)sensing technologies due to its renewable nature and remarkable properties.[7,15] These materials are not only biocompatible and sustainable but also highly versatile, making them attractive for a variety of sensing platforms. One of the key advantages of LCB is its inherent biocompatibility and non-toxicity, making it ideal for biological sensing applications with minimal risk of adverse reactions or contamination.[7,186] In addition, renewable and biodegradable nature of LCB provides a more environmentally sustainable alternative to traditional sensing materials derived from fossil fuels or non-renewable sources.[52,183] The surface chemistry of LCB is highly amenable to modification, allowing for chemical treatments, surface grafting, or bioconjugation to introduce functional groups or biomolecules. This flexibility enables the customization of LCB for a wide range of sensing applications. LCB also demonstrates useful optical properties, such as

birefringence and transparency, which can be exploited in the development of optical sensors that rely on changes in light transmission or polarization.[187,188] In addition, LCB can exhibit photoluminescence or fluorescence properties, opening the door to fluorescence-based sensing techniques for detecting analytes.[189,190] Recent advancements have demonstrated that LCB can be engineered and combined with conductive materials to exhibit electrical conductivity or semiconducting behavior, thereby expanding its potential in electrochemical sensors and field-effect transistor-based sensing platforms.[6,16,40] These biological materials have shown promise for diverse applications such as wearable sensors,[191] point-of-care diagnostics,[192] and environmental monitoring.[7,28] The versatility of LCB extends to its ability to be processed into various forms including films,[16] fibers,[7,193] membranes[194,195] and aerogels.[52,191] These forms offer adaptability for diverse sensing applications. Flexible and lightweight LCB-based sensors can conform to irregular surfaces or be integrated into wearable devices for

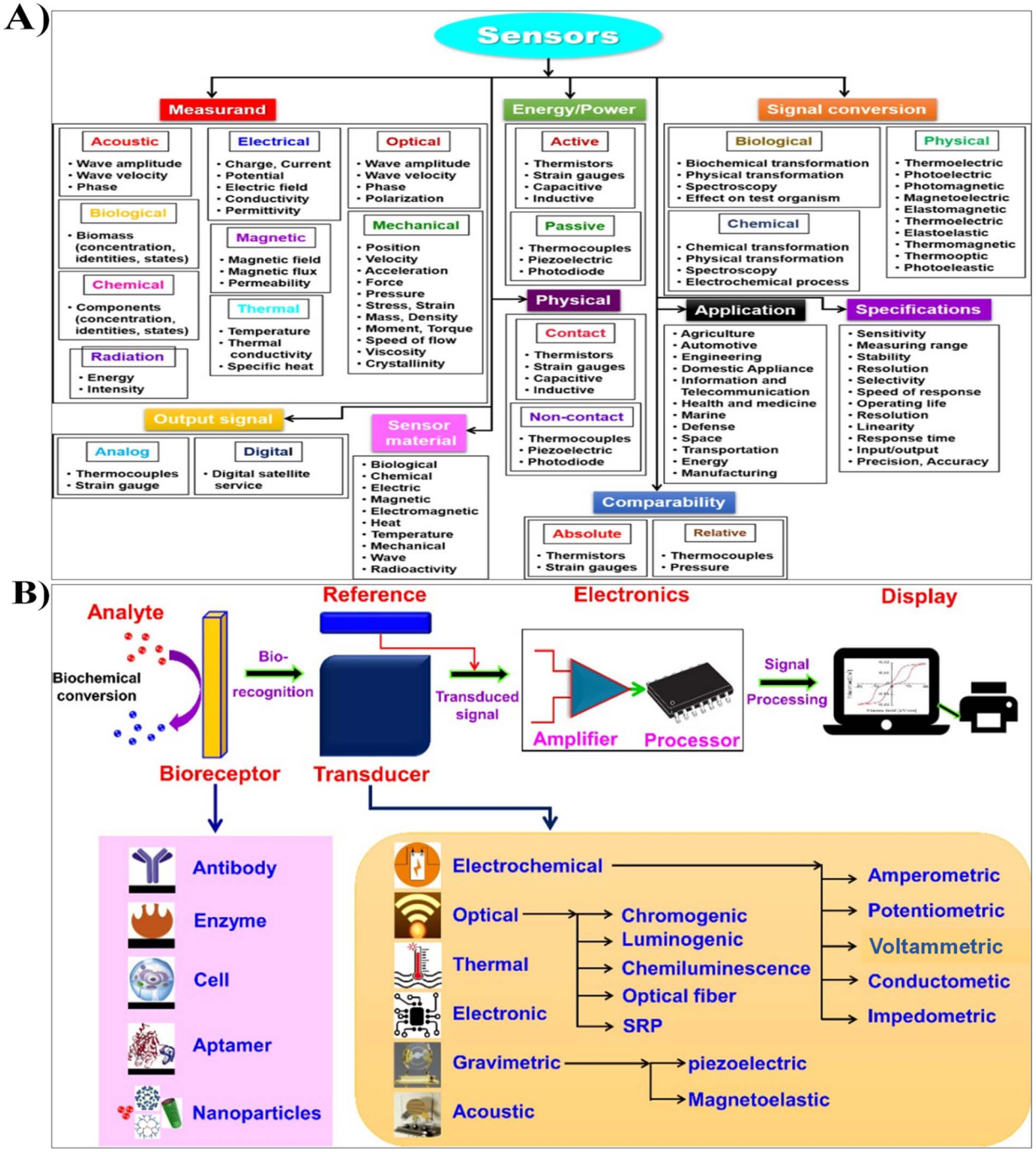

Fig. 2 (A) Classification of sensors based on measurand, energy source, physical contact, signal conversion, output type, comparability, sensor material, specifications, and applications. (B) Schematic representation of a typical biosensor. Reproduced with permission from ref. 11, copyright © 2021 MDPI.

continuous monitoring. Furthermore, the porous nature of LCB enhances sensitivity and selectivity by enabling the immobilization of sensing elements.[54,196,197]

(Bio)sensors are analytical tools that use sensing elements (such as catalysts) or biologically derived recognition systems, in combination with a transducer, to measure the concentration of target analytes. These systems convert biochemical reactions into quantifiable physical signals. Electrochemical methods and (bio)sensors are highly sought after due to their simplicity, high sensitivity, selectivity, rapid response time, and versatility in detecting a wide range of chemical compounds.[9,14,198] The selectivity and sensitivity of sensors depend largely on the properties of the receptor elements, where the analyte interacts. Achieving high sensitivity requires effective analyte recognition and efficient signal transduction.[9,199,200] Sensors can be categorized based on the physical quantity or analyte they measure. This includes factors like energy source (active/passive), physical contact (contact/non-contact), comparability (absolute/relative), analog/digital output, and signal detection (physical, chemical, thermal, biological) (Fig. 2A).[11]. (Bio)sensors integrate biological elements with electronic components, incorporating analytes, bioreceptors, transducers, electronics, and displays to detect physiological changes or biochemical materials. They are capable of detecting low concentrations of specific pathogens, toxic chemicals, or pH levels, finding applications in fields such as medical diagnosis, environmental monitoring, and drug analysis (Fig. 2B).[11]

Lignocellulosic materials could significantly enhance the selectivity and sensitivity of electrochemical sensors or biosensors when used as chemical surface modifiers. This is due to their high surface area, diverse chemical functionalities, macromolecular structure, biodegradability, high porosity, ultrafine network structure, renewability, and excellent mechanical properties, as well as their permselective coating capabilities.[27,44,189] Additionally, LCB could serve as suitable supports for biological molecules like enzymes[54,196] and as biotemplates/scaffolds for immobilizing guest materials such as nanoparticles and fluorescence-labeled compounds.[189,197] They are also used in the fabrication of bio-based organic/inorganic hybrid nanocomposites, which exhibit exceptional sensing properties.[192,197] Despite these attractive attributes, the

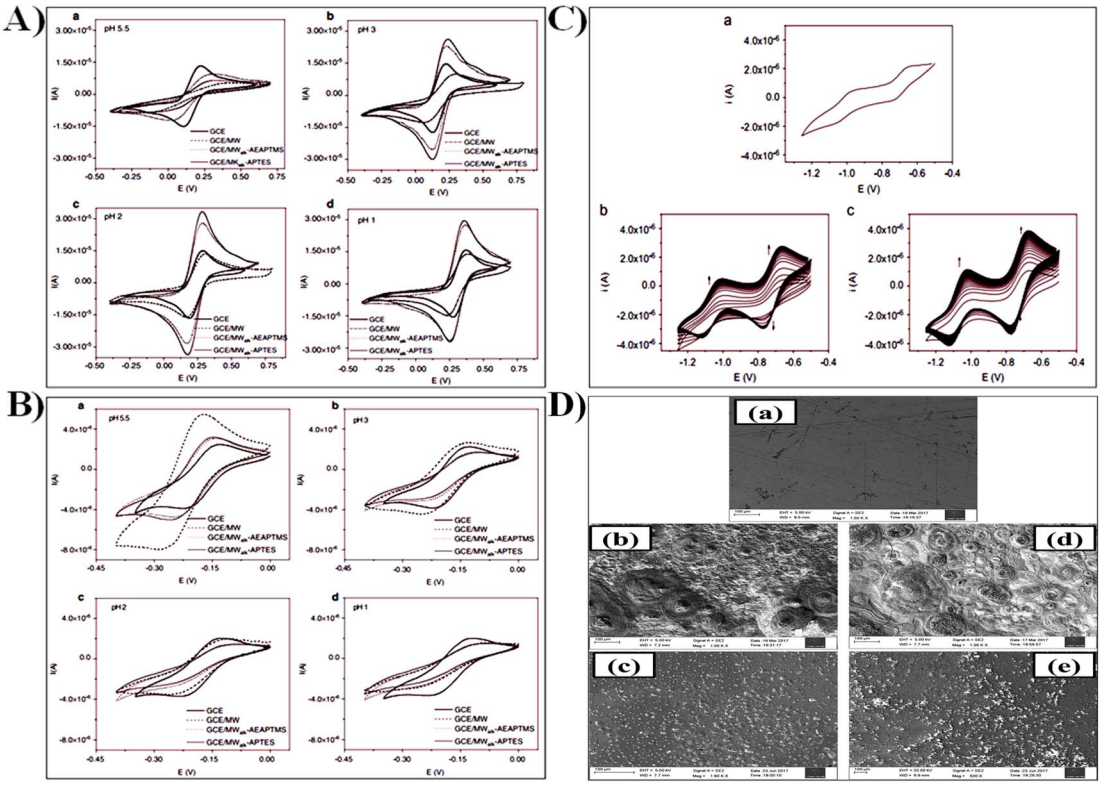

Fig. 3 (A) Cyclic voltammograms at equilibrium of $[Ru(NH_3)_6]^{3+}$ at a concentration of 2×10^{-4} mol L^{-1} recorded at various pH levels (a) 5.5, (b) 3, (c) 2, and (d) 1 on both nude and modified glassy carbon electrodes (GCE) in 0.1 mol per L KCl at a scan rate of 50 mV s^{-1},[201] copyright © 2015 De Gruyter. (B) Cyclic voltammograms at equilibrium of $[Fe(CN)_6]^{3-}$ at a concentration of 10^{-3} mol L^{-1} recorded at various pH levels (a) 5.5, (b) 3, (c) 2, and (d) 1 on both nude and modified GCE electrodes in 0.1 mol per L KCl at a scan rate of 50 mV s^{-1}. Reproduced with permission from ref. 201, copyright © 2015 De Gruyter. (C) Cyclic voltammograms of paraquat at a concentration of 5×10^{-5} mol L^{-1} recorded in 0.1 mol per L NaCl at a scan rate of 100 mV s^{-1} on (a) bare glassy carbon (BGC), (b) the pristine sawdust thin film electrode (PSTFE), and (c) that issued from sodium hydroxide treated sawdust (SSTFE) electrodes. Reproduced with permission from ref. 41, copyright © 2012 Elsevier. (D) Field-emission scanning electron microscopy (FESEM) micrographs of C38 steel: (a) freshly polished surface, (b) after 3 h immersion in 1 M HCl, (c) after 3 h immersion in 1 M HCl with 100 mg L^{-1} of alkaloid extract from *Rauvolfia macrophylla* stapf (AERMS), (d) after 3 h immersion in 0.5 M H_2SO_4, and (e) after 3 h immersion in 0.5 M H_2SO_4 with 100 mg per L AERMS. Reproduced with permission from ref. 203, copyright © 2019 American Chemical Society.

complex hybrid microstructure of LCB remains underutilized, particularly in the development of thin-film electrode devices.

Recent advancements have highlighted the use of LCB in electrochemical sensing applications. For instance, Njine-Bememba *et al.*[201] employed aminated pretreated Ayous sawdust functionalized with two organosilanes for the electrochemical analysis of probes ($[Fe(CN)_6]^{3-}$ and $[Ru(NH_3)_6]^{3+}$) *via* cyclic voltammetry (CV). The presence of silanes facilitated the gradual accumulation of anionic species while repelling cationic species as the solution was acidified (Fig. 3A and B).[201] Kenne *et al.*[41] fabricated thin-film electrodes using both native and NaOH-treated Ayous (triplochiton scleroxylon) sawdust, achieving enhanced selective detection and electroanalysis of paraquat when compared to bare glassy carbon electrodes (GCE) (Fig. 3C).[41] Following optimization, the detection limits (based on signal-to-noise (S/N) ratio of 3) for GCE modified by natural and NaOH-treated Ayous sawdust were found to be 5.49 $\times$ 10^{-9} mol L^{-1} and 3.02 $\times$ 10^{-9} mol L^{-1}, respectively.[41] Furthermore, alkaloid extracts from Rauvolfia macrophylla Stapf and Tabernaemontana contorta were investigated for their corrosion inhibition properties on C38 steel in 1 M HCl and 0.5 M H_2SO_4 using electrochemical techniques, including electrochemical impedance, potentiodynamic polarization, and mass loss measurements.[202,203] Field-emission scanning electron microscopy (FESEM) images showed a smooth surface before immersion (Fig. 3D(a)). After immersion in 1 M HCl and 0.5 M H_2SO_4 without inhibitor, severe damage occurred, with iron clusters and punctures (Fig. 3D(b and c)), due to iron oxidation. In the presence of alkaloid extract from *Rauvolfia macrophylla* stapf as shown in Fig. 3D(c–e), the steel surface remained rust-free, indicating effective corrosion prevention. These findings demonstrate the corrosion inhibition properties of the alkaloid extracts, attributed to their spontaneous chemical adsorption on the electrode surface, which forms a stable layer that enhances the sustainability of C38 steel in acidic environments.[202,203] In addition, two recent studies have explored coffee husks as lignocellulosic matrices to enhance sensor sensitivity for electrochemical quantification of organic substances. Njanja *et al.*[28] developed a lignocellulose-based amperometric sensor, using coffee husks as modifiers to prepare a composite carbon paste electrode (CPE) for methylene blue dye electroanalysis. The sensor showed a linear concentration range for methylene blue dye between 1 and 125 μmol L^{-1}, with a detection limit of 3 μM.[28] Mbokou *et al.*[29] evaluated the electroanalytical performance of a CPE modified with coffee husks for acetaminophen quantification in commercial pharmaceutical tablets. The sensor exhibited high sensitivity, with a linear response from 6.6 μM to 0.5 mM and a detection limit of 0.66 μM (S/N = 3). It successfully determined the acetaminophen content in commercialized tablets (Doliprane 500 and Doliprane 1000), yielding recovery rates ranging from 98% to 103%.[29] Additionally, Radotić *et al.*[51] investigated maize cell walls as modifiers of a CPE for heavy metals electroanalysis, showing good performance under analytical conditions. Kuan *et al.*[204] developed lignocellulose-based analytical devices for bioanalysis, focusing on food and water safety and urinalysis. They used bamboo stirrers as fluidic channels to transport analytes, with a small piece of wood stirrer serving as a reaction zone. This approach enabled point-of-care diagnostics based on bamboo, achieving sensitivity and providing rapid, on-site detection of *Escherichia coli* (*E. coli*) in water.[204] Furthermore, Zhang *et al.*[205] doped lignocellulose with nitrogen to prepare binary composites modified with metal sulfides for non-enzymatic sensing of ascorbic acid, dopamine, and nitrite. The fabricated electrodes demonstrated excellent electrocatalytic activity toward these analytes, with good sensitivity, a wide linear range, and low detection limits of 3.0 μM for ascorbic acid, 0.25 μM for dopamine, and 0.20 μM for nitrite.[205]

Kim *et al.*[186] developed a two-step procedure to prepare biomass-derived carbon for modifying GCE to accurately quantify acetaminophen. Using cyclic voltammetry and differential pulse voltammetry, the modified electrode exhibited high sensitivity, selectivity, and a low detection limit of 0.004 μM for acetaminophen. Evaluation of these sensors in real samples confirmed their superior electrochemical performance.[186] Similarly, Chen *et al.*[206] synthesized biomass-derived N-doped porous carbon-based sensors for the simultaneous determination of dihydroxybenzene isomers, using pig lung as a biomass precursor. The sensors achieved detection limits of 0.078 μmol L^{-1} for catechol, 0.057 μmol L^{-1} for resorcinol, and 0.371 μmol L^{-1} for hydroquinone.[206] In addition, Somba *et al.*[15] prepared alkali-activated carbon from Theobroma cocoa pods as a sensing platform for the electrochemical determination of xanthine (Xa) in fresh fish samples. Using differential pulse voltammetry, the sensors were optimized for various parameters affecting Xa determination, resulting in a calibration curve ranging from 1.0 to 12.0 μM, with a detection limit of 0.264 μM. The sensor was evaluated for interference, reproducibility, and stability, and was successfully applied in fresh fish sample analysis.[15]

Furthermore, biomass has also proven to be an effective material for enzyme immobilization in electrochemical sensors, offering a sustainable and efficient platform for biosensor development.[14,207] Deffo *et al.*[14] leveraged this potential by developing a second-generation uric acid biosensor, chemically immobilizing the enzyme uricase on functionalized multi-walled carbon nanotubes grafted onto lignocellulosic material derived from palm oil fiber, using a ferrocene mediator.[14] Differential pulse voltammetry (DPV) results demonstrated a rapid bioelectrode response toward uric acid (0.185 V), with high sensitivity (41.14 μA mM^{-1}) and a low detection limit (19 μM) within a linear range of 10–1000 μM. The low Michaelis–Menten constant (K_m = 31.364 μM) indicated a high affinity between uric acid and the enzyme at the electrode surface. Furthermore, the biosensor detected uric acid in just 2 s, a fast response attributed to the advantageous characteristics of the LCB used.[14] Additionally, numerous studies have explored the calcination of LCB and the successful use of resulting activated carbons as electrode modifiers for sensitive pollutant detection in various matrices. These activated carbons, characterized by high surface area and porosity, improved the performance of modified sensors by increasing sensitivity and selectivity in detecting pollutants in diverse environments like water, air, and soil.[53,208–211]

Table 2 Overview of studies performed on lignocellulosic biomass as (bio)sensing components in electrochemical applications[a]

Electrodes	Electrochemical methods	Analytes	Linear range (μM)	Detection limit (μM)	Real medium	Ref.
PSTFE/GCE	SWV	Paraquat	0.1–0.725	0.005	—	41
SSTFE/GCE			0.05–0.6	0.003		
CHs/CPE	SWV	Methylene blue	1–125	3	River water	28
CHs/CPE	SWV	Acetaminophen	6.6–500	0.66	Commercialized tablets (Doliprane® 500 and Doliprane 1000)	29
C/CPE	SWV	Pb^{2+}	0.1–100	0.02	Tap water	51
			0.1–50	—		
X/CPE			0.1–100	—		
			0.1–100	—		
L/CPE		Cu^{2+}	0.1–20	0.08		
			0.1–20	—		
CW/CPE			0.1–20	—		
			0.1–20	—		
N-LC/CoS_2-MoS_2/GCE	CA	Ascorbic acid	9.9–6582	3.0	Urine	205
		Dopamine	0.99–261.7	0.25		
		Nitrite	0.5–5160	0.20		
GPAC/GCE	DPV	Catechin	4–368	0.67	Green tea leaves	6
ZKAKC/GCE	DPV	Acetaminophen	0.01–20	0.004	Urine	186
HPCs/GCE	DPV	Catechol	0.5–320	0.078	River water	206
		Resorcinol	0.5–340	0.057		
		Hydroquinone	1–360	0.371		
N,P-MMC/GCE	CA	H_2O_2	100–10 000	6.8	—	215
CNANAs/GCE	CA	H_2O_2	5–1760	3.53	Human urine and serum	52
CNSs/GCE	CA	Nitrite	0.2–350	0.0146	Lake and sea water	208
CA-Zn/GCE	DPV	Caffeine	39.8–458	28.5	Coca-Cola and Pepsi	209
CA-ZnFe/GCE			39.8–637	16.0		
GCE/ACCP	DPV	Xanthine	1.0–12.0	0.264	Fresh fish	15
VCPTE	CA	Acetaminophen	120–5800	88	Resprin, Resfenol, Tylenol, Vick Pyrena	212
PCPET	CA	Hydroquinone	75–1600	8.1	Cosmetic creams (Clariderm, Claripel)	213
StCPET	CA	Hydroquinone	62–1500	8.5	Cosmetic creams (Clariderm, Claripel)	214
UOx/Fc/FMWCNT-POF/Pt	DPV	Uric acid	10–1000	19	Urine	14

[a] GCE: glassy carbon electrode; PSTFE: pristine sawdust thin film electrode; SSTFE: sodium hydroxide treated sawdust thin film electrode; SWV: square wave voltammetry; CHs: coffee husks; CPE: carbon paste electrode; C: cellulose, X: xylan, L: lignin; CW: cell wall; CoS_2-MoS_2: binary metal sulfide composite; N-LC: N-doped lignocellulose; CA: chronoamperometry; GPAC: graphene sheet-like porous activated carbon; DPV: differential pulse voltammetry; ZKAKC: $ZnCl_2$-KOH activated kelp carbon; HPCs: nitrogen doped hierarchical porous carbon materials; N,P-MMC: nitrogen and phosphorus co-doped hierarchical micro/mesoporous carbon; CNANAs: carbon nanoballs aggregation networks-based aerogels; CNSs: carbon nanospheres; CA-Zn: carbon activated with $ZnCl_2$; CA-ZnFe: carbon activated with $ZnCl_2$:$FeCl_3$; ACCP: activated carbon cacao pods; VCPTE: vaseline carbon paste tissue electrode; PCPET: paraffingraphite powder modified with sweet potato tissue; StCPET: stearic acid-graphite powder modified with sweet potato tissue; UOx/Fc/FMWCNT-POF/Pt: uricase coated ferrocene, functionalized multiwalled carbon nanotube and palm oil fiber on bare platinum.

Lignocellulosic biomass is also used as an enzyme source for electrochemical catalysis of organic molecules using enzymatic biosensors. Fatibello-Filho *et al.*[212] used chronoamperometry to determine paracetamol using an avocado tissue (*Persea americana*) biosensor. The dry avocado tissue powder provided polyphenol oxidase, which catalyzed the oxidation of paracetamol to *N*-acetyl-*p*-benzoquinoneimine. The resulting current, obtained at 70 seconds, was proportional to the paracetamol concentration (1.2×10^{-4} to 5.8×10^{-3} mol L^{-1}) with a detection limit of 8.8×10^{-5} mol L^{-1}.[212] Similarly, Cruz *et al.*[213] used sweet potato tissue peroxidase to determine hydroquinone in cosmetic creams. The enzyme catalyzed the oxidation of hydroquinone to quinone, which was reduced electrochemically back to hydroquinone at −0.22 V.[213] Another biosensor based on stearic acid-graphite powder and sweet potato (*Ipomoea batatas* (L.) Lam.) tissue peroxidase showed high catalytic performance, compatibility with non-aqueous solvents, and long lifetime.[214] A summary of recent bio(sensing) research studies based on LCB is provided in Table 2. In recent years, studies on LCB for electrochemical applications have demonstrated their potential in developing various sensors with notable performance characteristics.[15,29,41,201] For example, the pristine sawdust thin film electrode (PSTFE) was employed to detect paraquat using square wave voltammetry (SWV), achieving a linear range of 0.1 to 0.725 μM and a detection limit of 0.005 μM, showcasing its high sensitivity.[41] Meanwhile, sodium hydroxide treated sawdust thin film electrode (SSTFE) extended the applications of LCB by detecting similar analytes with improved performance.[41] Coffee husk-based carbon paste electrodes (CHs/CPE) were successfully used to detect methylene blue and acetaminophen, with the former being detected in river water within a linear range of 1 to 125 μM and a detection limit of 3 μM,[28] while the latter was detectable in commercial tablets with a linear range of 6.6 to 500 μM and a detection limit of 0.66 μM.[29] Additionally, cellulose-based carbon paste electrodes (C/CPE) were utilized for lead ion (Pb^{2+}) detection in tap water, with an impressive detection limit of 0.02 μM within a linear range of 0.1 to 100 μM.[51] On the other hand, the nitrogen-doped lignocellulose with CoS_2–MoS_2 composite (N-LC/CoS_2–MoS_2/GCE) displayed a broad range for detecting ascorbic acid, dopamine, and nitrite, underscoring its versatile sensing capability.[205] Moreover, graphene sheet-like porous activated carbon (GPAC/GCE) showed effective detection of catechin from green tea leaves, with a detection limit of 0.67 μM within a range of 4 to 368 μM.[6] In contrast, carbon nanospheres (CNSs/GCE) demonstrated superior nitrite detection in lake and sea water with an exceptionally low detection limit of 0.0146 μM.[208] The advancements in electrode materials, including carbon activated with $ZnCl_2$ (CA-Zn/GCE) and its iron-composite variant (CA-ZnFe/GCE), have expanded the range of detectable substances such as caffeine and other analytes, illustrating their applicability in diverse matrices.[209] The application of various electrochemical methods, including differential pulse voltammetry, square wave voltammetry and chronoamperometry, highlights the evolution of lignocellulosic-based sensors from basic to highly sophisticated detection platforms across various environmental and commercial samples.[15,28,29]

3. Nanocellulose based sensing platforms

The extraction methods used significantly influenced the properties of the resulting cellulose, with key factors such as treatment duration, solvent concentration, and temperature playing crucial roles in optimizing cellulose yield and quality. The extracted cellulose exhibited favorable mechanical properties, making it a promising material for diverse applications. Table 3 summarizes several studies focused on the isolation and characterization of cellulose materials with notable properties derived from various LCB, demonstrating their potential for various applications.[216–219] These studies explore a diverse range of biomass sources, including agricultural residues such as sugarcane bagasse[217] and coconut fibers,[217] as well as date palm biomass,[220] jackfruit rind,[139] and oil palm mesocarp fiber.[218] The extraction methods employed varied widely, incorporating multiple pre-treatments such as Soxhlet extraction with organic solvents[217] and alkaline/acid treatments.[139,220] Following the initial treatments, the lignocellulosic biomass underwent a series of additional processing steps, including bleaching, delignification, and further purification techniques such as centrifugation and sonication. These varied methodologies aimed to optimize both processing efficiency and the quality of the extracted cellulose. Bleaching typically involves the use of chemicals like sodium chlorite, while delignification is often achieved through acid treatment, such as sulfuric acid, to break down lignin and facilitate cellulose isolation.[217–219] The studies highlighted significant variability in the pre-treatment conditions, including the concentration of chemicals, duration of treatment, and temperature, all of which impacted the final cellulose quality and yield.[139,218,221–223] This variability displays the need for the development of optimized extraction protocols tailored to the specific characteristics of different biomass sources. Achieving an ideal balance between high yield and desirable material properties remains a considerable challenge. To address this, further refinement of extraction methods is essential, including the fine-tuning of chemical treatments, mechanical processes, and reaction conditions, in order to improve both the efficiency and the performance of the extracted cellulose for various industrial applications.

Various forms of cellulose have been extracted from a diverse range of LCB, including microcrystalline cellulose (MCC),[217] α-cellulose,[220] cellulose nanofibrils (CNFs),[224] cellulose nanocrystals (CNCs).[216,224] Each type of extracted cellulose possesses distinct properties influenced by the extraction and pre-treatment processes, as summarized in Table 3. For instance, cellulose extracted from sugarcane bagasse and corn cob exhibited high crystallinity, reaching up to 89%, along with significant thermal stability, making it particularly suitable for applications in composite nanoreinforcement.[217] This enhanced crystallinity and thermal resistance were attributed to the effective removal of non-cellulosic components and optimized extraction conditions.[217] Crystallinity index and degradation temperature are key indicators of structural order and thermal resilience, respectively, both of which directly impact

Table 3 Summary of some studies on extraction and characterization of cellulose from various biomass sources[a]

Biomass used	Extraction methods involved	Type of extracted cellulose	Properties of extracted cellulose	Ref.
- Sugarcane bagasse (SB) - Corn cob (CC) - Coconut fibers (CF) - Hybrid combinations: SB-CC and SB-CF	- Dewaxing using Soxhlet extraction with benzene and methanol - Delignification involved sodium chlorite, glacial acetic acid, washing, and filtering - Alkaline treatment removed hemicellulose and lignin using sodium hydroxide - Acid hydrolysis extracted microcrystalline cellulose with 2 wt% sulfuric acid - Purification included dialysis, centrifugation, and sonication for stable cellulose suspension	Microcrystalline cellulose (MCC)	- SB-CC had 89% while SB-CF had 84.39% crystallinity - SB-CC had 0.8903 mm size and 0.272 PDI; SB-CF had 0.2297 mm size and 0.289 PDI - Degradation of samples started at ~111.67 °C, significant decomposition at ~350 °C, lignin degraded at ~379 °C - FTIR showed higher cellulose content; X-ray diffraction confirmed improved crystallinity in hybrid biomasses	217
- Date palm trees (10–15 years old) from Al-Ain, UAE; parts investigated: Rachis, leaflet, and fiber	- Samples were washed with deionized water and dried in a shaded area - Soxhlet extraction was used to remove resins and waxes - Extract-free biomass was leached with 0.1 M HCl at 100 °C for 2 h - Residue was treated with 0.1 M NaOH at 100 °C with stirring for 2 h - Dried cellulose was bleached with acetic acid, hydrogen peroxide, and sulfuric acid - α-Cellulose was determined using 17.4% NaOH and washing in 20% acetic acid	- Isolated cellulose - α-Cellulose	- Cellulose content varied: rachis 78.63%, leaflet 75.64%, fiber 70.40%; crystallinity index was 52.27% - Decomposition of cellulose started at 200–250 °C; major degradation occurred between 180–350 °C - Functional groups were similar; key peaks included OH, CH, C–O–C, with residual lignin peaks - Rachis and fiber celluloses had porous rod-like structures; leaflet cellulose was less defined - Major crystalline peaks were at $2\theta = 22°$; crystallinity indexes were high, indicating well-ordered structures	220
- Bleached hardwood (Birch, Betula) Kraft pulp	- Hardwood pulp was treated with imidazole/water mixtures at different water contents - Treatment occurred at 120 °C for 24 hours, followed by agitation and water quenching - Treated pulp was sonicated, yielding a turbid supernatant, which was then purified and characterized	- Cellulose nanofibrils (CNFs) - Cellulose nanocrystals (CNCs)	- CNFs had width of 8 ± 4 nm and length several micrometers - CNCs measured 4 ± 2 nm wide and 156 ± 37 nm long - CNFs and CNCs had a crystallinity index of ~67% and ~73% - Both CNFs and CNCs retained 9–10% of residual xylan content	224
- Jackfruit rind (*Artocarpus heterophyllus*)	- Dewaxing, moderate alkali delignification, and bleaching with alkaline hydrogen peroxide - Extraction of CNFs using organic–inorganic acid hydrolysis using acetic acid–HCl mixture under mild hydrothermal conditions - Homogenization: post-hydrolysis to produce CNFs	- Cellulose nanofibers (CNFs)	- CNFs had an average diameter of ~28 nm, as shown by TEM. - PXRD confirmed cellulose I structure and 87.36% crystallinity - FTIR confirmed removal of hemicellulose and lignin - TGA/DTA showed initial degradation at 100 °C and peak at 324–340 °C	139

Table 3 (*Contd.*)

Biomass used	Extraction methods involved	Type of extracted cellulose	Properties of extracted cellulose	Ref.
			- SEM and EDX verified fiber purity and elemental composition - Chemical composition: 48.02% carbon and 51.98% oxygen - DLS provided size distribution data; CNFs had a narrower range - Mean zeta potential was 24.1 mV	
- Waste date leaves obtained from a UAE farm	- Date leaves were washed, dried, and crushed to a particle size of 120 μm - The leaves were soaked in brine solution for 24 h - The soaked material was treated with brine at pH 3–4 and 80 °C for 6 h - The resulting cellulose was filtered, washed, and dried	- Needle-shaped cellulose fibers	- Needle-shaped cellulose fibers had a high crystallinity index of 64.75% - Proximate analysis showed higher volatile matter, lower ash, and moisture - Ultimate analysis of cellulose fibers showed higher carbon and hydrogen - Higher thermal degradation temperature noted in treated fibers - Crystallinity index increased from 53.58% to 64.75% after treatment - Pretreatment method yielded long, needle-shaped fibers with high thermal stability	222
- Non-edible parts of jackfruit (*Artocarpus heterophyllus*) peel	- Sodium chlorite method: dewaxed jackfruit peel was treated with sodium chlorite, bleached, and alkali-treated	- Isolated cellulose	- The isolated cellulose demonstrated high crystallinity (83.42%) as shown by XRD analysis, with a sharp endothermal peak at 323 °C in DSC and a stable thermal profile in TGA	237
	- Acetic acid and nitric acid: biomass was treated with NaOH, bleached, and purified with acids and ethanol - Formic acid treatment: hemicellulose removed, then cellulose was bleached with formic acid and hydrogen peroxide - SCNCs production: cellulose was hydrolyzed with H_2SO_4, then processed to obtain spherical cellulose nanocrystals	- Spherical cellulose nanocrystals (SCNCs)	- The SCNCs had an average diameter of 130 nm and exhibited a zeta potential of −11.6 mV, indicating their stability in suspension	
- Traditional Chinese medicine residues, primarily plant rhizomes	- Carboxylated cellulose nanocrystals (CNCs) were prepared using sequential periodate-chlorite oxidation - The process involved soaking the cellulose in water, reacting it with sodium periodate ($NaIO_4$) and sodium chlorite ($NaClO_2$), and then purifying the oxidized fibers to obtain dialdehyde cellulose (DAC) - These DACs were subsequently treated to produce CNCs with high carboxyl content	- Carboxylated cellulose nanocrystals (CNCs)	- The CNCs had an average length of 139.3 nm and a width of 10 nm - The crystallinity index of the CNCs decreased following oxidation, but the cellulose I structure was preserved - The thermal stability of CNCs decreased with reduced particle size and crystallinity, as revealed by TGA - FTIR analysis indicated changes in hydrogen bonding with decreasing particle size	221

Table 3 (*Contd.*)

Biomass used	Extraction methods involved	Type of extracted cellulose	Properties of extracted cellulose	Ref.
- Pomegranate peels, both outer and inner layers, as the biomass source for cellulose extraction	- The extraction process involved a multi-step approach starting with delignification using sodium hydroxide to remove lignin, followed by mercerization to produce holocellulose - Subsequent bleaching with sodium chlorite and acid treatment was used to purify and further process the cellulose	- Holocellulose - α-Cellulose	- Extracted cellulose exhibited enhanced crystallinity and reduced particle size - FTIR confirmed the presence of characteristic cellulose peaks - XRD analysis showed increased cellulose crystallinity, particularly in the outer layer compared to the inner layer - The chemical revealed a notable increase in cellulose content to 71% in treated samples from an initial 60% in untreated peels	238
- Cocoa pod husks (CPH) from the Colombian cocoa industry	- CPH was pre-treated with 2% sodium chlorite at 80 °C, then hydrolyzed with sodium hydroxide - The fibers were bleached with 5% sodium hypochlorite and dried to produce tCPH - A control sample (tCPHnpe) was treated similarly without high pressure	- Cellulose microfibers	- The treatment reduced lignin by 14% and increased holocellulose content - FTIR spectra revealed higher cellulose in tCPH, with less hemicellulose and lignin - tCPH had lower moisture content at 5.91% compared to 6.72% of CPH - XRD showed tCPH crystallinity increased to 42.84%, while that of CPH was 28.83% - SEM images showed tCPH with well-defined cellulose microfibers, while tCPHnpe had agglomerated fibers	239
Date palm stem waste	- Date palm stem waste was first bleached using acidified sodium chlorite ($NaClO_2$) to remove non-cellulosic components - The biomass was then treated with sodium hydroxide (NaOH) to further remove lignin - Cellulose was subjected to hydrolysis using 62 wt% sulfuric acid (H_2SO_4) at 45 °C for 45 minutes to produce CNCs	- Cellulose nanocrystals (CNCs)	- CNCs exhibited high thermal stability with degradation temperatures of 249.5 °C and thermal analysis temperatures ranging from 290–297 °C - CNCs had a high activation energy (125.6 kJ mol^{-1}), reflecting a robust crystalline structure with strong hydrogen bonding - CNCs demonstrated good physical stability with a ζ potential of −29.3 mV and a narrow particle size distribution, indicating stable suspension	223
Oil palm mesocarp fiber (OPMF) sourced from FELDA Serting Hilir Palm Oil Mill, Kuala Lumpur, Malaysia	- The extraction process involved multiple steps. First, OPMF was treated with NaOH solution to remove lignin and hemicelluloses - Following alkali treatment, the fiber was bleached using a combination of acetate buffer, aqueous chlorite, and distilled water to purify it - Finally, CNCs were extracted through acid hydrolysis with H_2SO_4 followed by centrifugation, dialysis, and sonication	- Cellulose nanocrystals (CNCs)	- Extracted CNCs exhibited increased crystallinity (77.80%) compared to the original OPMF (44.61%) - This enhancement in crystallinity was attributed to the removal of amorphous regions and non-cellulosic components - CNCs showed improved thermal stability and a rod-like morphology with an average diameter of 4.52 nm, as confirmed by SEM and TEM - CNCs exhibited rod-like shapes with diameters ranging from 1 to 6 nm	218

Table 3 (*Contd.*)

Biomass used	Extraction methods involved	Type of extracted cellulose	Properties of extracted cellulose	Ref.
Pseudo stem fiber of *Ensete ventricosum* (commonly known as ensete fiber), a type of banana plant fiber	- The extraction process involved a two-step pretreatment - Initially, the fiber was subjected to alkali treatment to remove hemicellulose, followed by an alkalinized hydrogen peroxide delignification process to further purify the cellulose - Optimal conditions for the extraction of CNCs were determined using response surface methodology	- Cellulose nanocrystals (CNCs)	- The cellulose exhibited an increased crystallinity index from 65% to 75%, indicating enhanced structural order - CNCs demonstrated improved thermal stability, as revealed by TGA - The chemical structure was modified compared to the raw fiber, showing alterations due to the pretreatment processes - Morphological analysis *via* SEM confirmed a rod-like shape of CNCs	219

[a] SB stands for sugarcane bagasse, CC is corn cob, and CF represents coconut fibers. MCC denotes microcrystalline cellulose, and FTIR refers to Fourier-transform infrared spectroscopy. TGA stands for thermogravimetric analysis, while PXRD is powder X-ray diffraction. SEM and EDX denote scanning electron microscopy and energy-dispersive X-ray spectroscopy, respectively, and DLS stands for dynamic light scattering. PDI refers to polydispersity index. CNCs are cellulose nanocrystals, CNFs are cellulose nanofibrils, and HEL signifies hydrotropic extracted lignin. IL denotes ionic liquid, EOL stands for ethanol organosolv lignin, and H_2SO_4 is sulfuric acid. NaOH refers to sodium hydroxide, and $NaClO_2$ stands for sodium chlorite. TEM is transmission electron microscopy, and SCNCs are spherical cellulose nanocrystals. DAC represents dialdehyde cellulose, CNCs can also refer to carboxylated cellulose nanocrystals, OPMF stands for oil palm mesocarp fiber, DSC is differential scanning calorimetry, and ζ potential denotes zeta potential.

the material performance in advanced applications.[139,220] X-ray diffraction analyses have consistently shown that cellulose fibers extracted from LCB display increased crystallinity, which contributes to superior mechanical properties and thermal stability.[216,217] For example, CNCs derived from LCB fibers exhibit exceptionally high crystallinity, thermal stability, and excellent mechanical properties, making them highly advantageous for green technologies and sensing applications.[218,219] Cellulose nanocrystals (CNCs) are highly crystalline, rod-like nanoparticles typically obtained through acid hydrolysis of cellulose fibers, a process that removes the amorphous regions while preserving the crystalline domains.[56,225] CNCs exhibit high tensile strength, a high surface area, and remarkable reinforcing capabilities in composite materials. Their surface contains abundant hydroxyl groups, enabling functionalization for diverse applications.[56,224–226] CNCs have proven to be highly valuable in the development of advanced materials, including nanocomposites, biofuels, and technologies for environmental remediation.[149,216,221] In addition, CNFs are composed of long, flexible fibrils with lengths that can extend up to several micrometers. These nanofibers exhibit a high aspect ratio and crystallinity, which contributes to their remarkable mechanical properties.[227,228] CNFs are characterized by their high strength, flexibility, and large surface area, which impart exceptional mechanical and thermal properties.[56,229] These attributes make CNFs highly versatile for numerous applications, such as reinforcing composite materials, enhancing the mechanical properties of paper[230] and textiles,[231] and serving as a bio-based material for sustainable packaging[232] and tissue engineering.[171,172,233] Additionally, their high surface area allows for effective incorporation of functional additives, making it suitable for advanced applications in electronics,[39,234] sensors,[193,230] and medical devices.[235,236]

3.1. Properties of nanocellulose

Nanocellulose, derived from cellulose fibers, has garnered significant attention due to its exceptional properties and diverse applications across various industries. Cellulose-based nanostructures, including cellulose nanofibers (CNFs), cellulose nanocrystals (CNCs), and bacterial nanocellulose (BNC), display remarkable mechanical strength, stiffness, and lightweight characteristics.[61,226,240] CNFs are flexible, elongated fibers typically ranging in diameter from 2 to 50 nm, with lengths extending from hundreds of nanometers to several micrometers. They exhibit a large surface area, high aspect ratios (length-to-diameter ratios), often exceeding 1000.[56,241,242] CNFs possess remarkable mechanical properties, making them excellent for reinforcing composite mechanical properties. The tensile strength CNFs can vary depending on their source and processing methods. Individual CNFs are reported to have tensile strengths ranging from 2 to 6 GPa.[56,243] However, when these fibers are used in composites or nanopapers, the tensile strength is influenced by factors like fiber bonding and orientation. For example, cellulose nanopapers with random fibril orientation have a theoretical maximum tensile strength of approximately 200 MPa.[243] Moreover, CNCs are rigid, crystalline

rod-like particles commonly produced through acid hydrolysis of cellulose, with diameters ranging from 3 to 20 nm and lengths between 100 and 500 nm.[56,225] With high crystallinity and surface areas, CNCs are known for their exceptional mechanical properties, with reported theoretical tensile strengths ranging from 7.5 to 7.7 GPa, positioning them among the strongest naturally occurring materials.[56,244,245] BNC synthesized by bacteria such as *Gluconacetobacter xylinus*, forms a three-dimensional network with fiber diameters ranging from 20 to 100 nm. It is highly water-retentive, containing 90–99% water, and is known for its high purity, excellent biocompatibility, and tensile strengths up to 200 MPa.[246,247] As a result, nanocellulose is widely used as a reinforcement additive in composite materials, improving mechanical performance while maintaining a low weight profile.[248,249] The high surface area-to-volume ratio of nanocellulose enables efficient adsorption and absorption processes, making it highly suitable for applications such as water purification, drug delivery, and wound healing.[61,236,250] Its biocompatibility, biodegradability, and ease of modification further expand its utility in biomedical applications, including tissue engineering and controlled drug release.[56,251,252] Moreover, nanocellulose exhibits interesting thermal stability, optical transparency, and light-scattering properties, making it an ideal material for various advanced applications. These include flame-retardant materials, thermal insulators, and optically transparent films for flexible electronics and display technologies.[39,232,249] The leading properties of nanocellulose arise from its high aspect ratio, large surface area, and abundance of hydroxyl (–OH) groups.[61,172,253] Hydrogen bonding plays an important role in stabilizing its structure, contributing to exceptional mechanical strength, thermal stability, and chemical reactivity. Strong intermolecular hydrogen bonds between cellulose chains enhance tensile strength and stiffness, making nanocellulose an ideal reinforcement material for polymers and composites.[254,255] Additionally, hydrogen bonding influences nanocellulose crystallinity, which directly impacts its optical, barrier, and rheological properties.[256,257] The exposed hydroxyl groups facilitate interactions with water molecules and other polar or charged species, making nanocellulose highly effective in applications such as water treatment and biosensing. Furthermore, chemical modification enables tailored functionalities, expanding its potential for diverse applications.[227,258,259]

Nanocellulose exhibits interesting properties due to its allomorphic variations, including cellulose I, II, III, and IV (Fig. 4A).[260,261] These allomorphs significantly influence mechanical, chemical, and thermal properties of cellulose, determining their suitability for biomedical applications and the development of high performance nanocomposites.[56,261,262] Cellulose Iα, the predominant allomorph in natural cellulose, features a well-organized crystalline structure with parallel cellulose chains in an anti-parallel arrangement, reinforcing intermolecular hydrogen bonding. These properties make it ideal for high-durability applications such as papermaking, textiles, and biomedical scaffolds.[254,260,263] Meanwhile, cellulose Iβ differs in hydrogen bonding configuration, affecting its mechanical strength and enzymatic degradation susceptibility.[234,264] Cellulose II, or regenerated cellulose, undergoes

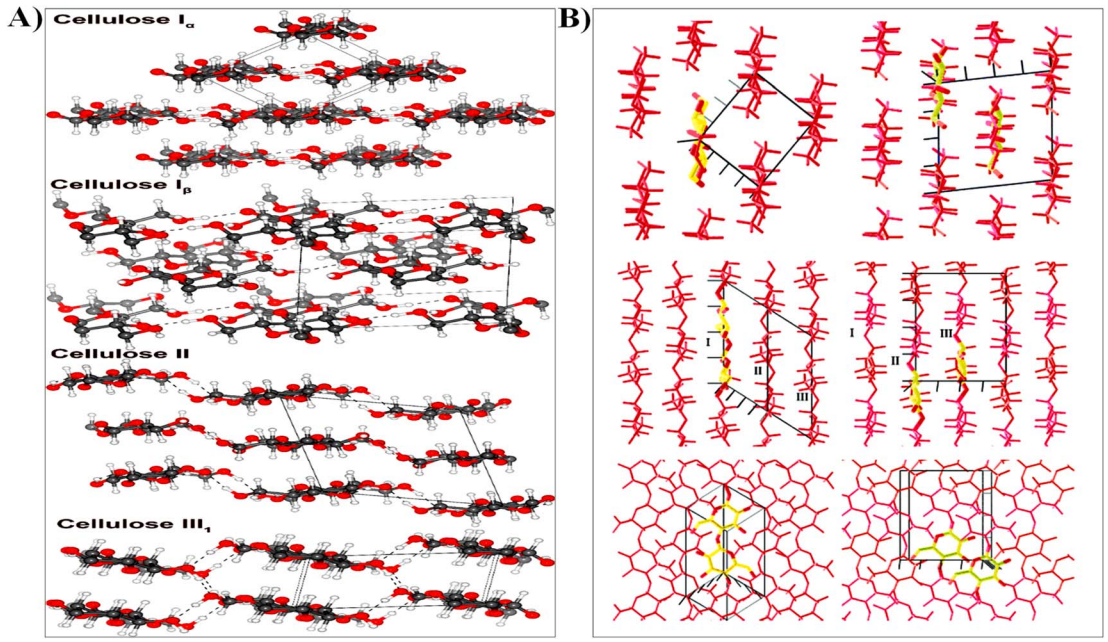

Fig. 4 (A) Refined crystal structures depicting cellulose allomorphs Iα, Iβ, II, and III1, with C, O, and H atoms represented by gray, red, and white spheres, respectively. Dashed lines denote hydrogen bonds. Reproduced with permission from ref. 234, copyright © 2020 Elsevier. (B) Visualizations of cellulose Iα and Iβ' crystal structures along chain axes (top), perpendicular to chain axes and within hydrogen-bonded sheets (middle), and perpendicular to hydrogen-bonded sheets (bottom). Red skeletal models represent cellulose chains, while the asymmetric unit of each structure is delineated by thicker lines, with carbons depicted in yellow. Unit cells are illustrated in white. Reproduced with permission from ref. 271, copyright © 2003 American Chemical Society.

structural transformation for increased chemical accessibility, making it valuable in textiles, flexible packaging, and filtration membranes.[248,265] Cellulose III, derived from treated cellulose I, offers heightened reactivity, making it suitable for drug delivery, coatings, and composite materials.[266,267] Cellulose IV, the amorphous form, lacks long-range order but retains fundamental chemistry of the cellulose, excelling in adhesives, flexible films, and packaging due to its enhanced bonding, flexibility, and barrier properties.[268–270] The crystal structures of cellulose Iα and Iβ are similar along the chain axis but differ perpendicular to it within hydrogen-bonded sheets. In both, the second sheet (II) is shifted upward by ∼c/4 relative to the first (I).[271] However, in Iα, the third sheet (III) is also shifted upward by ∼c/4 relative to II, while in Iβ, it shifts downward, resulting in a ∼c/2 displacement between sheets II and III. The conversion from Iα to Iβ likely occurs through chain slippage without disrupting hydrogen-bonded sheets, involving a ∼c/2 shift at the II–III interface (Fig. 4B).[271]

Cellulose, particularly at the micro- and nanoscale, is highly valued for its mechanical, chemical, optical, and rheological properties. As a key structural component in plants, cellulose provides mechanical strength through tight intra- and intermolecular bonds, forming microfibrils with high tensile strength.[272,273] The mechanical robustness of cellulose is primarily attributed to its highly crystalline regions. For instance, a bundle of stretched crystalline cellulose chains demonstrates an elastic modulus between 110 and 220 GPa, tensile strength between 7.5 and 7.7 GPa, and a density of 1.6 g cm^{-3}. However, the transversal modulus of crystalline nanocellulose is significantly lower, typically ranging from 15 to 30 GPa.[274–277] Rheological studies on nanocellulose have revealed interesting behavior. Dynamic rheology of microfibrillated cellulose (MFC) suspensions in water has shown gel-like properties across a concentration range of 0.125% to 5.9% w/w, with storage moduli varying from 1.5 Pa to 105 Pa.[278] CNCs typically exhibit a lower aspect ratio compared to CNFs, which have a much higher aspect ratio due to their smaller diameter and extended length.[272,279]

Surface chemistry studies have provided insights into the complex molecular composition of nanocellulose.[280–282] Despite the presence of hydrogen bonding, nanocellulose possesses a high density of hydroxyl groups, which facilitate interactions with organic chemicals.[272,283] Additionally, its inherent hydrophilicity and chirality promote surface functionalization through various chemical reactions, including esterification, oxidation, grafting, hydrophobization, and cationization.[53] The surface area of nanocellulose has been reported to exceed 30 m^2 g^{-1},[284,285] with a degree of polymerization (DP) typically greater than 900 glucose units, depending on its source and extraction method. In their review, Hallac and Ragauskas[286] summarized the DP of celluloses from various sources, measured after nitration using the viscometric method. They found that native wood celluloses generally had DPs ranging from 3900 to 5500, with species such as trembling aspen, jack pine, and white birch showing higher values. In contrast, non-woody celluloses, such as bagasse and wheat straw, had significantly lower DPs, around 925 and 1045, respectively.[286] Despite its high molecular weight and crystalline structure, nanocellulose exhibits limited water absorption. Non-toxic, biodegradable, and biocompatible, cellulose appears white and can form transparent or white gels.[287] Various techniques have been developed to incorporate ionic charges onto the surface of nanocellulose, as illustrated in Fig. 5.

Fig. 5A illustrates several pathways for modifying cellulose using small molecules, each offering unique advantages and applications. Esterification involves introducing ester groups onto cellulose chains, improving its solubility and compatibility with various solvents and matrices. This modification is particularly useful in applications that require enhanced solubility and interactions with other materials.[288,289] Acylation, which is the process allowing the attachment of acyl groups to the hydroxyl groups of cellulose, effectively alters its chemical properties and opens up new functional applications.[290,291] Silanization, which involves attaching silane compounds to cellulose, enhances its compatibility with different matrices, making it ideal for composites and coatings where improved adhesion is required.[292] Isocyanate modification creates urethane linkages on cellulose surfaces, enabling further chemical modifications and enhancing its versatility.[293] These modification pathways provide versatile ways to tailor cellulose for a wide range of applications.

Fig. 5B illustrates cellulose modification through grafting techniques, which allow for precise tailoring of cellulose properties. One prominent method, ring-opening polymerization (ROP), offers fine control over both the length and composition of polymer chains. This enables the creation of cellulose-polymer hybrids with specific attributes, such as enhanced strength and flexibility.[294] Additionally, techniques like atom transfer radical polymerization (ATRP) and reversible addition–fragmentation chain transfer (RAFT) polymerization provide controlled methods for grafting polymers onto cellulose, significantly enhancing its properties.[295,296] ATRP uses a transition metal catalyst to mediate the polymerization process, allowing for the growth of well-defined polymer chains from cellulose substrates. This method offers control over molecular weight, polydispersity, and polymer composition, and can introduce functionalities that alter cellulose properties, such as increased hydrophilicity or modified mechanical properties.[296,297] On the other hand, RAFT polymerization employs a chain transfer agent to control the polymerization process, resulting in polymers with specific architectures and functionalities.[295] RAFT allows scientists to graft polymers onto cellulose with controlled structures, further enhancing properties like biodegradability and compatibility with various environmental conditions.[298,299]

Fig. 5C illustrates various methods for modifying cellulose surfaces with macromolecular compounds, each offering tailored solutions for specific applications. The first approach (a) involves attaching polymers with isocyanate groups to cellulose, creating stable urethane linkages that enhance the material properties and compatibility.[293,298] The second method (b) entails reacting polymer amines with preoxidized cellulose aldehyde groups, leading to the formation of imine linkages, which modify the cellulose surface characteristics.[298] The third

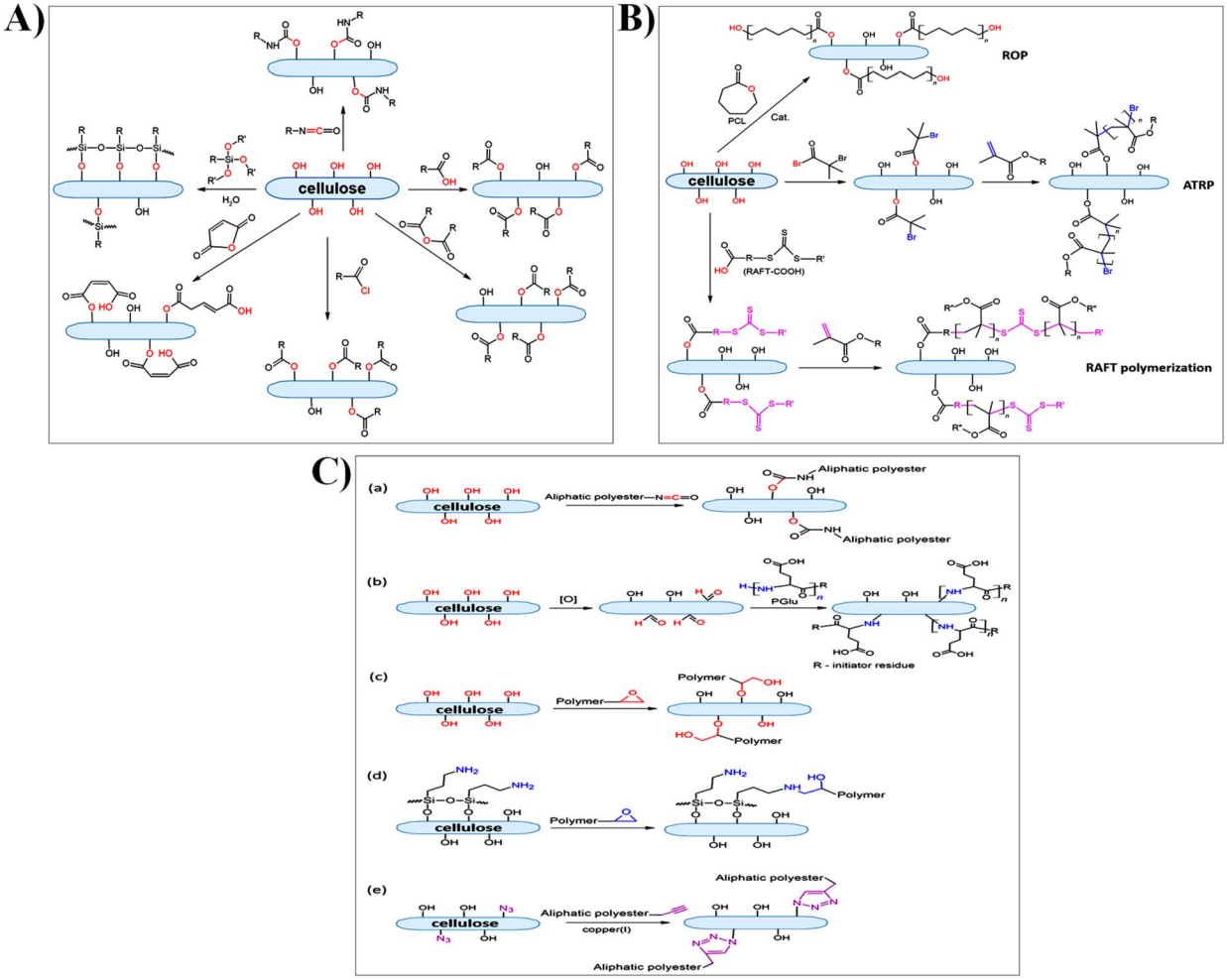

Fig. 5 (A) Schematic representation illustrating pathways for modifying cellulose using small molecules, including esterification, acylation, silanization, and modification with isocyanates. (B) Examples showcasing cellulose modification through grafting techniques such as ring-opening polymerization (ROP), atom transfer radical polymerization (ATRP), and reversible addition–fragmentation chain transfer (RAFT) polymerization. (C) Various methods explored for modifying the cellulose surface with macromolecular compounds using grafting techniques: (a) attachment of polymers containing isocyanate groups, (b) interaction of polymer amines with aldehyde groups of preoxidized cellulose, (c and d) modification of cellulose with epoxy-bearing polymers, and (e) modification *via* "click" reactions. Reproduced with permission from ref. 298, copyright © 2022 MDPI.

and fourth methods (c and d) involve incorporating epoxy-bearing polymers, resulting in the creation of robust hybrid materials with improved performance and stability. Finally, the fifth method (e) employs "click" chemistry, where polymers functionalized with azide or alkyne groups react with cellulose aldehyde groups to form covalent bonds. This approach further diversifies the potential applications of modified cellulose.[298] Click chemistry offers a robust and efficient strategy for the grafting of presynthesized polymers onto various substrates, particularly in the context of cellulose-based materials. A notable example is provided by Krouit *et al.*,[300] who functionalized cellulose fibers *via* esterification with 10-undecynoic acid, thereby introducing terminal alkyne groups suitable for subsequent copper(I)-catalyzed azide–alkyne cycloaddition (CuAAC). This heterogenous click reaction, performed in tetrahydrofuran (THF) at room temperature over 48 hours, enabled the grafting of azide-functionalized polycaprolactone (azide-PCL) onto the modified cellulose surface. The successful azidation of PCL was confirmed through a combination of Fourier-transform infrared spectroscopy, X-ray photoelectron spectroscopy, and nuclear magnetic resonance, and achieved a high reaction yield exceeding 90%.[300] Expanding on this approach, Mincheva *et al.*[301] demonstrated a similar CuAAC reaction involving azidized cellulose nanocrystals (CNCs) and a propargyl-terminated poly(L-lactide) (PLLA) in THF at 50 °C. The resulting grafting yielded a polymer-functionalized CNC surface with a PLLA content of approximately 12 wt%, thereby highlighting the versatility of click chemistry in the development of tailored polymer–cellulose hybrid materials.[301] These studies highlighted the potential of click chemistry not only for efficient surface modification but also for achieving precise control over grafting density and polymer architecture in cellulose-based composite systems.[300,301]

Table 4 Overview of recent studies focused on cellulose-based electrode materials for (bio)sensing of diverse analytes

Electrode materials	Analytes	Linear range	Detection limit	Main results achieved	Ref.
Cellulose nanofibers/Fe_3O_4 composite modified glassy carbon electrode (GCE)	Hydrazine	0.001–140 M	0.5 nM	Enhanced detection of hydrazine with a 2.3× increase in oxidation current and a 60 mV reduction in oxidation potential compared to unmodified GCE. Recovery range: 97.6–104.9%	193
Fe_3O_4 incorporated cellulose nanofiber composite (Fe_3O_4/CNF) as part of a modified carbon paste electrode (CPE)	4-Chlorophenol (4-CP)	1.0 nM–170 μM	0.5 nM	- Fe_3O_4/CNF/CPE demonstrated enhanced sensitivity for detecting 4-CP compared to a bare CPE - The oxidation current of 4-CP increased by over 1.67 times and the oxidation potential decreased by approximately 120 mV at optimal conditions - The sensor performance was validated with a recovery range of 98.52–103.66% in drinking water and wastewater samples	304
Cellulose nanofibers (CNF), graphene oxide (GO), chitosan-graphene oxide composite, acetylcholinesterase (AChE)	Chlorpyrifos (organophosphate pesticide)	25–1000 nM	2.2 nM	- The biosensor exhibited high sensitivity for detecting chlorpyrifos with good performance across the linear range of 25–1000 nM - The detection and quantification limits were 2.2 nM and 73 nM, respectively - The use of CNF and GO improved the sensor sensitivity, making it a precise, quick, and eco-friendly method for monitoring chlorpyrifos contamination in water and juice samples	30
CelloZIFPaper_*in situ* and CelloZIFPaper_*ex situ* (ZIF-8 integrated into cellulose pulp or TEMPO-oxidized cellulose nanofibrils)	Toxic heavy metals, such as lead ions (Pb^{2+})	—	8 μM for lead ions (Pb^{2+})	- The study demonstrated that porous zeolitic imidazolate frameworks (ZIF-8) integrated into cellulose-based papers could be used effectively as adsorbents for heavy metal removal from water, with capacities ranging from 66.2 to 354.0 mg g^{-1} - These materials served as working electrodes for selective electrochemical sensing of toxic metals, advancing Lab-on-CelloZIFPaper technologies for label-free heavy metal detection	309
TEMPO-oxidized cellulose nanofibers (TOC) loaded with silver nanoparticles (AgNPs) and/or graphite (Gr), crosslinked by tannic acid	Dopamine (DA)	0.005–250 μM	0.0005 μM (S/N = 3)	- TOC/AgNPs/Gr composite-modified electrode exhibited enhanced electrochemical performance for dopamine detection - It demonstrated a wide linear range, low detection limit, high sensitivity, and excellent anti-interference characteristics - Sensors also met clinical criteria for reproducibility, selectivity, stability and recovery, offering a promising approach for dopamine quantification	305
Cellulose nanocrystals (CNC)/polyaniline (PANI) composite films	Humidity, pH, organic solvents	—	—	- The study developed CNC-PANI and CNC-glucose-PANI films with bright structural color through optimized self-assembly - These films showed responsiveness to humidity, pH, and organic solvents, with changes in color and conductivity	303

Table 4 (*Contd.*)

Electrode materials	Analytes	Linear range	Detection limit	Main results achieved	Ref.
				- A two-layer CNC-PANI film was incorporated into a circuit, displaying color changes and increased conductivity in response to stimuli - Additionally, a PANI electrochromic device with CNC films demonstrated rapid color change from green to blue upon applying up to 1.5 V, with good cyclability and potential applications in information encryption and anti-counterfeiting using the chiral nematic CNC pattern	
Polyaniline/multiwalled carbon nanotubes/carboxymethyl cellulose (PANI/MWCNTs/CMC)	Ascorbic acid	0.05–5 mM	0.01 mM	- PANI/MWCNTs/CMC composite was successfully synthesized and characterized, exhibiting enhanced electrical and electrocatalytic properties due to the synergistic effects of its components - The composite demonstrated a large surface area, high pore volume, and good dispersion in aqueous solutions - As an electrochemical sensor, it showed a linear detection range for ascorbic acid and a high sensitivity of 100.63 $\mu A\ mM^{-1}\ cm^{-2}$	310
MnO_2/cellulose nanowhiskers hybrid materials	Hydrogen peroxide	0.2–400 μM	0.04 μM (S/N = 3)	- The MnO_2/cellulose hybrid sensor demonstrated high sensitivity (0.70 $\mu A\ \mu M^{-1}$) and fast electrochemical response - The sensor showed excellent performance with a high recovery rate (93–110%) in real sample detection - Characterization techniques confirmed the formation and uniform distribution of MnO_2 nanoparticles on cellulose nanowhiskers, enhancing electrocatalytic properties and making it suitable for sensor applications	311
2,2,6,6-Tetramethylpiperidine-1-oxyl (TEMPO)-oxidized cellulose nanocrystals (TOCNCs) and L-cystines (L-Cys) modified gold (Au) electrode (TOCNC/L-Cys/Au)	Enantiomers of phenylalanine (Phe), leucine (Leu), and valine (Val)	—	—	- TOCNC/L-Cys/Au electrode discriminated between enantiomers of the amino acids Phe, Leu, and Val, which are relevant to metabolic diseases - The sensor showed significant differences in peak currents for different amino acid enantiomers, confirmed by cyclic voltammetry (CV) and differential pulse voltammetry (DPV) - The electrode demonstrated effectiveness in distinguishing D- and L-Phe and showed potential for chiral sensing and metabolic disease diagnosis	312
Graphene oxide/cellulose nanofibril composite (GO/CNF) modified carbon paste electrode (GO/CNF/CPE)	*p*-Nitrophenol	3.0 nM–210 μM	0.8 nM	- The GO/CNF/CPE demonstrated high sensitivity, selectivity, and accuracy for detecting *p*-nitrophenol in water samples - The sensor showed a wide linear range and a low detection limit, making it effective for environmental monitoring and analysis	313

Table 4 (*Contd.*)

Electrode materials	Analytes	Linear range	Detection limit	Main results achieved	Ref.
Graphite/cellulose nanofibers-silver nanoparticles (Gr/CNF-AgNPs)	Ascorbic acid (AA), dopamine (DA), paracetamol (PA)	Wide range for all analytes	0.029 μmol L^{-1} for AA, 0.034 μmol L^{-1} for DA, 0.019 μmol L^{-1} for PA	- The study developed a voltammetric biosensor using a composite of cellulose nanofibers (CNFs) extracted from sugar cane bagasse and *in situ* synthesized silver nanoparticles (AgNPs) - The AgNPs-CNFs nanocomposite electrode exhibited a large surface area, high selectivity, and low detection limits for AA, DA, and PA - It demonstrated excellent anti-interference properties and was used to analyze these analytes in human urine and blood serum	314
PANI/D-CMC/ZnO (polyaniline/dialdehyde carboxymethyl cellulose/ ZnO nanoparticles)	Hydrogen peroxide (H_2O_2)	0.50 to 5 μM and 10 to 50 μM	0.45 μM	- The study developed a highly sensitive voltammetric sensor for H_2O_2 using a hybrid PANI/ D-CMC/ZnO material - The sensor demonstrated high conductivity and a good performance with a linear range and low detection limit of 0.45 μM for H_2O_2 under optimal conditions (pH 5.7) - The sensor effectively measured H_2O_2 in real samples, such as milk	306
PANI/cellulose/WO_3 composite	Acetone	0 to 100 ppmv	10 ppm	- An electrochemical sensor was developed using a composite of polyaniline (PANI) and tungsten trioxide (WO_3) doped with cellulose - The sensor operates effectively at room temperature, detecting acetone with a high sensitivity and accuracy - It demonstrated a linear response with an R^2 value of 0.99415 and a relative standard deviation (RSD) of 5% - The sensor achieved a detection limit of 10 ppm, overcoming the challenge of high operating temperatures typically associated with acetone sensing	4
Fe_3O_4@cellulose nanocrystals/Cu nanocomposite (Fe_3O_4@CNC/Cu) on a graphite screen-printed electrode	Venlafaxine	0.05–600.0 μM	0.01 μM	- The Fe_3O_4@CNC/Cu nanocomposite was successfully synthesized using a plant extract as a green reducing agent - This nanocomposite was used to modify a graphite screen-printed electrode, enabling sensitive detection of venlafaxine - The sensor demonstrated a wide linear range and a low detection limit for venlafaxine - It proved to be selective and precise for detecting venlafaxine in urine, water, and pharmaceutical samples	308

Table 4 (*Contd.*)

Electrode materials	Analytes	Linear range	Detection limit	Main results achieved	Ref.
Quaternized cellulose nanoparticles (QCs)/ acetylene black (AB)/ enzymes composite electrodes	Hydrogen peroxide (H_2O_2), glucose	—	—	- The QCs-AB composite electrodes demonstrated excellent electrocatalytic performance with fast response, high sensitivity, and good stability for detecting H_2O_2 and glucose - The composite material facilitated effective direct electron transfer for glucose oxidase (GOD) and hemoglobin (Hb) immobilized on the electrode - This approach offers a promising platform for the development of unmediated enzyme biosensors	207
Cellulose microfibers supported reduced graphene oxide (rGO) composite	Fenitrothion	Up to 1.134 mM	8 nM	- The cellulose microfibers supported rGO composite electrode demonstrated superior electro-reduction ability and lower reduction potential for fenitrothion compared to other modified electrodes - It showed a reduction potential 141 mV lower than a chemically reduced rGO-cellulose microfibers composite - The electrode achieved a wide linear response range and a low detection limit, and it was successfully used for detecting fenitrothion in various water samples	315
Composite sensor of cellulose nanocrystals (CNCs) and multiwall carbon nanotubes (MWCNTs)	Tryptophan (Trp) enantiomers (L-Trp and D-Trp)	—	—	- The chiral sensor demonstrated rapid, high-sensitivity, and stable discrimination of Trp enantiomers, with a 3.5-fold higher peak current ratio for L-Trp compared to D-Trp under optimal conditions (pH 7.0, 25 °C) - The sensor performance varied with CNC type (s-CNCs from H_2SO_4-hydrolysis *vs.* h-CNCs from HCl-hydrolysis), highlighting different affinities and chiral recognition effects - The combination of CNC chiral recognition and MWCNTs signal amplification provided an effective method for distinguishing Trp enantiomers	316
Nanoporous gold electrode arrays on cellulose membranes	Oxygen (O_2)	0.054 to 0.177 v/v %	0.0075%	- A novel, cost-effective, and flexible paper-based electrochemical O_2 sensor was developed using nanoporous gold electrode arrays on cellulose membranes and an ionic liquid electrolyte (BMIMPF6) - The sensor demonstrated high sensitivity, a low detection limit, and a rapid response time of less than 10 s, making it highly promising for environmental monitoring and gas sensing applications	195

Table 4 (*Contd.*)

Electrode materials	Analytes	Linear range	Detection limit	Main results achieved	Ref.
Assembly of cellulose grafted with hydroxypropyl-β-cyclodextrins (CMC-CD), multi-walled carbon nanotubes (MWCNTs) and copper ions on the surface of a GCE	Tryptophan (Trp) enantiomers (L-Trp and D-Trp)	—	—	- The developed sensor exhibited significant chiral recognition capability for Trp enantiomers, with a differential pulse voltammetry (DPV) oxidation peak current ratio (IL/ID) of 2.2 - The sensor showed a stronger electrochemical signal for L-Trp compared to D-Trp, indicating a higher affinity for L-Trp. The sensor was successfully applied to quantify D-Trp in a racemic mixture	307

3.2. Nanocellulose in (bio)sensor applications

Nanocellulose, encompassing various forms, stands out as a class of environmentally friendly materials with remarkable properties, making them increasingly prominent in modern technology.[56,61,302] In the context of biosensor materials derived from cellulose, the significance of cellulose and its derivatives including cellulose-based composites has been extensively explored. Nanocelluloses, in particular, have proven highly valuable in a wide array of biosensing applications, enabling the detection of diverse analytes across multiple fields.[193–195,302] The research summarized in Table 4 underscores the growing trend of using cellulose-based materials to enhance the sensitivity, selectivity and performance of electrochemical sensors. These cellulose-based materials, often integrated with additional functional components, have proven to be highly effective in improving sensor capabilities for detecting a wide range of analytes.[193,195,230,302] Various cellulose-based composites, achieved by incorporating in cellulosic matrices, additive materials such as metal oxides,[193] graphene,[30] or polyaniline,[303] have been integrated into electrodes to detect a range of analytes, including hydrazine,[193] 4-chlorophenol,[304] dopamine,[305] hydrogen peroxide,[306] and tryptophan enantiomers.[307] These composite materials, when used as electrodes, exhibit improved sensor performance, marked by lower detection limits, broader linear ranges, and enhanced signal responses compared to unmodified electrodes.[30,305–307] These advancements are attributed to the interesting physicochemical properties of cellulose, which when combined with conductive materials like carbon nanotubes or metal nanoparticles, result in superior electrochemical activity.[30,306,308] Additionally, the incorporation of cellulose derivatives in composite films has enabled the development of multifunctional sensors that are responsive not only to chemical analytes but also to environmental factors such as humidity and pH.[303] By functionalizing cellulose with specific groups or embedding it with conductive nanoparticles, these composite films can detect a wide range of environmental changes. For instance, cellulose-based sensors can undergo physical transformations, such as swelling or shrinking in response to variations in humidity or pH, leading to changes in conductivity or optical properties that are easily measurable. This makes them ideal for real-time monitoring applications in diverse fields where both chemical and environmental parameters should be continuously assessed.[303] The research described in Table 4 highlights recent advancements in the development of cellulose-based electrode materials for the (bio) sensing of a broad range of analytes.

3.2.1 Enhancing gas sensor performance with nanocellulose-based composites. Nanocellulose has found extensive applications, particularly in the development of gas sensors. Gas sensors, also known as gas detectors, play a vital role in detecting and identifying various gases for safety and environmental monitoring purposes. They are widely used to detect toxic or explosive gases and measure gas concentrations.[317] Emerging technologies in hazardous gas sensing require easy-to-use, cost-effective solutions for widespread adoption.[21,22] In this regard, nanocellulose, with its renewable

nature, low cost, abundance, high porosity, mechanical strength, and flexibility, offers promising properties for modifying gas sensor materials. Traditionally, gas sensors have been fabricated using inorganic semiconductor metal oxides such as TiO_2, Fe_2O_3 and ZnO.[318–320] However, these materials often suffer from instability due to the ionic conduction charge on their surfaces. In contrast, organic conducting polymers possess free electrons along their polymer chains, which enhance their conductivity. Additionally, semiconductor metal oxides typically require high operating temperatures, while organic conducting polymers like polyaniline (PANI) or polypyrrole (PPy), offer cost-effective synthesis and faster response times at moderate temperatures.[317,321] Combining semiconductor metal oxides or organic conducting polymers with nanocellulose can significantly enhance electrical conductivity, sensitivity and performance of resulting modified sensors.[21,313,314,322] Several studies have focused on incorporating nanocelluloses into electrically conductive matrices to enhance the electrical properties of the resulting composites, as well as the performance of sensors modified with these electrically conductive cellulose-based composites.[308,323] For example, composite nanofibers of cellulose/TiO_2/PANI prepared a room temperature showed improved ammonia sensing performance at room temperature (Fig. 6A), attributed to enhanced surface area and specific surface characteristics of composites due to PANI presence in the electrode materials (Fig. 6B).[324] The ammonia sensing performance was assessed using a custom test system at room temperature (Fig. 6C). TiO_2 contributed to enhanced response values and sensitivity of developed sensors. Selectivity tests revealed the sensor high specificity to ammonia over acetone, ethanol, and methanol at 250 ppm concentration, showcasing its practical applicability (Fig. 6D).[324] Similarly, Hu *et al.*[194] successfully fabricated a novel formaldehyde sensor using nanofibrous polyethyleneimine (PEI)/BNC membranes coated on quartz crystal microbalance. This sensor exhibited good selectivity towards formaldehyde and demonstrated excellent reversibility, reproducibility, and linearity with increasing formaldehyde concentrations.[194] In addition, Rahman *et al.*[325] fabricated electrospun nanofibers and solution-casting nanofilms from environmentally friendly cellulose acetate blended with glycerol, mixed with PPy, and doped with tungsten oxide (WO_3) nanoparticles. They developed sensing membranes for the detection of H_2S gas at room temperature.[325] The sensors operated at 20 °C and detected H_2S concentrations as low as 1 ppm. They demonstrated rapid response times of 22.8 and 31.7 s for the nanofiber and nanofilm sensors, respectively, with excellent reproducibility, stability, and low humidity dependence.[325] In a recent work, cellulose was used as an eco-friendly support for a flexible gas sensor, which was developed using spray-coated oxidized single-walled carbon nanotube (Oxy-SWCNT) bundles.[326] The oxygen functionalization of the outer SWCNTs enhanced solution processability and gas selectivity, while the inner SWCNTs provided efficient charge transport. The cellulose-supported sensor outperformed silicon-based sensors, showing an improved NO_2 response and cross-sensitivity to other gases due to polar glycosidic linkages.

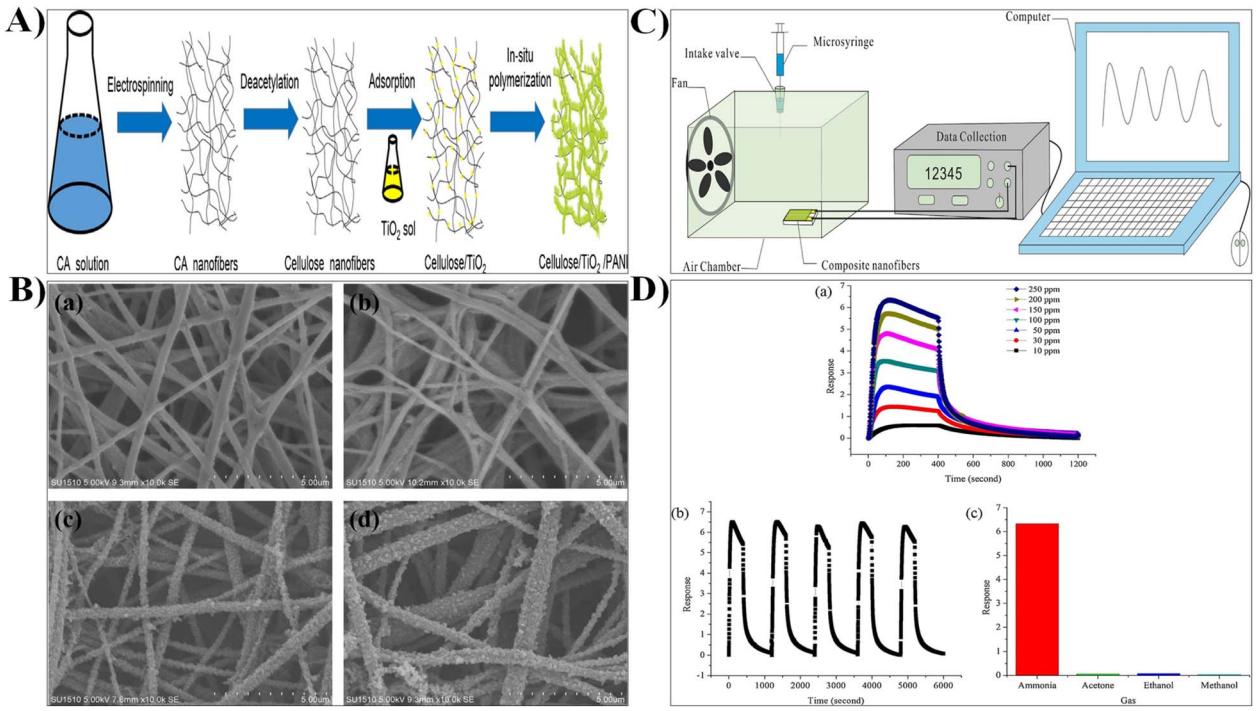

Fig. 6 (A) Scheme depicting the formation of cellulose/TiO_2/PANI composite from cellulose acetate (CA). (B) Scanning Electron Microscopy (SEM) images showcasing cellulose (a), cellulose/TiO_2 (b), cellulose/PANI (c), and cellulose/TiO_2/PANI composite nanofibers (d). (C) Schematic representation of the homemade gas sensing test system. (D) Response to varying concentrations of ammonia (a), repeatability to 250 ppm ammonia (b), and selectivity (c) of cellulose/TiO_2/PANI composite nanofibers. Reproduced with permission from ref. 324, copyright © 2016 Elsevier.

Surface roughness engineering with halloysite nanotubes further enhanced the NO_2 response, achieving an ultralow detection limit of 0.43 ppb.[326]

Bacterial nanocellulose, renowned for its abundant hydroxyl (–OH) groups and enhanced mechanical properties, has been combined with metal oxides to design composite materials for gas sensors. These sensors showed promising responses to a range of chemical compounds, including nitrogen dioxide, acetone, and ethanol, at ambient temperatures.[22] Additionally, leveraging the electrical conductivity and stability of aniline with cellulose nanopaper cross-linked with amino graphene has led to the development of CO_2 gas sensors with heightened sensitivity and rapid response characteristics across the range of CO_2 concentrations tested.[21] In industrial applications, carbon-derived materials interacting with cellulose –OH groups can form a network widely used for chemical gas sensing.[20,327] For instance, the integration of conductive carbon-based materials in cellulose matrix highlighted the potential of composite materials for precise chemical gas sensing applications. Im *et al.*[328] developed an integrated cellulose polymer concentrator/single-walled carbon nanotube (SWCNT) sensing system for detecting benzene, toluene, and xylenes (BTX)

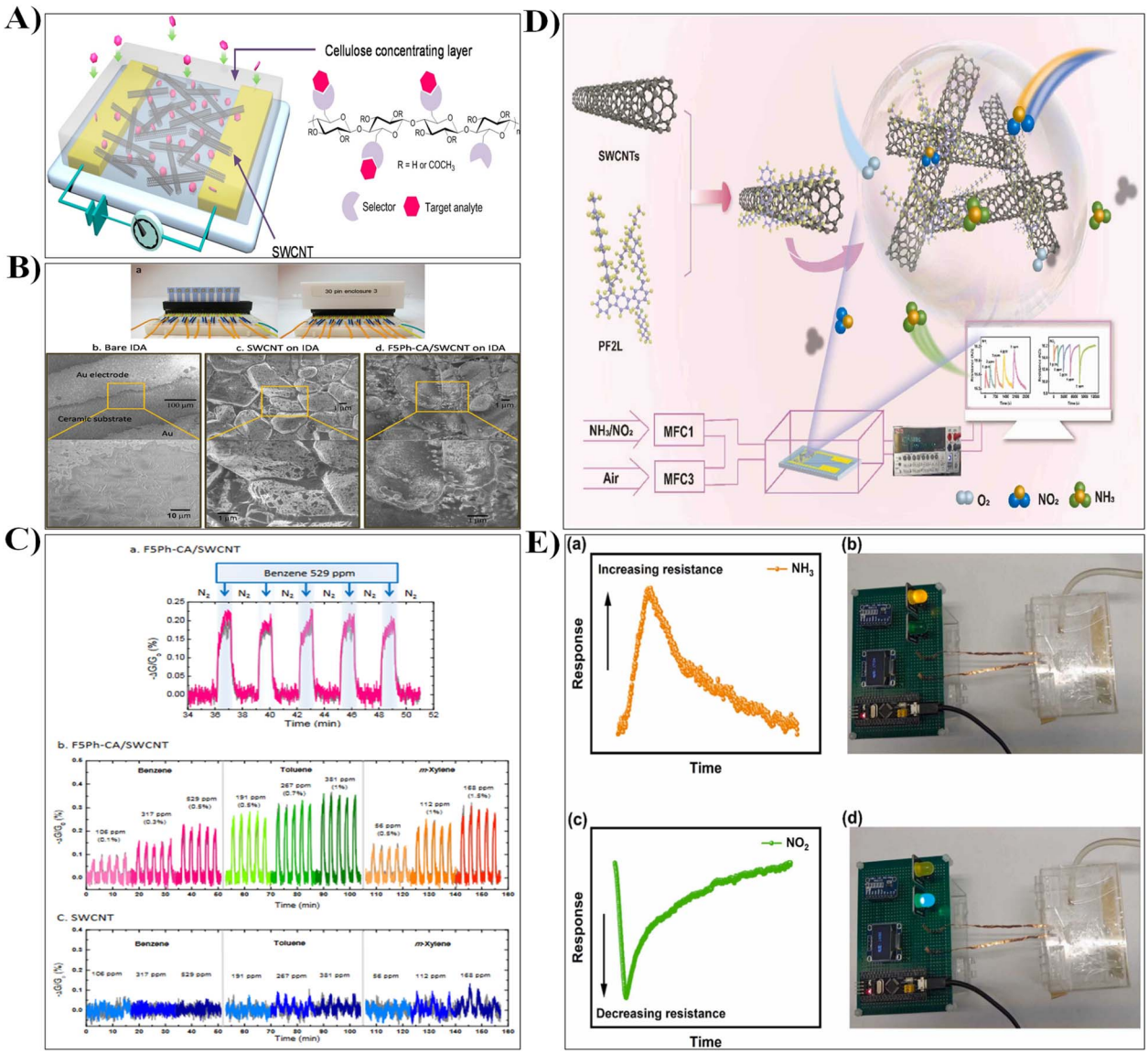

Fig. 7 (A) Illustration of the integrated polymer concentrator/single-walled carbon nanotubes (SWCNT) sensing system. The cellulose concentrating layer absorbed and concentrated analytes, delivering them rapidly to the SWCNT sensing layer. (B) (a) Images of the array device with 9 sensors deposited on interdigitated microelectrode array (IDA). SEM images of (b) bare IDA, (c) SWCNTs on IDA, and (d) F5Ph-CA/SWCNT on IDA. (C) (a) Normalized conductance changes [$-\Delta G/G_0$ (%)] of F5Ph-CA/SWCNT system when exposed to 529 ppm benzene, (b) normalized conductance changes when exposed to benzene, toluene, and *m*-xylene vapors compared to pristine SWCNT sensor (c). Duplicate sensor responses were consistent, as shown by grey curves representing the second sensor response. Reproduced with permission from ref. 328, copyright © 2016 MDPI. (D) Sensing performance plot of PF2L/sc-SWCNTs sensors for detecting NH_3 vapor and NO_2. (E) LED-based detection of NH_3 vapor (a and b) and NO_2 (c and d) using the PF2L/sc-SWCNTs sensor. Reproduced with permission from ref. 329, copyright © 2024 Elsevier.

vapors, as shown in Fig. 7A. SEM images (Fig. 7B) of the developd composite materials revealed a reduced SWCNT network after coating with cellulose acetate.[328] The system exhibited high sensitivity, with limits of detection for benzene, toluene, and *m*-xylene vapors recorded at 55 ppm, 19 ppm, and 14 ppm, respectively. Furthermore, the sensor demonstrated excellent selectivity and fast response times, reaching equilibrium in less than 10 seconds (Fig. 7C).[328] Zhang *et al.*[329] synthesized a polymer with two Schiff base side chains (PF2L) *via* the Suzuki coupling reaction, improving polymer solubility. They used PF2L to selectively sort semiconductor single-walled carbon nanotubes (sc-SWCNTs) from commercial SWCNTs, forming PF2L/sc-SWCNTs composites. The incorporation of side chains enhanced π–π interactions within the polymer and between the polymer and sc-SWCNTs, promoting better dispersion of the nanotubes.[329] The resulting PF2L/sc-SWCNTs-based gas sensors were fabricated using a drop-coating method and tested for gases with different properties, such as NH_3 and NO_2 (Fig. 7D). The sensors exhibited responses of 2.415% for NH_3 and 14.85% for NO_2 at 1 ppm. The response and recovery times for NH_3 were 50 s and 220 s, respectively, and for NO_2, 59 s and 733 s. They also developed an LED-based detection device for selective NH_3 and NO_2 discrimination as displayed in Fig. 7E, showcasing the potential of this device for dual gas sensing.[329]

3.2.2 Versatile nanocellulose-based chemical sensor platforms. Studies have explored the integration of nanocellulose into chemical sensing, demonstrating its potential across various platforms. Different nanocellulose-based sensing systems have been developed, showcasing their versatility in different dimensional forms. One-dimensional (1D) systems enhance sensitivity and specificity. In 1D systems, nanocellulose is often used in the form of fibers to construct highly sensitive and specific sensors. These fibers exhibit remarkable responsiveness due to their structural alignment and high aspect ratio, which enhances their interaction with targeted analytes.[330] Two-dimensional (2D) platforms, such as papers and films, offer increased surface area and porosity for improved detection. These 2D structures are particularly effective at enhancing sensor performance by providing a large number of reactive sites for analyte interaction, which in turn increases the detection sensitivity. The high porosity of 2D nanocellulose materials facilitates the rapid diffusion of target molecules, allowing for quicker and more efficient sensing responses. Additionally, the ability to produce nanocellulose films and papers at low cost and large scale has spurred their use in a variety of applications.[325,327] Three-dimensional (3D) matrices, like aerogels and hydrogels, provide precise control over sensors and facilitate better analyte interactions. 3D nanocellulose systems can be engineered to have specific structural characteristics, such as pore size and mechanical strength, which can be optimized for particular sensing applications.[331,332] Aerogels, for instance, are highly porous, lightweight materials characterized by low density and high surface area, making them ideal for applications requiring rapid analyte diffusion and high adsorption capacity.[331,333] When functionalized with conductive materials or nanoparticles, these 3D aerogels can be used as electrodes in electrochemical sensors or as platforms for the detection of gases, biomolecules, and environmental pollutants.[331,333,334] Hydrogels, on the other hand, are water-absorbing materials that undergo significant swelling and contraction in response to environmental changes, such as pH, temperature, or ionic strength. These properties allow hydrogels to be used in sensors that detect changes in biological environments or chemical processes.[335–337]

3.2.2.1 1D fiber-based sensors. These sensors offer numerous advantages, such as flexibility and excellent mechanical properties, making them ideal for a variety of applications. The orientation of nanofibers within a single fiber is a crucial factor influencing their performance.[338] Nawaz *et al.*[330] developed a highly selective and sensitive fluorescent sensor, Phen-MDI-CA, for detecting Fe^{2+}. This sensor was synthesized by chemically bonding 1,10-phenanthroline-5-amine (Phen) to cellulose acetate (CA) fibers, using 4,4′-methylene diphenyl diisocyanate (MDI) as a crosslinker.[330] The synthesized Phen-MDI-CA dissolved easily in DMSO and dimethylformamide, enabling the creation of versatile materials such as fluorescent inks, flexible films, coatings, and microspheres, all emitting bright blue fluorescence (Fig. 8A). The process involved homogeneous reaction conditions, which ensured a robust sensor structure, as depicted in Fig. 8B.[330] This work demonstrates the potential of 1D fiber-based sensors for high-performance analyte detection. Fluorescence-based detection showed a linear correlation between emission intensity and Fe^{2+} concentration, with a detection limit of 2.6 ppb. Selectivity tests confirmed the high specificity of the sensor for detecting Fe^{2+} ions. In comparison, UV-visible absorption also displayed selectivity but with a higher detection limit of 4.0 ppb (Fig. 8C).[330]

In another study conducted by Yao *et al.*,[339] a novel multicolor (green, yellow, and orange) macrofiber-based biosensor was developed using moderately oriented bacterial cellulose nanofibers (BCNs) through a wet spinning process.[339] This biosensor assembled CdTe-loaded BCNs onto a 1D structure, enabling pH and glucose sensing functionalities. The resulting macrofibers exhibited sigmoidal pH dependence and high sensitivity to glucose concentrations, promising significant advancements in biosensing by providing a versatile platform for precise and efficient analyte detection.[339] Moreover, Teodoro *et al.*[340] synthesized a hybrid material comprising cellulose nanowinkers and silver nanoparticles (AgNPs) for colorimetric detection of H_2O_2. The hybrid sensor demonstrated high sensitivity and selectivity, achieving impressive limits of detection (0.014 μM for concentrations ranging from 0.01–30 μM and 112 μM for concentrations from 60–600 μM).[340] Orelma *et al.*[341] developed an optical cellulose fiber specifically designed for water sensing applications. They observed a reversible attenuation of over 30 dB upon immersion in water. This innovative approach highlights the potential of cellulose-based materials in advancing sensor technologies, particularly in the area of water quality monitoring.[341] Furthermore, Kumari *et al.*[342] combined cellulose extracted from pine needles with lysine Schiff base to fabricate a sensor-adsorbent for mercury ions. They achieved using this developd sensor a maximum adsorption capacity of 258.75 mg g^{-1}.[342] Fu *et al.*[343] introduced a simple

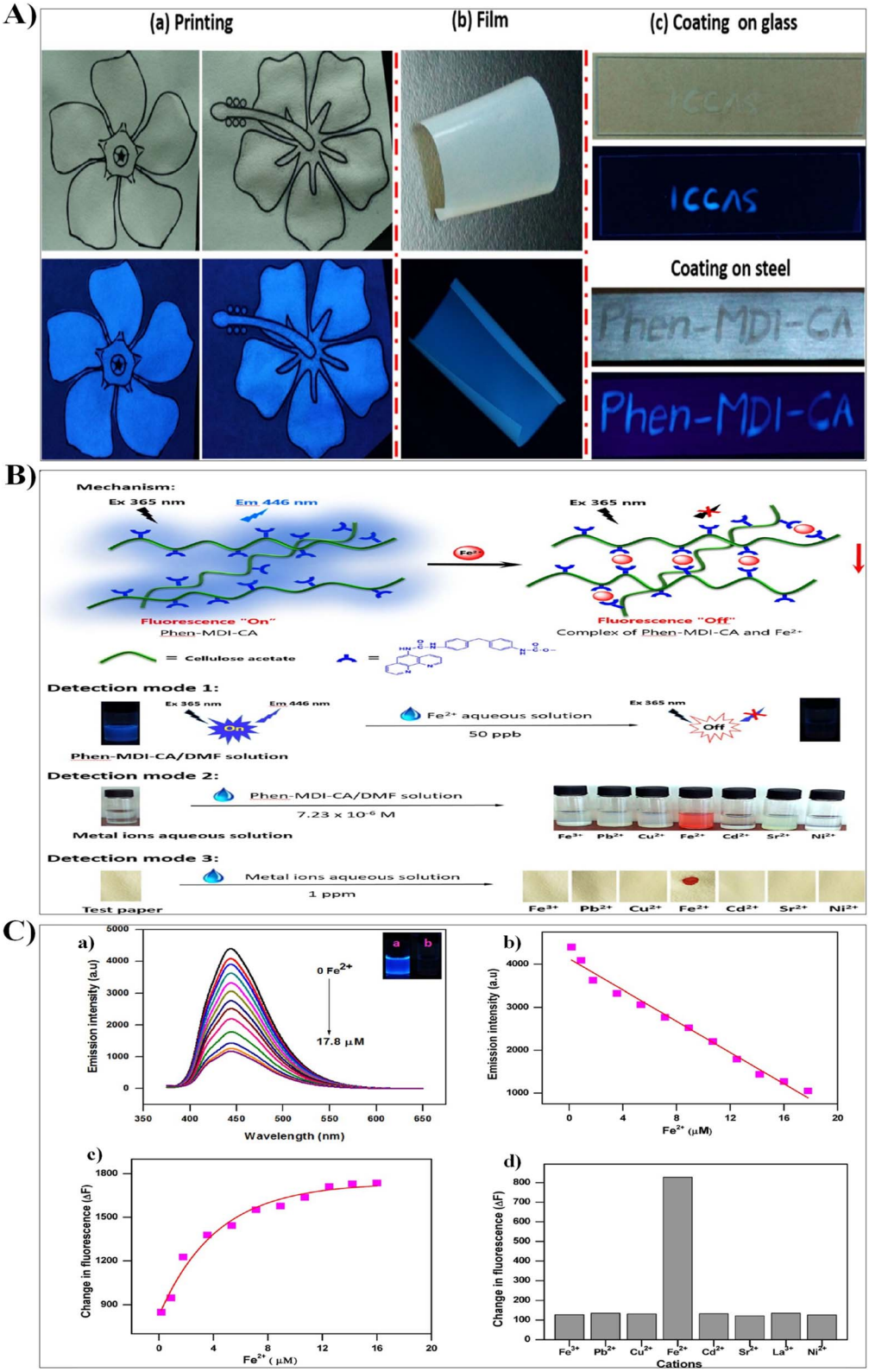

Fig. 8 (A) Photos of Phen-MDI-CA in different material forms under visible and 365 nm UV light: (a) fluorescent printing on filter paper, (b) flexible fluorescent film, and (c) coatings on glass and steel. (B) Fe^{2+} ion detection in multimode. Detection mode 1: fluorescence quenching upon adding Fe^{2+} aqueous solution (50 ppb) into Phen-MDI-CA (7.23×10^{-6} M in DMSO). Detection mode 2: visual color change upon adding Phen-MDI-CA into a metal-ion aqueous solution. Detection mode 3: visual color change of test papers by adding metal ions (1 ppm). (C) (a) Fluorescence spectra of Phen-MDI-CA with different Fe^{2+} ion concentrations. Inset: photos of Phen-MDI-CA/DMSO solutions before and after Fe^{2+} ion addition under UV light. (b) Emission intensity *vs.* Fe^{2+} concentration. (c) Effect of Fe^{2+} concentration on emission intensity change. (d) Fluorescent response of Phen-MDI-CA with various metal aqueous solutions (0.045 μM) using 365 nm excitation wavelength for all measurements. Reproduced with permission from ref. 330, copyright © 2018 American Chemical Society.

method for synthesizing and immobilizing polyaniline nanorods onto carboxymethyl cellulose (CMC)-modified cellulose nanofibers, specifically designed for biosensing applications. This resulted in a biosensor with a detection limit of 0.374 M and a linear response range from 0.497 M to 2.27 mM.[343] Moreover, Davis and co-workers[344] developed a novel method to encapsulate ionic fluorescent dendrimers (AFD) into cellulose acetate (CA) nanofibers, enabling the detection of metalloproteins through a quenching mechanism. Fig. 9A shows the schematic of the electrospinning setup, dendrimer encapsulation, and the deacetylation process used in this study. High-resolution UV confocal microscopy was employed to visualize protein detection.[344] Fig. 9B presents fluorescence images of AFD-doped cellulose nanofibers before and after incubation with a 10 μM cyt c solution, illustrating a significant quenching effect. This method demonstrated potential for the sensitive and selective detection of metalloproteins, with distinct responses for each protein interacting with the fluorescent fibers, showcasing its promising application in biosensing technologies (Fig. 9C).[344]

Chauhan *et al.*[345] developed a simple, low-cost, eco-friendly, and disposable conducting paper substrate (RCP) decorated with electrospun cellulose acetate fibers (CAEFs) for biosensor applications. The CAEFs were electrospun at 16 kV, with a flow rate of 0.2 mL h^{-1} and a 15 cm tip-to-collector distance, yielding fibers with a diameter of 330 ± 3.50 nm and a hydrophilic nature (contact angle of 38.07 ± 5.10°). The CAEF/RCP electrode was functionalized with antibodies for detecting 25-OH vitamin D3 (AB-25OHD_3), confirmed through various characterization techniques (Fig. 10A).[345] The electrochemical behavior of the BSA/AB-25OHD_3/CAEF/RCP immunoelectrode was studied using cyclic voltammetry (CV) and electrochemical impedance spectroscopy (EIS) in PBS solution (pH 7). The optimal concentration of AB-25OHD_3 was determined to be 50 μg mL^{-1}. CV analysis revealed a decrease in peak current as the electrode surface was modified, with the peak current dropping from 87 μA for RCP to 2.26 μA after BSA/AB-25OHD_3/CAEF/RCP modification. EIS analysis showed an increase in charge-transfer resistance (R_{ct}) from 1.08 kΩ for RCP to 4.24 kΩ for BSA/AB-25OHD_3/CAEF/RCP, confirming the electrode modifications (Fig. 10B). The electrochemical response of the BSA/AB-25OHD_3/CAEF/RCP immunoelectrode was further studied using chronoamperometry in PBS for 25-OHD3 concentrations ranging from 10 to 100 ng mL^{-1} with a five-minute incubation time. The chronoamperometry was performed at −0.15 V with pulses every 0.1 s for 160 s. The current increased with higher concentrations of 25-OHD_3, reaching a plateau after 80 ng mL^{-1}, indicating a saturated antibody–antigen interaction.[345] This current variation was attributed to electrode surface rearrangement and enhanced charge transfer *via* $[Fe(CN)_6]^{3-/4-}$, potentially influenced by changes in the isoelectric point (IEP). A calibration curve for 25-OHD_3 concentrations was derived

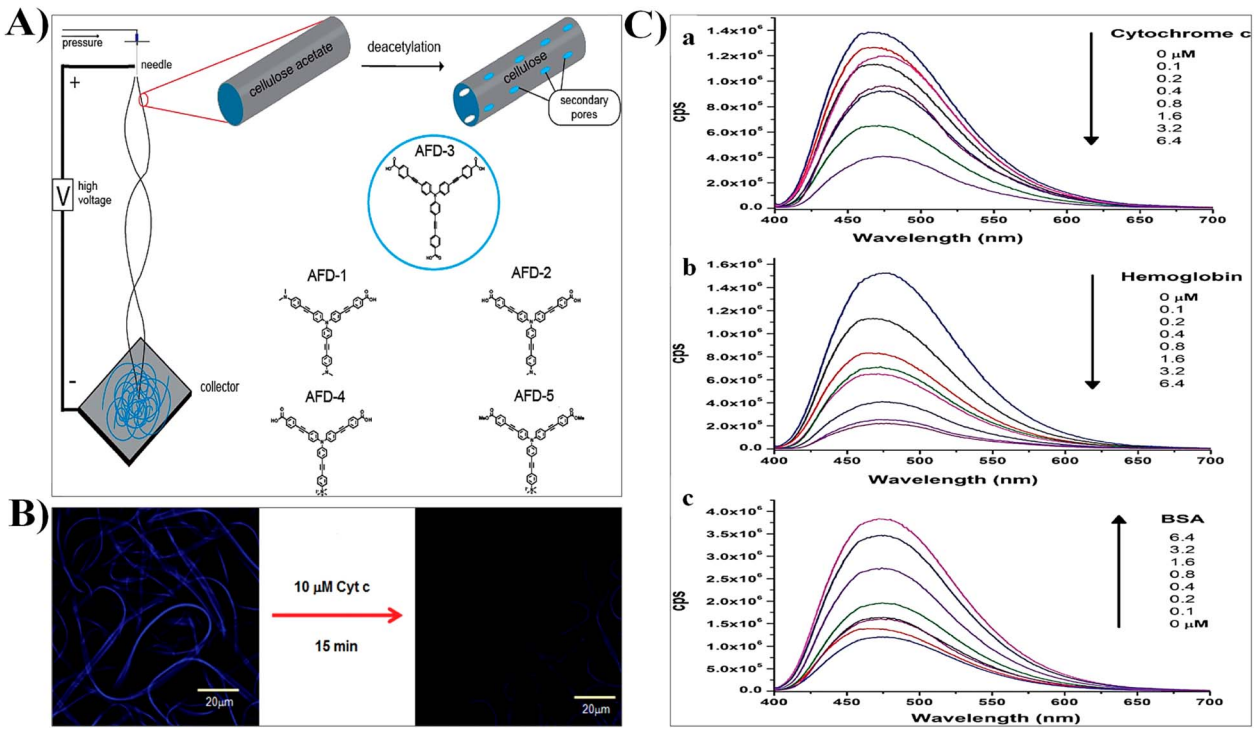

Fig. 9 (A) Schematic representation of the electrospinning setup, encapsulation of the fluorescent dendrimer, and deacetylation process employed in this study. Five water-soluble fluorescent dendritic compounds (AFD-1, AFD-2, AFD-3, AFD-4, and AFD-5) composed of phenylene-ethynylene repeating units are depicted. (B) Confocal fluorescence images of electrospun nanofibers before (left) and after (right) incubation in a 10 μM cyt c solution for 15 min. (C) Fluorescence emission spectra of AFD-functionalized nanofibers in response to various concentrations of cyt c, Hgb, and BSA ($\lambda_{Ex}/\lambda_{Em}$ = 370/475 nm). Reproduced with permission from ref. 344, copyright © 2010 American Chemical Society.

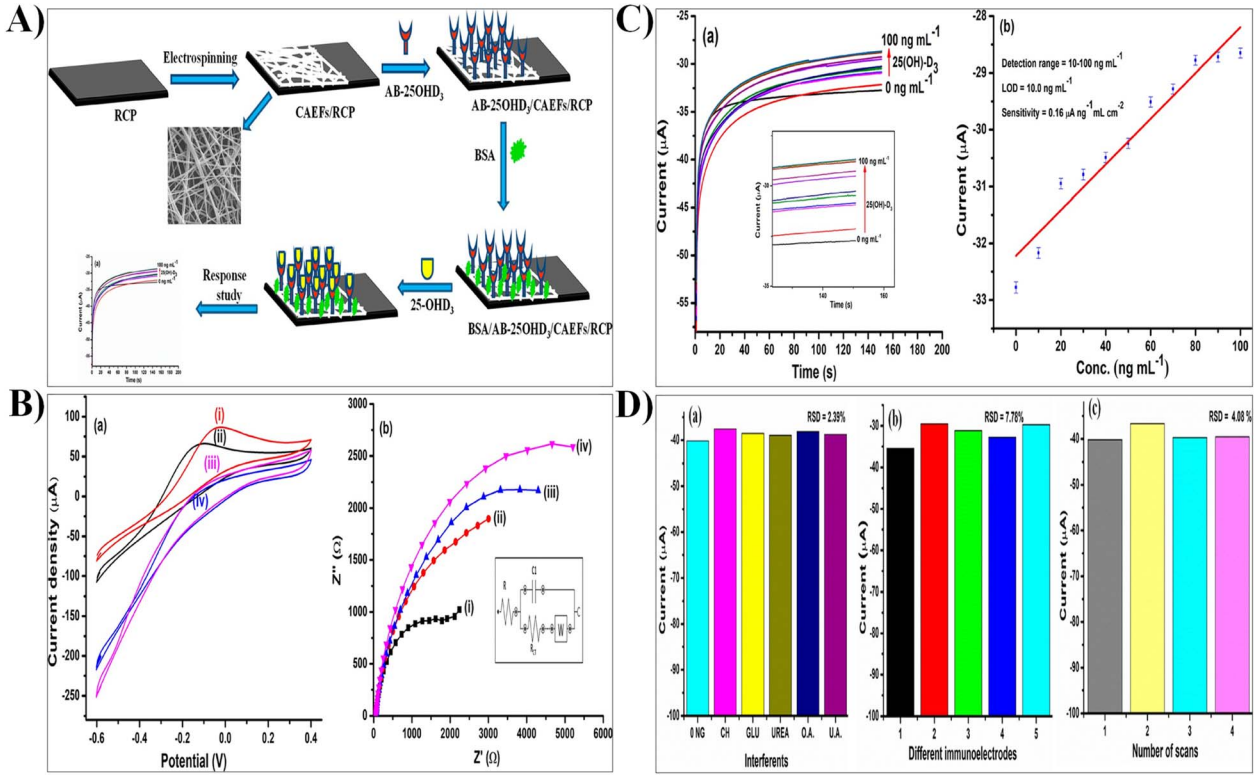

Fig. 10 (A) Production process of the cellulose acetate-based immunosensor. (B) Electrochemical characterization including cyclic voltammetry (CV) and electrochemical impedance spectroscopy (EIS) of different electrodes: (i) RCP, (ii) CAEF/RCP, (iii) AB-25OHD$_3$/CAEF/RCP, and (iv) BSA/AB-25OHD$_3$/CAEF/RCP immunoelectrode. (C) Evaluation of the BSA/AB-25OHD$_3$/CAEF/RCP immunoelectrode response in phosphate-buffered saline containing $[Fe(CN)_6]^{3-/4-}$ *via* chronoamperometry, along with the calibration curve relating peak current to 25-OHD3 concentrations. (D) Assessment of immunoelectrode selectivity, reproducibility, and repeatability in PBS containing $[Fe(CN)_6]^{3-/4-}$. Reproduced with permission from ref. 345, copyright © 2019 American Chemical Society.

(Fig. 10C). The selectivity, reproducibility, and repeatability of the BSA/AB-25OHD$_3$/CAEF/RCP immunoelectrode were evaluated and found to be satisfactory. The relative standard deviation (RSD) was below 5%, indicating good reproducibility. Tests with interfering compounds like cholesterol, glucose, urea, oxalic acid, and uric acid showed no significant change in current values. The immunoelectrode demonstrated good reproducibility (RSD = 7.78%) and repeatability (RSD = 4.08%) during successive measurements of 25-OHD$_3$ at a concentration of 10 ng mL^{-1} (Fig. 10D).[345]

3.2.2.2 2D nanocellulose-based substrates. They offer interesting advantages due to their transparency, low thermal expansion, high strength and stiffness, flexibility, and remarkable mechanical properties. These characteristics make them highly suitable substrates for flexible electronics applications, particularly in sensors and actuators development.[39] Ren *et al.*[47] fabricated an amperometric glucose biosensor using a composite film comprising gold nanorods and cellulose acetate. Glucose oxidase enzyme was incorporated into the composite film by mixing with gold nanorods and cross-linking with cellulose acetate medium using glutaraldehyde.[47] The optimized biosensor showed high sensitivity (8.4 A cm^{-2} mM^{-1}), a low detection limit (2×10^{-5} M), a wide linear range (from 3×10^{-5} to 2.2×10^{-3} M), good storage stability, reproducibility, and a strong affinity for glucose.[47] Esmaeili *et al.*[346] explored polypyrrole–cellulose nanocrystal (PPy/CNC) composites combined with glucose oxidase (GOx) for biosensing of glucose (Fig. 11A). In Fig. 11B(a), field emission scanning electron microscopy (FESEM) revealed a globular, dense PPy structure, while PPy/CNC displayed an open, porous structure.[346] No phase separation was observed, indicating homogeneous polymerization on the CNC surface. The PPy/CNC nanostructure exhibited uniform, fibrous morphology, as previously observed. Aggregates on the screen-printed electrode (SPE) surface were evenly distributed (Fig. 11B(b)). CV on SPE/PPy/CNC and SPE/PPy electrodes demonstrated stable redox peaks with CNC enhancing surface area, enzyme immobilization, and electron transfer.[346] SPE/PPy/CNC electrode exhibited well-defined redox peaks, with a formal potential estimated at 0.265 V (Fig. 11C). The biosensor showed high sensitivity (approximately 0.73 μA mM^{-1}) over a dynamic response range from 1.0 to 20 mM glucose, with a low limit of detection (LOD) of (50 ± 10) μM, indicating potential for sensitive glucose detection in various applications (Fig. 11D).[346]

Koga *et al.*[230] introduced a novel approach by combining oxide nanowires, cellulose nanofibers, and pencil-drawn electrodes to fabricate a paper-based disposable molecular sensor. This composite structure exhibited mechanical robustness

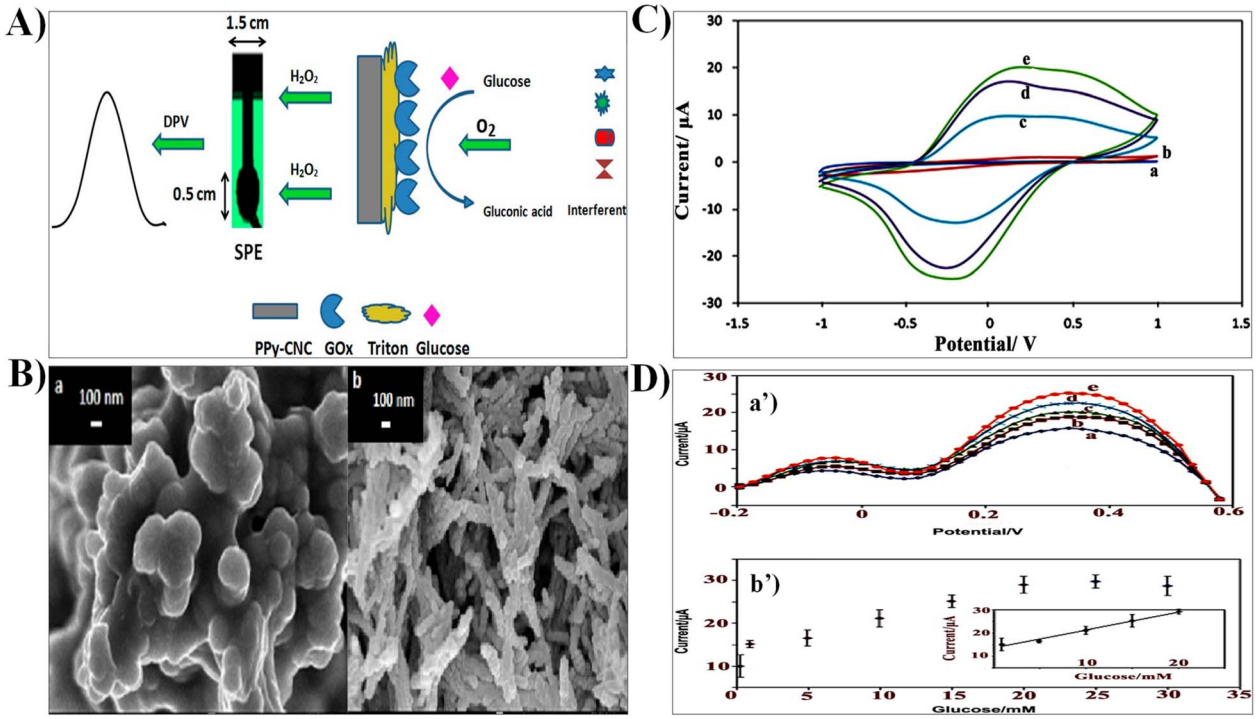

Fig. 11 (A) Schematic representation of an electrochemical glucose biosensor using PPy/CNC membrane. (B) Microstructures of (a) PPy and (b) porous PPy/CNC nanocomposite on SPE surface. (C) Cyclic voltammetry graphs: unmodified bare SPE (a); modified PPy/GOx electrode (b); and PPy/CNC/GOx electrodes with CNC concentrations of 0.3 (c), 0.5 (d), and 0.9 wt% (e). (D) Differential pulse voltammetry (DPV) graph (a′) with glucose concentrations of 1 (a), 5 (b), 10 (c), 15 (d), and 20 mM (e); and analytical curve (b′) of PPy/CNC/GOx glucose biosensor in 50 mM buffer solution (pH = 7) at 0.5 V s^{-1} scan rate *versus* Ag/AgCl electrode. Reproduced with permission from ref. 346, copyright © 2015 MDPI.

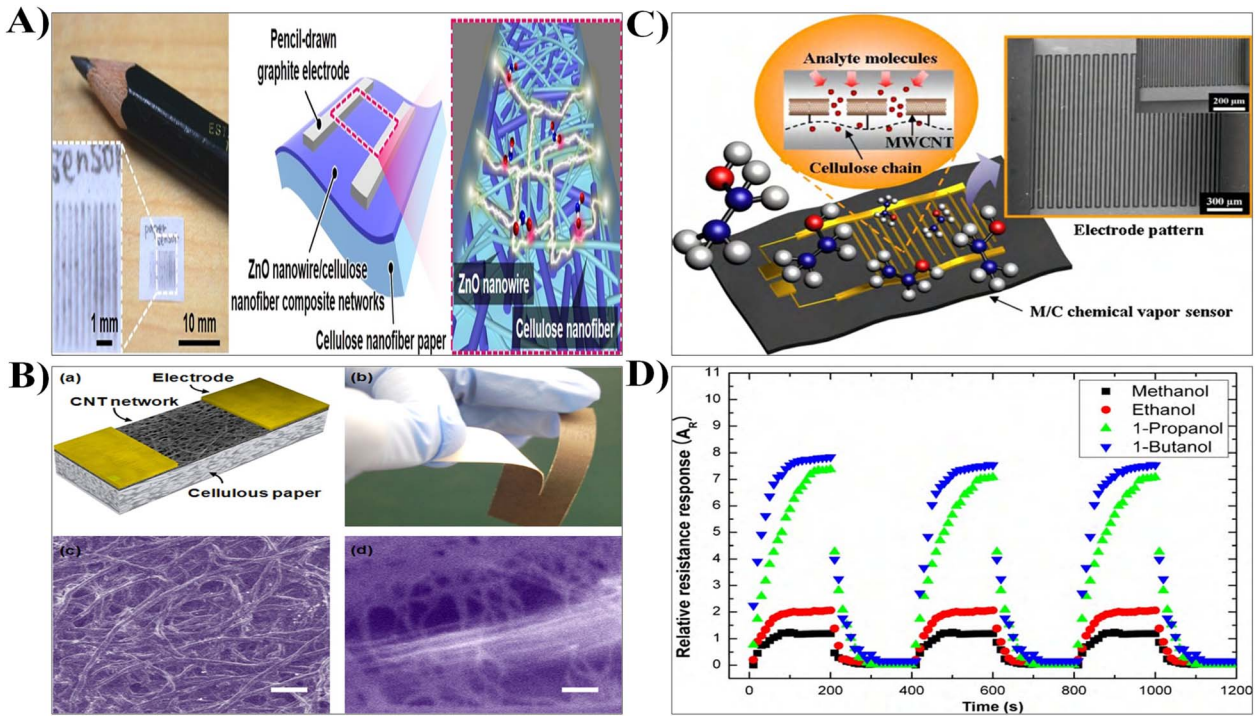

Fig. 12 (A) The design of a disposable molecular sensor made with ZnO metal oxides, cellulose nanofibers, and pencil-drawn electrodes. Reproduced with permission from ref. 230, copyright © 2019 American Chemical Society. (B) (a) A humidity sensor on cellulose paper, (b) flexible and customizable CNT networks, (c) SEM image of cellulose paper, and (d) magnified cross-linked CNTs. Reproduced with permission from ref. 17, copyright © 2012 American Chemistry Society. (C) A developed paper-based chemical sensor, and (D) its electrical response to specific chemicals. Reproduced with permission from ref. 327, copyright © 2010 Elsevier.

while serving as an efficient bridging network for the nanowire sensor. It facilitated effective access to target molecules while ensuring reliable electrical contact with the electrodes.[230] The sensor design and functionality are illustrated in Fig. 12A. This integrated sensor offers a cost-effective, portable, and disposable solution for molecular sensing in environmental monitoring, healthcare diagnostics, and food safety.[230] Moreover, numerous studies have explored the integration of carbon-based materials such as multi-walled carbon nanotubes (MWCNTs), carbon nanotubes (CNTs), and graphene, to enhance the mechanical and piezoelectric properties of nanocellulose composites.[17,48,347] For instance, Wan *et al.*[48] developed a biocompatible cellulose-CNT composite for cell sensing applications. This composite effectively immobilized leukemia K562 cells on a gold electrode, forming an impedance-based cell sensor with a detection limit of 2.6×10^3 cells per mL, highlighting its potential in biomedical applications.[48] Additionally, Qi *et al.*[347] introduced a novel humidity sensor using a cellulose-CNT composite for water trapping applications. These films demonstrated rapid response times and high sensitivity, with a relative electrical resistance change ranging from 5500% to 500%.[347] In another study, Han *et al.*[17] designed a similar humidity sensor using cellulose paper embedded with CNTs. The developd sensor exhibited a linear response up to a relative humidity of 75%. Both sensors displayed high reproducibility and long-term stability.[17,347] The conductance shift of the nanotube network entangled within the cellulose matrix served as the basis for humidity sensing. The sensor exhibited a linear response behavior up to a relative humidity of 75%, with excellent repeatability and minimal hysteresis.[17] Fig. 12B depicts the configuration of the developed humidity sensor, showcasing its design and functionality.[17] These innovative approaches highlight the potential of carbon nanotube-cellulose composites in the development of highly sensitive and reliable humidity sensing devices.[17,347] Beyond humidity sensing, Yun *et al.*[327] prepared a chemical vapor sensor using a composite of MWCNTs and cellulose paper (Fig. 12C). This sensor effectively detected vaporized analyte molecules such as methanol, ethanol, 1-butanol, and 1-propanol, exhibiting reversible and rapid relative resistance responses based on analyte concentration (Fig. 12D).[327]

Xu *et al.*[348] developed highly sensitive thin-film sensors using cellulose-graphene composites for alcohol recognition. Fig. 13A illustrates the structure of these thin-film sensors, highlighting

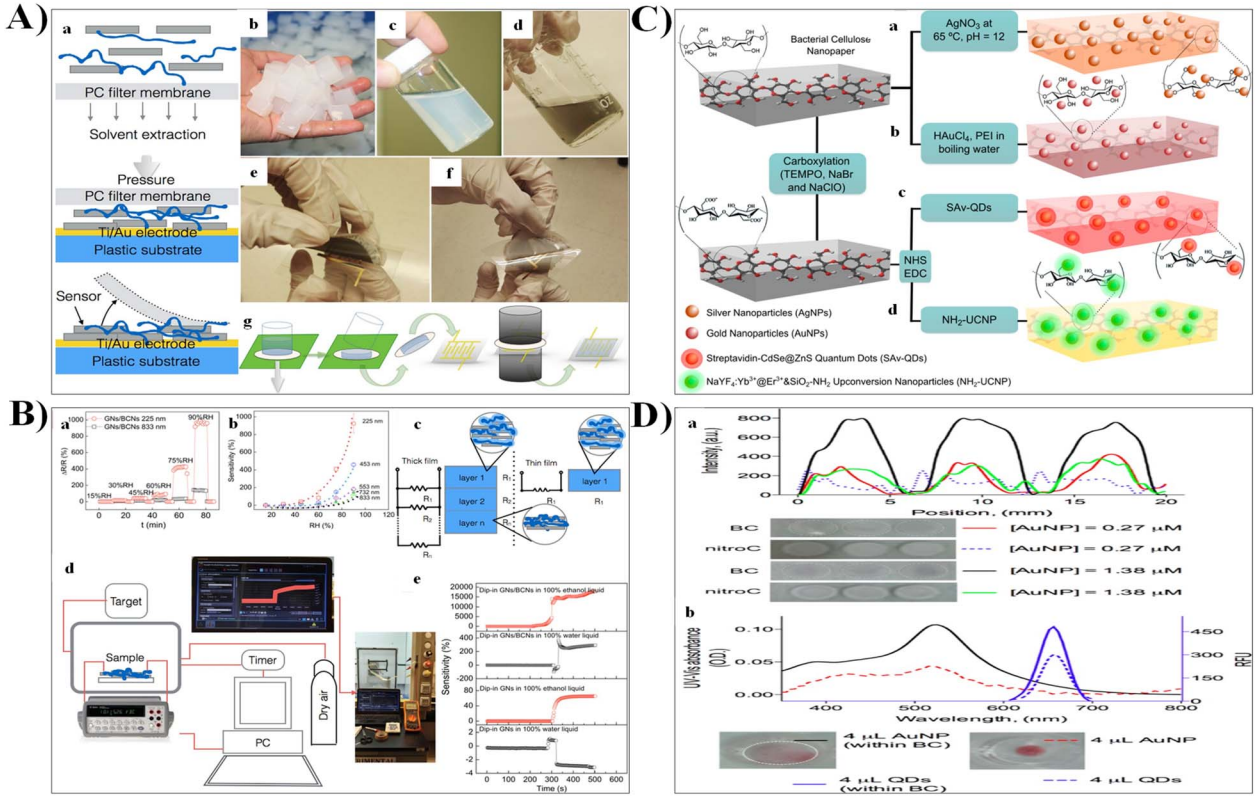

Fig. 13 (A) Illustration of the assembly process from raw material to thin-film sensor device (from a to g). Reproduced with permission from ref. 348, copyright © 2017 Springer Nature. (B) (a) Resistivity changes of 225 nm-thick and 833 nm-thick GN/BCN sensors under varying relative humidity (RH). (b) Sensitivity of GN/BCN sensors to different %RH levels. (c) Electrical configuration models in thick and thin GN/BCN films. (d) Experimental setup for evaluating GN/BCN sensor response to alcohol or water vapors. (e) Sensitivity of GN/BCN sensors detecting liquid-phase ethanol and water. Reproduced with permission from ref. 348, copyright © 2017 Springer Nature. (C) Various steps (from a to d) in the creation of nanopaper-based composites. Reproduced with permission from ref. 350, copyright © 2015 American Chemical Society. (D) Use of nanopaper as a preconcentration platform: (a) Colorimetric profile and images of AuNP deposited on bacterial cellulose nanopaper and nitrocellulose (nitroC). (b) UV-vis/photoluminescent spectra of 4 μL of [AuNP] = 1.84 μM and 4 μL of [QDs] = 100 nM on BC and microwells, respectively. QDs were excited at 480 nm. Reproduced with permission from ref. 350, copyright © 2015 American Chemical Society.

their enhanced sensitivity for alcohol detection.[348] By assembling graphene nanosheets (GNs) with BCNs, they created a thin-film alcohol-sensing device that exhibited significantly higher sensitivity to vapor-phase ethanol compared to sensors made from pure graphene nanosheets.[348] The GN/BCN sensor demonstrated rapid response and recovery times and was capable of detecting alcohol concentrations ranging from 10% to 100% (Fig. 13B).[348] Furthermore, Veeralingam *et al.*[349] developed a one-step process to fabricate cellulose paper by directly growing $NiSe_2$, resulting in a low-cost, flexible, wearable multifunctional sensing platform that integrated with smartphones.[349] This platform demonstrated remarkable potential for various healthcare applications, including non-invasive periodontal diagnosis through human saliva analysis for oral health monitoring.[349] Additionally, it functioned as a breath analyzer for detecting breath-related diseases and as a gesture sensor to facilitate communication for individuals with hearing impairments. This multifunctional sensing platform represents a significant advancement in personalized healthcare monitoring, offering an accessible and seamless solution for diverse medical needs.[349] In another study, Morales-Narváez *et al.*[350] developed a nanopaper-based optical sensing platform for detecting biologically relevant analytes (Fig. 13C). They demonstrated the superiority of bacterial cellulose (BC) as a preconcentration platform, enabling the analysis of small volumes (~4 μL) of optically active materials.[350] To construct the sensing platform, they printed sensor spots on bacterial cellulose plates, incorporating cuvettes to develop a colorimetric-based detection system. The sensor comprised nanopaper embedded with silver and gold nanoparticles (AuNPs) to enhance detection sensitivity. As shown in Fig. 13D(a), the colorimetric profiles of bare BC and nitrocellulose spots, drop-casted with AuNPs, revealed a 2.4-fold signal enhancement with BC, confirming its superior preconcentration ability. BC also improved measurements of small volumes of optically active nanomaterials like AuNPs and quantum dots (QDs), as shown in Fig. 13D(b).[350]

3.2.2.3 3D nanocellulose substrates based (bio)sensors. In the realm of (bio)sensors, 3D nanocellulose substrates have garnered significant attention due to their interesting

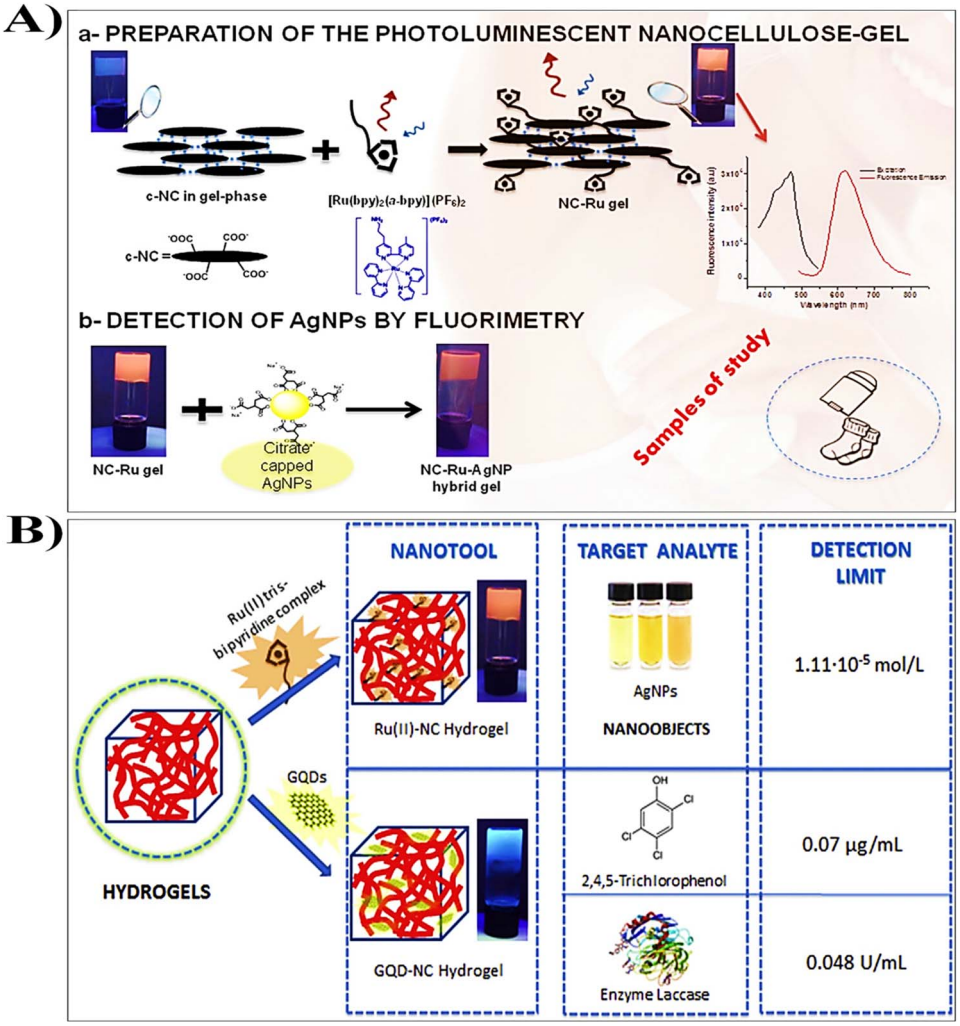

Fig. 14 (A) Illustration of the sensor and electrochemical response to chemicals tested. Reproduced with permission from ref. 352, copyright © 2016 Elsevier. (B) Analytical applications of different fluorescent nanocellulose based hydrogels with remarkable performances for enzyme immobilization and toward diverse target analytes. Reproduced with permission from ref. 353, copyright © 2017 Elsevier.

properties and versatility. Often utilized in the form of hydrogels, these substrates are characterized by their high water-swelling capacity and are typically formed through chemical or physical crosslinking processes. Hydrogels, as polymer gels, consist of 3D networks capable of absorbing large amounts of water, making them an ideal matrix for supporting various biomolecules.[350,351] Ruiz-Palomero *et al.*[352] fabricated a nanostructured conductive hydrogel-based sensor using cellulose nanocrystals. This sensor incorporated photosensitive ruthenium bipyridine moieties to detect silver nanoparticles in real samples, as illustrated in Fig. 14A. The researchers engineered flexible luminescent gels based on carboxylated nanocellulose platforms, achieving excellent sensing performance with a broad response range of 1.85×10^{-5} to 1.48×10^{-4} mol L^{-1} and a detection limit (LOD) of 1.11×10^{-5} mol L^{-1}.[352] Similarly, Wang *et al.*[331] explored nanofibrillated cellulose aerogels modified with carbon nanotubes to achieve mechanoresponsive conductivity and pressure-sensing capabilities. By integrating nanocellulosic materials with carbon nanotubes, they developed a highly responsive electroactive platform with potential applications in pressure sensing and functional materials for large-scale implementation.[331] Furthermore, Ruiz-Palomero *et al.*[353] provided a comprehensive summary of nanocellulose-based sensing materials for detecting various target analytes, as depicted in Fig. 14B. Their findings highlight the significant role of cellulose-based substrates in advanced sensing technologies, with applications spanning environmental monitoring, biomedical diagnostics, and beyond.[353]

4. Hemicellulose and sensor technology

Hemicellulose plays a crucial role in maintaining the structural integrity and biochemical properties of plants.[71] Unlike cellulose, which is a homopolymer composed of linear glucose chains, hemicellulose is a heterogeneous polysaccharide made up of various monosaccharides, including xylose, arabinose, mannose, galactose, and glucose (Fig. 15).[71,72] Additionally, hemicellulose molecules are branched polysaccharides, with structural variations depending on plant species and tissue type, contributing to the diversity of LCB.[354,355] In hardwoods, hemicellulose consists primarily of glucuronoxylan, whereas in softwoods, it mainly comprises glucomannan, with smaller amounts of glucuronoxylan. Unlike cellulose, which forms highly ordered crystalline structures, hemicellulose is an amorphous polymer that surrounds cellulose microfibrils within the plant cell wall. This structure provides flexibility and resilience, allowing plants to withstand mechanical stress and environmental fluctuations.[71,356] The branched lateral chains of hemicellulose establish a network through hydrogen bonding with cellulose microfibrils and covalent interactions with lignin, thereby enhancing the rigidity and stability of the cellulose–hemicellulose–lignin matrix.[71,357] Hemicellulose primarily consists of pentoses, hexoses, and carboxylic acids, forming branched polymers with a relatively low molecular weight and a degree of polymerization ranging between 150 and 200.[358,359]

4.1. Hemicellulose properties

One of the defining characteristics of hemicellulose is its heterogeneity. The composition and structure of hemicellulose vary significantly depending on plant species, tissue type, and growth conditions.[361,362] Additionally, hemicellulose exhibits interesting rheological properties, influencing the texture of both plant cell walls and food products. Its role in the cell wall is to strengthen the structure by interacting with cellulose and lignin, providing high stability to plant cell walls necessary for industrial uses.[363] The hydrophilic nature and low molecular weight of hemicellulose enable hydrothermal extraction and hydrolysis, while their chemical modification enhances their potential in various applications.[364] The amorphous nature and

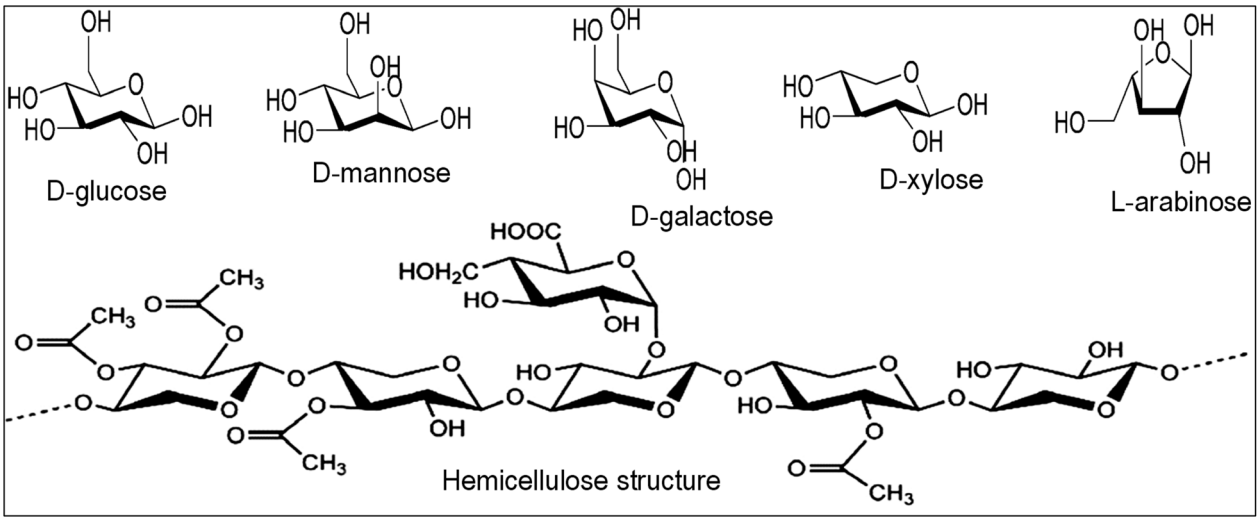

Fig. 15 Typical hexoses and pentoses found in hemicellulose. Reproduced with permission from ref. 143, copyright © 2013 Royal Society of Chemistry. Chemical structure of hemicellulose. Reproduced with permission from ref. 360, copyright © 2017 Elsevier.

branched architecture of hemicelluloses make them more susceptible to solubilization under specific conditions. A key characteristic of hemicelluloses is their ability to dissolve in water at elevated temperatures, typically between 180 and 230 °C, under pressures ranging from 1 to 3 MPa.[361,365,366] These conditions promote the hydrolysis of glycosidic bonds within the hemicellulose matrix, leading to the degradation of complex polysaccharides into simpler sugars. This solubilization process is essential for various industrial applications, particularly in biomass pretreatment for biofuel production. Under hydrothermal conditions, hemicelluloses can be effectively extracted from LCB, improving the accessibility of cellulose and lignin for subsequent enzymatic or chemical processing. Additionally, this property facilitates the production of value-added sugars, such as xylose and arabinose, which serve as precursors for bio-based chemicals and materials.[361,365–367] While cellulose modification is widely studied, chemical modification of hemicellulose is less frequently reported due to its structural heterogeneity, which complicates precise modification strategies.[368]

4.2. Hemicellulose in (bio)sensing applications

Despite its renewability, biocompatibility, and low cost, hemicellulose faces several challenges as an electrode material modifier for sensing applications. One primary limitation is its structural heterogeneity and complexity, which can result in inconsistent sensor performance and difficulties in achieving uniform modification of electrode surfaces.[369,370] Moreover, the inherently low electrical conductivity of hemicellulose poses a limitation, as efficient signal transduction is essential for sensor performance.[371,372] Its mechanical stability is also a concern, as hemicellulose-based materials can be prone to swelling and degradation in aqueous environments, potentially compromising the durability and reliability of the sensors.[373] To address these limitations, hemicelluloses are often combined with other materials to fabricate electroactive hemicellulose-based composites. By blending hemicelluloses with electrically conductive polymers and nanoparticles, researchers can significantly enhance their electrochemical properties, mechanical strength, and chemical stability.[370,371] This approach helps overcome the inherent low conductivity of hemicelluloses and addresses issues related to moisture sensitivity and thermal degradation.[370,371] However, while chemical modifications or composite formation with conductive materials can improve conductivity, these modifications may compromise the functional properties of the material.[374] Furthermore, the stability and reproducibility of hemicellulose-based electrodes under varying environmental conditions (*e.g.*, pH, temperature) remain significant challenges. Exposure to extreme or fluctuating conditions can lead to the degradation or leaching of hemicellulose components, compromising the structural integrity of the electrodes, which in turn affects sensor performance, reducing accuracy and reliability.[375,376] The lack of standardized fabrication methods for hemicellulose-based electrodes also limits their scalability and integration into practical biosensing devices. Nonetheless, hemicellulose-based materials are gaining increasing attention for biosensing applications due to their natural abundance, biodegradability, and functional groups (hydroxyl, carbonyl, and carboxyl) that facilitate interactions with biomolecules.[16,371,377,378] These materials, primarily composed of polysaccharides, offer a promising platform for sustainable biosensor development. The diverse chemical functionalities in hemicelluloses are crucial for the effective functionalization of electrode surfaces, enhancing the performance of biosensing applications by facilitating interactions with other materials to fabricate high-performance composites.[371,378] Moreover, their porous structure increases surface area and promotes faster electron transfer, which is essential for high-sensitivity detection.[378]

The research studies summarized in Table 5 highlight a wide range of progress in sensor technologies using hemicellulose-based materials, each showcasing interesting features and promising applications. A key area of progress is the development of durable and multifunctional hydrogels. For example, nano-polydopamine-reinforced hemicellulose-based hydrogels demonstrated excellent mechanical properties, stable electrochemical performance, and strong self-adhesive capabilities, making them effective for use in motion sensors and transdermal drug delivery systems.[371] A multifunctional hybrid hydrogel combining hemicellulose-decorated polypyrrole, polyvinyl alcohol, tannic acid, and polyacrylamide exhibited exceptional transparency, conductivity and stretchability, making it suitable for wearable sensors in human motion monitoring.[379] Additionally, hemicellulose/polypyrrole composite hydrogels were developed to be stretchable, water-retentive, and anti-freezing, with enhanced conductivity and mechanical properties, showcasing their potential in wearable devices and sports monitoring.[370] In another study, ionic PAA-TA@HC-Al^{3+} hydrogels were successfully fabricated and they demonstrated remarkable stretchability, toughness, and self-recovery. Additionally, they showed strong self-adhesion and protective properties, making them highly effective for detecting various movements.[19] Hemicellulose-derived ratiometric fluorescent aerogels showcased ultra-trace detection capabilities for arsenite ions and ciprofloxacin, with high adsorption capacities, indicating their potential for environmental monitoring and contamination remediation.[380] Moreover, xylan hemicellulose-based conductive hydrogels, with MXene incorporated, displayed high tensile strength and extreme stretchability, highlighting their potential for use in stretchable and durable conductive materials.[381] Moreover, the development of hemicellulose-based sensors marks significant progress in bacterial and fungal detection, leveraging the natural biocompatibility, biodegradability, and versatility of hemicellulose.[377] By incorporating carbon-based nanoparticles such as nitrogen-doped carbon dots, into the hemicellulose matrix and using the resulting composites as fluorescent biosensors, these sensors exhibit enhanced stability, rigidity, and improved antibacterial and antifungal properties. This makes them highly effective against a broad range of pathogens, including both Gram-negative and Gram-positive bacteria, as well as fungi. Additionally, the ability of the hydrogel to selectively interact with

Table 5 Advancements in hemicellulose-based sensor technologies: performance metrics and applications across diverse platforms

Electrode materials	Analytes/parameters measured	Main results achieved	Ref.
Nano-polydopamine-reinforced hemicellulose-based hydrogels	Body movements (*e.g.*, throat vibrations)	- The hydrogels demonstrated excellent mechanical properties, stable electrochemical performance, and strong self-adhesive capabilities - They withstood 1000 compression cycles without significant damage, had a tensile strain of 101%, and showed superior adhesion to skin compared to fibrin glue - The hydrogels also served as effective motion sensors and drug patches for transdermal drug delivery	371
Multifunctional hybrid hydrogel incorporating hemicellulose-decorated polypyrrole (H/PPY), polyvinyl alcohol (PVA), tannic acid (TA), and polyacrylamide (PAM)	Strain signals of index finger and elbow flexion, pulse beat	- The hybrid hydrogel exhibited high transparency (79.6% at 2 mm thickness), conductivity (3.12 S m^{-1}), mechanical strength (325.4 kPa), and stretchability (1497.2%) - It demonstrated effective strain and pulse monitoring capabilities and good adhesion to various substrates, including human skin - The hydrogel improved properties make it suitable for wearable sensors in human motion monitoring	379
Hemicellulose/polypyrrole (H/PPY) composite hydrogels	Human motion signals (finger bending, wrist bending, throat deformation)	- The study developed stretchable, water-retentive, and anti-freezing H/PPY hydrogels for epidermal strain sensors - The hydrogels demonstrated enhanced conductivity (from 2.1 to 5.1 S m^{-1}), reduced freezing/thawing temperatures (−43.1 °C and −22.1 °C), and impressive mechanical properties including high tensile strain (1094.9%), compressive strength (1790.2 kPa), and toughness (2.82 MJ m^{-3}) - The sensors showed excellent remoldability and durability, with good performance after 250 cycles and effective detection of various human motions - These hydrogels are promising for applications in wearable devices, sports monitoring, medical monitoring, and soft robotics	370
Tannic acid modified hemicellulose nanoparticles (TA@HC) embedded in ionic PAA-TA@HC-Al^{3+} hydrogels	Strain, pulse, and breathing movements	- The ionic hydrogel demonstrated exceptional stretchability (1060%), toughness (1.52 MJ m^{-3}) and self-recovery (87%) - It offered strong self-adhesion, anti-ultraviolet, anti-oxidative, and antibacterial properties - As a wearable strain sensor, it accurately detected and differentiated large and micro movements, including weak pulses and breathing	19
Hemicellulose-derived ratiometric fluorescent aerogel	Arsenite ions (As(III)) and ciprofloxacin (CPR) antibiotic	- The hemicellulose-based fluorescent aerogel, fabricated from oxidized rice straw and crosslinked with chitosan, demonstrated ultra-trace level detection of As(III) with a limit of 3.529 pM and CPR with a limit of 55.2 nM - The aerogel also showed high adsorption capacities of 185 μg g^{-1} for As(III) and 454 mg g^{-1} for CPR. - It was applied to real water samples, proving its potential for effective remediation of these contaminants	380
Stretchable and tough xylan hemicellulose-based conductive hydrogels, with MXene incorporated as conductive fillers	Strain and movement in human motion	- Xylan-based hydrogels were fabricated with high tensile strength (0.34 MPa), extreme stretchability (2098.4%), and notable toughness (3.79 ± 0.95 MJ m^{-3}) - Incorporating MXene improved these properties further to 0.51 MPa tensile strength and 5.95 ± 1.19 MJ m^{-3} toughness - The hydrogels demonstrated reliable sensitivity as strain sensors for monitoring human movements, showcasing their potential for use in stretchable and tough conductive materials, especially with the inclusion of renewable xylan and bio-based resources	381

Table 5 (*Contd.*)

Electrode materials	Analytes/parameters measured	Main results achieved	Ref.
CM-Hemi@Ca-N-CDs hydrogel was synthesized from sugarcane bagasse using carboxymethyl hemicellulose (CM-Hemi), N-doped carbon dots (N-CDs), and calcium chloride	Bacterial and fungal detection	- CM-Hemi@Ca-N-CDs hydrogel exhibited strong antibacterial activity against both *Escherichia coli* and *Staphylococcus aureus* - Hydrogel sensors demonstrated antifungal activity by detecting *Candida albicans* through selective interaction and inhibition response - CM-Hemi@Ca-N-CDs exhibited stronger binding affinities with microbial proteins, confirmed by molecular docking - Fluorescence microscopy was used to detect color emission differences upon microorganism interaction, indicating analyte-specific sensor responses - DFT calculations indicated improved stability of CM-Hemi@Ca-N-CDs hydrogel, with low energy gap and high electron affinity achieved	377

microbial cell walls further enhances its potential for sensitive and targeted microbial detection.[377]

Several studies have explored hemicellulose-derived biomass composites for (bio)sensing applications, with promising results.[370,379,382]

4.2.1 Wearable sensors. In wearable sensor applications, smart functional fillers, such as plant-derived hemicellulose, can significantly enhance the mechanical properties of ionic hydrogels. Tannic acid-modified hemicellulose nanoparticles (TA@HC) and Fe^{3+} were incorporated into PAA hydrogels, accelerating gelation within 30 s at room temperature.[372] The TA and Fe^{3+} system activated sodium persulfate (SPS), generating hydroxyl radicals that facilitated rapid gelation. The resulting PAA/TA@HC/Fe^{3+} hydrogel exhibited exceptional mechanical strength (up to 5600% strain), adhesiveness, rapid self-healing, and reproducible adhesion to various substrates.[372] By selectively coating Fe^{3+} on the upper surface, an asymmetric adhesive hydrogel was created, allowing for comfortable skin contact while repelling pollutants, making it an effective pressure sensor.[372] Zhao *et al.*[374] developed hemicellulose-based conductive hydrogels reinforced with MXene to address challenges in flexible sensing applications, such as low sensitivity and poor interface matching. These hydrogels exhibited exceptional self-adhesion (3.12 kPa on skin), high stretchability (>1700%), and reliable electrical conductivity (0.045 S m^{-1}), enabling their use as adaptable strain sensors. The synthesis involved crosslinking polyacrylamide (PAM) with hemicellulose and MXene, forming a porous, hydrogen-bond-rich structure (Fig. 16A). The hydrogels demonstrated excellent adhesion on substrates like wood, glass, and skin, with optimal hemicellulose content enhancing performance (Fig. 16B).[374] Their strain sensors reliably detected mechanical deformations with a gauge factor of 2.1 up to 400% strain and retained stability over repetitive cycles (Fig. 16C). Additionally, the hydrogels effectively monitored human motion, capturing signals from finger bends and movements of joints such as elbows and knees (Fig. 16D). The dynamic physical interactions and structural integrity of the material ensured high sensitivity, repeatability, and long-term durability, making it suitable for wearable sensing technologies. This study highlighted the synergistic potential of hemicellulose and MXene in creating multifunctional hydrogels with significant advancements in adhesion, conductivity, and flexibility, opening pathways for innovative applications in bioelectronics and human motion detection.[374]

4.2.2 Chemical and environmental sensing. Jiang *et al.*[383] synthesized a hybrid material composed of hemicellulose, a nitrogen-rich deep eutectic solvent, and carbon QDs for the ultrasensitive detection of silver ions and L-cysteine using an 'off–on' sensing mechanism.[383] This probe exhibited high selectivity towards silver ions, achieving a low detection limit of 21 nM. The same composite film was successfully applied for detecting L-cysteine within a dynamic range of 0–100 μM, achieving a detection limit of 242 nM.[383] Furthermore, Yang *et al.*[384] employed a microwave-assisted synthesis method to produce xylan-derived carbon QDs for tetracycline sensing. Under optimized conditions, a novel sensing platform capable of detecting tetracycline in a linear range of 0.05–20 μM was

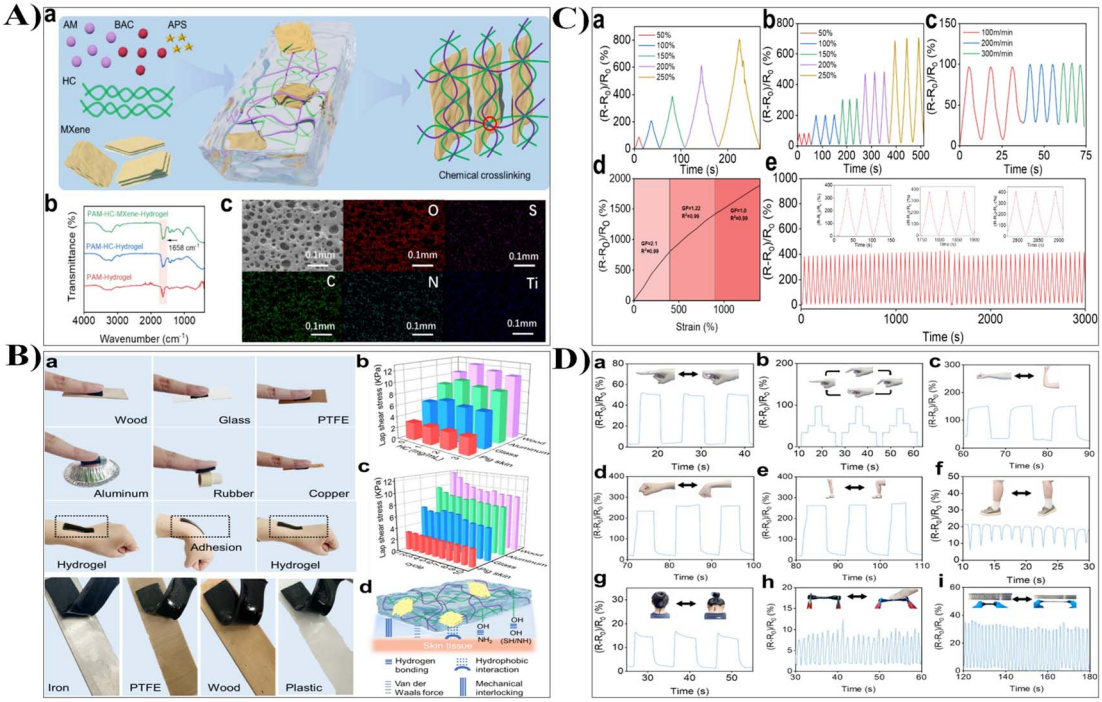

Fig. 16 (A) (a) Schematic representation of hemicellulose-based conductive hydrogels. (b) FT-IR spectra of PAM hydrogels, HC-PAM hydrogels, and MXene-HC-PAM hydrogels. (c) Surface morphology and elemental distribution analyzed using SEM and EDS. (B) (a) Photographs demonstrating MXene-HC-PAM hydrogel adhesion on various substrates. (b) Shear bond strength of hydrogels with different hemicellulose concentrations on various substrates. (c) Adhesion durability of MXene-HC-PAM hydrogel over 10 cyclic tests on different substrates. (d) Schematic of the adhesion mechanism on human skin. (C) (a) Relative resistance changes of MXene-HC-PAM hydrogel under varying strain levels. (b) Reproducibility of relative resistance changes tested across three cycles at different strains. (c) Impact of tensile speed on relative resistance changes at 50% strain. (d) Gauge factor (GF) of MXene-HC-PAM hydrogel. (e) Stability of relative resistance during a 3000 s cyclic test at 150% strain. (D) (a and b) Relative resistance variations during finger bending at different angles with the hydrogel applied. (c–g) Monitoring relative resistance changes when the hydrogel adhered to the elbow, wrist, knee, ankle, and neck. (h) Relative resistance changes under compression. (i) Cyclic stretching-induced relative resistance changes over 60 seconds. Reproduced with permission from ref. 374, copyright © 2024 Elsevier.

established, with a detection limit of 6.49 nM.[384] Similarly, polyamine-functionalized carbon dots derived from xylan were investigated for the detection of tannic acid.[385] This research established an acid detection platform using hybrid materials in both water and ethanol solutions. The dynamic range for tannic acid detection ranged from 0.1 to 5 μM, with detection limits of 36.8 nM and 44.9 nM determined for water and ethanol solutions, respectively.[385] Furthermore, Dammak *et al.*[386] combined cellulose nanocrystals and xylans to develop multilayer thin films for detecting xylanase activity. These films exhibited sensitivity to xylanase action, with their performance evaluated against a conventional colorimetric method, which detects reducing sugars released through enzymatic hydrolysis.[386] In addition, hemicellulose-based sensors also hold promise for environmental applications. Helim *et al.*[382] developed a sensor using hemicellulose extracted from *Opuntia Ficus Indica cactus* and agarose, creating a sensitive layer on a gold electrode (Fig. 17A). CV was employed to evaluate the electrochemical behavior and electron transfer kinetics of the sensor using $[Fe(CN)_6]^{3-/4-}$ (Fig. 17B). The functionalized gold electrodes (modified with agarose or agarose/hemicellulose) exhibited decreased current and shifted potential. Kinetic characterization of modified electrodes using CV technique indicated diffusion-controlled redox processes.[382] EIS confirmed increased charge transfer resistance post-modification as shown in Fig. 17C, aligning with CV results. Detection of lead ions (Pb^{2+}) showed a decrease in charge transfer resistance, as positively charged ions facilitated redox marker transfer.[382] In this study, the functional groups of hemicellulose to form complexes with metal ions and leveraged agarose gelling properties for membrane stability. It demonstrated a high affinity for Pb^{2+} due to the chemical structure of hemicellulose, outperforming detection for Hg^{2+}, Ni^{2+}, and Cu^{2+}. Square wave voltammetry revealed a detection limit of 1.3 fM for Pb^{2+}. Application of the sensor in river and sea water using the standard addition method confirmed its efficacy in lead detection (Fig. 17D).[382]

4.2.3 Medical sensing. In the medical sector, hemicellulose-based hydrogels have been successfully developed for sensing applications. A recent study introduced nano-polydopamine-reinforced hemicellulose-based hydrogels with multistage pore structures (Fig. 18A), which maintained stable mechanical properties even after 1000 cyclic compressions. The hydrogel exhibited an ultimate tensile strain of 101%, surpassing that of native skin.[371] With a shear adhesion strength of 7.52 kPa to skin tissue, the hydrogel outperformed

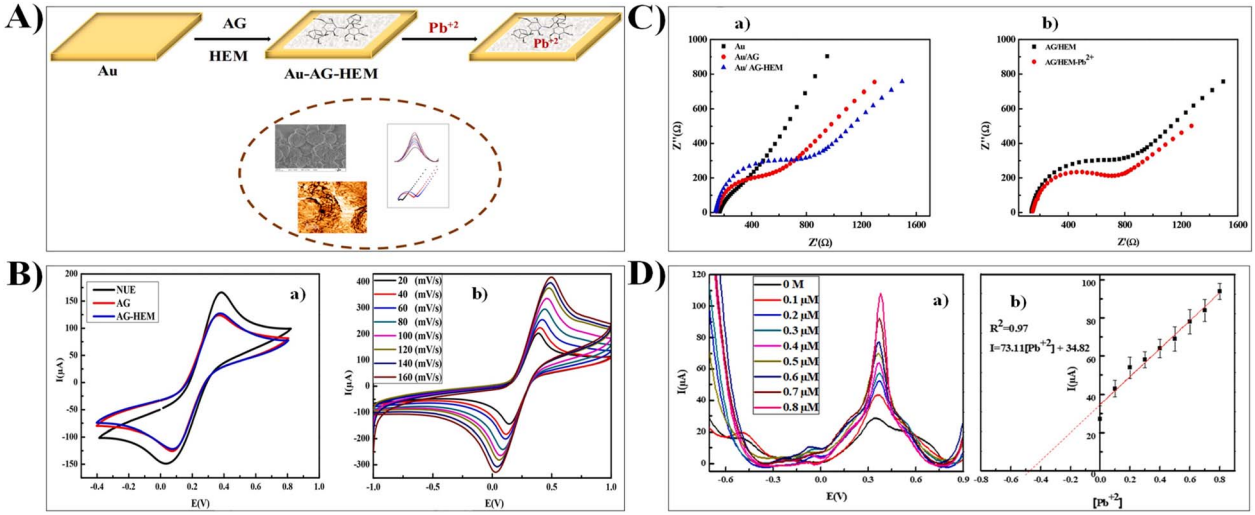

Fig. 17 (A) Schematic of gold sensor modified with biocopolymers AG-HEM for lead ion detection (Au: gold, AG: agarose, HEM: hemicellulose). (B) (a) Cyclic voltammograms of bare electrode (solid line), Au modified with AG (dashed line), and Au-AG-HEM (dotted line) in 5 mM $[Fe(CN)_6]^{3-/4-}$ at 80 mV s^{-1} scan rate; (b) Cyclic voltammograms of Au-AG-HEM at different scan rates in the same solution. (C) Nyquist plots post gold electrode modifications with AG and AG/HEM (a) and after lead ion detection at 1 μM concentration (a). Measurements conducted in $[Fe(CN)_6]^{3-/4-}$ solution, frequency range 0.1 Hz to 100 kHz, DC potential 10 mV, and applied potential 0.2 V. (D) (a) Square wave voltammetry (SWV) for Pb^{2+} determination in river water after successive Pb^{2+} additions; (b) Corresponding calibration curve. Reproduced with permission from ref. 382, copyright © 2023 Elsevier.

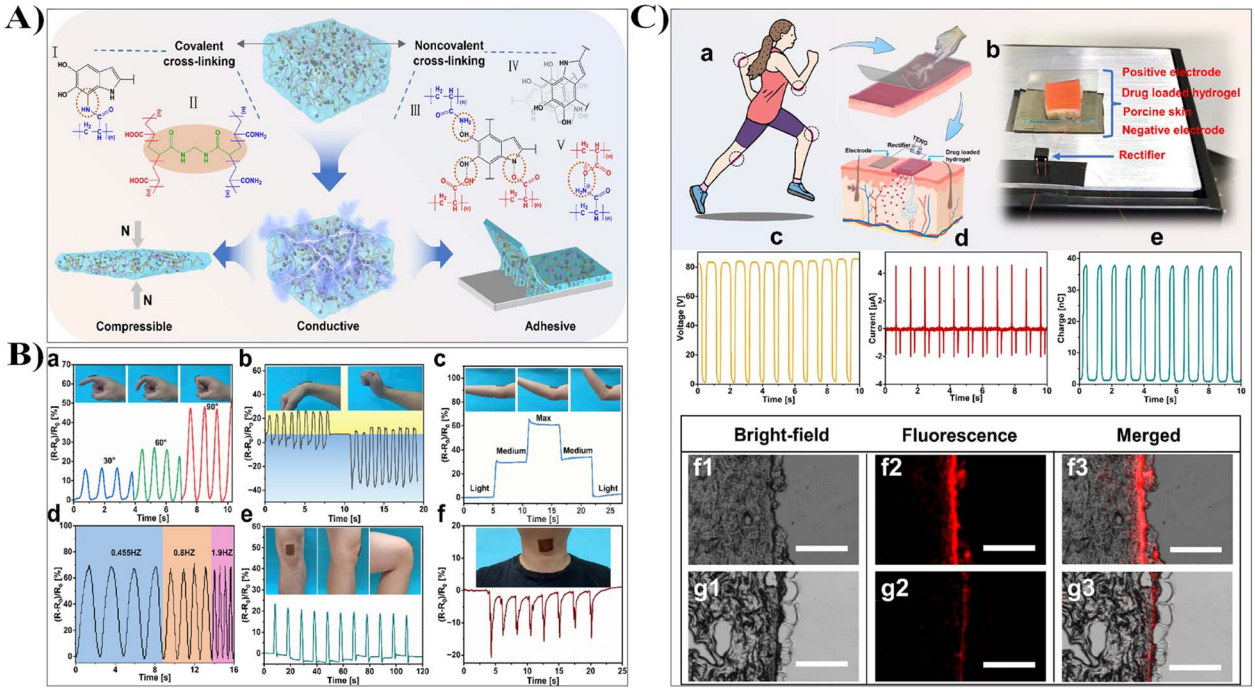

Fig. 18 (A) Schematic representation of the conductive, self-adhesive, and compressive hydrogel with internal cross-linking. (B) Real-time monitoring of various human movements with sensors attached to different body parts: (a) finger, (b) wrist, (c and d) elbow, (e) knee joint, and (f) throat. (C) Schematic diagram illustrating the self-powered transdermal drug delivery (TDD) closed-loop therapy system, along with characterization of triboelectric nanogenerator (TENG) and cross-sectional histological images of skin after rhodamine 6G (R6G) delivery from a patch for 6 hours: (a) TENG and TDD closed-loop therapy system illustration, (b) experimental setup mimicking human motion-driven TDD using a linear motor, (c–e) open-circuit voltage (VOC), short-circuit current (I_{SC}), and transferred charge (Q_{SC}) of the TENG, (f) placement of drug-loaded hydrogel patch on the positive electrode, (g) skin under natural conditions (without TENG connection). Scale bar: 100 μm. Reproduced with permission from ref. 371, copyright © 2023 American Chemical Society.

fibrin glue (Greenplast). The addition of nano-polydopamine enhanced electrical conductivity and reduced impedance. The nanocomposite hydrogel demonstrated exceptional mechanical strength, stable electrical conductivity, and self-adhesive characteristics. It also exhibited motion-sensing capabilities, with a gauge factor (GF) of approximately 1.04 and a response time of 150 ms.[371] The hydrogel-based sensor accurately monitored various movements, such as finger, wrist, and elbow bending, with distinct resistance variations (Fig. 18B). It showed frequency-independent behavior and dynamic stability during knee bending, indicating its potential for limb control and healthcare applications, including monitoring swallowing disorders (Fig. 18C). This multifunctional hydrogel acts as a real-time motion sensor, cationic drug carrier and electrically stimulated drug patch, offering promising implications for next-generation flexible materials in health monitoring and self-administration.[371]

5. Lignin and its (bio)sensor applications

Lignin is a complex aromatic polymer and a fundamental structural component in the support tissues of vascular plants and certain algae. It provides rigidity and resistance to decay, particularly in woody plants. The structural composition of lignin is illustrated in Fig. 19. Chemically, lignin consists of cross-linked phenolic polymers and is one of the most abundant renewable biopolymers on Earth, accounting for approximately 40% of total biomass.[75,387] Structurally, lignin is a three-dimensional polymer composed of phenylpropane units, primarily localized in the plant cell walls. Its building blocks are derived from three aromatic alcohol precursors: *p*-coumaryl, coniferyl, and sinapyl alcohols, which form phenolic subunits known as *p*-hydroxyphenyl (H), guaiacyl (G), and syringyl (S) moieties (Fig. 19).[388] Gymnosperms primarily contain G units, dicotyledonous angiosperms have a mix of G and S units, and monocotyledonous plants contain all three moieties.[389] The structure of lignin includes various bond types, such as β-O-4, β-5, β–β, and 5-5 linkages, which contribute to its rigidity and resistance to degradation (Fig. 19). Its high degree of aromaticity makes it resistant to chemical and biological breakdown. Additionally, lignin serves as a natural defense mechanism for plants, aiding in structural support, water and nutrient transport, and protection against parasitic attacks and environmental stressors.[390] The properties of lignin vary depending on its botanical origin, extraction method, and processing conditions, with hardwood lignin typically having a higher syringyl (S) to guaiacyl (G) ratio compared to softwood lignin.

Lignin extraction from LCB is a crucial step in biomass valorization for biofuel production, chemical synthesis, and advanced materials science.[389] Efficient extraction methods must be employed to isolate lignin while preserving its native chemical structure, ensuring its suitability for diverse downstream applications. Various extraction techniques, including organosolv, alkaline, and acid hydrolysis methods, have been developed, each offering distinct advantages and limitations regarding lignin purity, yield, and structural integrity (Table 6).[140,392–394] The choice of extraction method significantly influences the physicochemical properties of the recovered lignin, directly impacting its performance in specific applications. Following extraction, lignin typically undergoes purification steps using techniques such as solvent fractionation, precipitation, ultrafiltration, or chromatography to remove residual impurities and enhance its functionality.[140,395,396] Additionally, chemical modifications including oxidation, sulfonation, esterification, and hydrogenation are commonly employed to tailor physicochemical properties of lignin, improving its solubility, reactivity, and compatibility for targeted

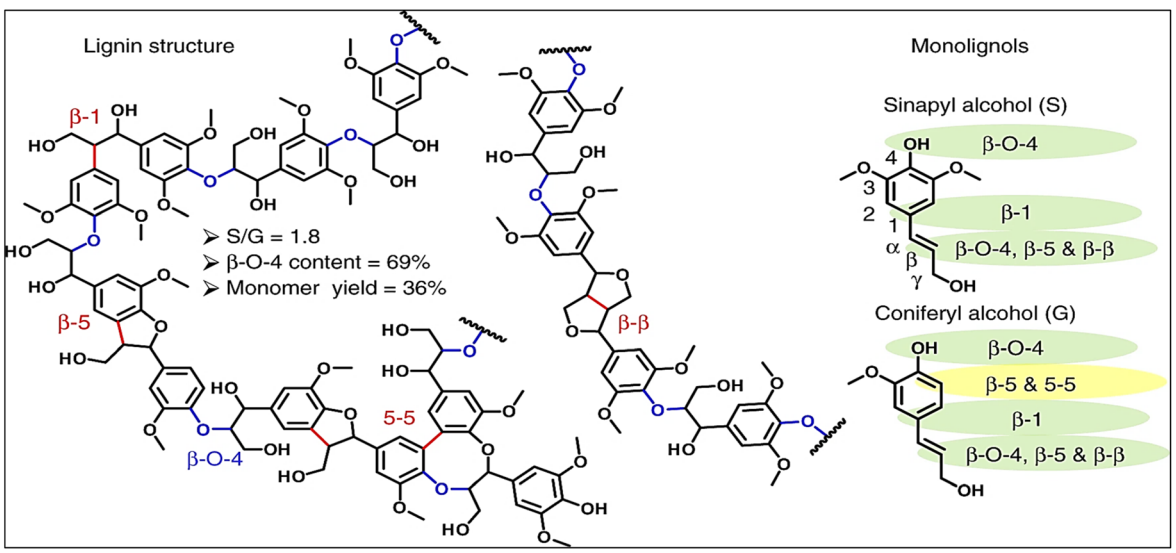

Fig. 19 Overview of lignin structure. Highlighted are sinapyl alcohol and coniferyl alcohol, the primary monomers, indicating reacting carbons with C–O or C–C bonds. A hypothetical lignin structure depicts these bonds, along with calculated S/G ratio, β-O-4 content, and monomer yield. Reproduced with permission from ref. 391, copyright © 2019 Springer Nature.

Table 6 Summary of studies on isolation of lignin from diverse LCB for diverse applications[a]

Biomass used	Extraction methods involved	Properties of extracted lignin	Ref.
Non-wood cellulosic biomass sources, including wheat straw, pine straw, alfalfa, kenaf, and flax fiber. Alfalfa yielded the most lignin (34%), followed by pine straw (22.65%), wheat straw (20.40%), and flax fiber (14.88%)	- Lignin was extracted from nonwood biomasses using a multi-step process - Biomass was first pulped with an 85% organic acid mixture for 2 h - Further delignification used PFA/PAA at 80 °C for 2 h - Delignified fibers were bleached, and lignin was precipitated and vacuum dried	- TGA revealed that lignin from wheat straw had the highest thermal stability with a char yield of 40.41%, followed by flax fiber (39.22%), alfalfa (35.04%), and pine straw (29.45%) - FTIR analysis revealed common features in lignin chemical structure, including formate ester and aromatic compounds - DSC showed higher enthalpy measurements for lignin from flax fiber (190.57 J g^{-1}) and alfalfa (160.90 J g^{-1}), indicating better thermal stability	396
Typha capensis (TC), a highly acetylated grass	- Milling (MWL): lignin was extracted from TC using a modified Bjorkman method and analyzed - Ionic Liquid (ILL): TC was treated with [EMIm][OAc], and lignin was separated, purified, and analyzed - Ethanol Organosolv (EOL): TC underwent autohydrolysis, ethanol/water, and sulfuric acid treatment before lignin separation and analysis	- TC and MWL had high acetyl content, 11 wt% and 8 wt%, respectively - ILL and EOL lost about 80% of their original acetyl groups - NMR spectra showed MWL had the most acetyl content, while EOL had the least - EOL experienced significant polysaccharide hydrolysis, and ILL may have acetylation shifts from lignin to cellulose	140
Eucalyptus urophylla	- Lignin was extracted using an ionic liquid-based microwave-assisted extraction (ILs-MAE) process, specifically utilizing [C2C1 im][OAc] and [C4C1 im]Cl ionic liquids, with varying microwave power and reaction times to assess extraction efficiency and lignin yield	- Up to 45.8% lignin was extracted using [C2C1 im][OAc] at 140 °C and 400 W - Extracted lignin had molecular weights ranging from 730 to 3870 g mol^{-1}, showing varying depolymerization - 2D HSQC NMR analysis showed significant degradation of β-O-4′ linkages and S/G ratio changes - Thermal stability and sugar content varied, reflecting extraction parameter effectiveness	132
Empty fruit bunches (EFB), palm mesocarp fiber (PMF), and palm kernel shells (PKS) from oil palm biomass	- Lignin was extracted with pyridinium formate (PyFor) under mild conditions - Parameters such as particle size, temperature, and time were optimized - The process was optimized using response surface methodology - Regenerated lignin was filtered and dried	- Maximum lignin extraction efficiencies were 92.01% for EFB, 91.23% for PMF, and 90.70% for PKS - The extraction process showed activation energies of 12 kJ mol^{-1} for EFB, 23 kJ mol^{-1} for PMF, and 28 kJ mol^{-1} for PKS - The extracted lignins were characterized using FTIR and ^{1}H NMR, and the sustainability of the PyFor solvent was confirmed	395
Sugarcane bagasse	- Alkaline extraction used 15% NaOH at 100 °C for 90 minutes, producing alkaline lignin (AL) - Ethanosolv extraction applied ethanol–water mixtures at 200 °C for 90 minutes, resulting in ethanosolv lignin (EL) - Hydrotropic extraction involved various solutions at 90 °C for 6 hours, yielding hydrotropic extracted lignin (HEL) - Lignin was precipitated by acidification or dilution with water in each extraction method	- Alkaline lignin (AL) had 57.85% carbon, a molecular weight of 2170 g mol^{-1}, and notable groups - Ethanosolv lignin (EL) had 61.33% carbon, a higher molecular weight of 3640 g mol^{-1}, and the highest HHV - Hydrotropic extracted lignin (HEL) also had 57.85% carbon, a molecular weight of 3802 g mol^{-1}, and similar HHV to AL - FTIR spectrum of HEL showed more aromatic and phenolic groups, with a maximum yield at 1.43 M sodium xylene sulfonate	401
Etek lignin, a byproduct from the acidic processing of wood to produce fermentable sugars	- Etek lignin underwent fast pyrolysis at 500 °C in a fluidized bed reactor with short residence time	- Pyrolytic lignins had varied carbon, hydrogen, and oxygen contents; heating values ranged from 22.7 to 27.2 MJ kg^{-1}	402

Table 6 (*Contd.*)

Biomass used	Extraction methods involved	Properties of extracted lignin	Ref.
	- Pyrolysis vapors were condensed, and aerosols were collected using electrostatic precipitators - Pyrolysis oil was mixed with sand and extracted through Soxhlet extraction with hexane and methanol - Resulting fractions were separated into soluble and insoluble types, then freeze-dried to obtain powders	- Methanol-insoluble fraction had a lower heating value of 9.7 MJ kg^{-1} - FTIR and 31P NMR analyses showed increased hydroxyl and carbonyl groups, with varied molecular weights - Pyrolytic lignins had lower molecular weights than original Etek lignin; DI (dichloromethane insoluble) lignin fraction had the highest - TGA revealed pyrolytic lignins decomposed at 110–120 °C; DI and WI (water immersed) fractions had greater stability	
The efficacy of three different deep eutectic solvents (DES) was investigated for extracting lignin from four types of food processing residues: rice husks, sugarcane bagasse, coffee chaff, and corn stover	- Biomass was ground, sieved to ≤180 μm, and treated with DES in an oil bath - The mixture was vacuum filtered, rinsed with ethanol, and precipitated with deionized water - The precipitate was dried to obtain lignin - Lignin was acetylated with acetic anhydride and pyridine for GPC analysis	- The extracted lignins showed varied molecular weight and polydispersity indices (PDI) based on the DES used - DES acetic acid: choline chloride (AACC) produced lignins with reduced molecular weight and high PDI for rice husks and sugarcane bagasse, while lactic acid: choline chloride (LACC) was most effective for coffee chaff and formic acid: choline chloride (FACC) for corn stover - Higher heating values (HHV) of the lignins extracted with AACC were notably higher than the control black liquor-derived lignin	403
Extracting lignin from bamboo biomass using nitrile-based ionic liquids (ILs) as pre-treatment solvents	- The extraction process involved the use of synthesized nitrile-based ionic liquids, specifically 1-propyronitrile-3-butylimidazolium chloride ([C2CNBim]Cl), 1-propyronitrile-3-allylimidazolium chloride ([C2CNAim]Cl), 1-propyronitrile-3-(2-hydroxyethyl)imidazolium chloride ([C2CNHEim]Cl), and 1-propyronitrile-3-benzylimidazolium chloride ([C2CNBzim]Cl) - The bamboo biomass was treated with these ILs under controlled conditions (temperature, time, and particle size) to extract lignin	- The lignin was characterized by FTIR, NMR, TGA, and elemental analysis - [C2CNBzim]Cl was the best IL, extracting up to 53% of lignin efficiently - Cellulose crystallinity stayed the same, and lignin showed expected functional groups after extraction - The ILs were highly recyclable, maintaining efficiency across several cycles - Successful lignin isolation was confirmed through functional group analysis and extraction efficiency	404
Extraction of lignin from two types of biomass: softwood and brewer's spent grains (BSG)	- Lignin was extracted using deep eutectic solvents (DES) composed of choline chloride (ChCl) combined with two different hydrogen bond donors (HBDs): lactic acid (LA) and glycerol (Gly) - The pretreatment was conducted at temperatures of 60 °C and 80 °C. The process involved mixing the biomass with DES, followed by filtration, ethanol washing, and precipitation of lignin using ethanol/water mixture as an antisolvent. The resulting lignin precipitate was then dried	- Lignin features varied based on the DES and temperature used in extraction - ChCl yielded higher β-O-4 linkages and narrow molecular weight distributions, especially at 80 °C	407

Table 6 (*Contd.*)

Biomass used	Extraction methods involved	Properties of extracted lignin	Ref.
		- ChCl resulted in lower yields and less β-O-4 preservation compared to other methods - NMR showed ChCl preserved G subunits and β-O-4 bonds better in softwood lignin	
Three types of poplar species were used: wild-type poplar (*P. nigra* × *P. maximowiczii*), and two genetically modified variants with high-S (F5H-64) and low-S (1035-41) lignin content	- Lignin was extracted using acetic acid/formic acid/water, acetone/water, and methanol/water as solvent mixtures - Biomass was heated with solvents, then filtered, concentrated, and precipitated to isolate lignin - Methanol treatment yielded 58–69% lignin, higher than 47–54% from acetic acid/formic acid - Acetone extraction resulted in 62–67% lignin yield, less effective than methanol	- Lignin properties varied based on the solvent used for extraction - Methanol yielded more monomeric phenolic products, achieving over 60% product yield - Methanol preserved lignin structure by minimizing carbon–carbon bond formation - SEM and NMR analyses showed methanol produced larger, regular particles with unique substitution patterns	405
Wheat straw and rice husk as LCB sources	- Lignin was extracted using protic ionic liquids consisting of pyridinium cations and dihydrogen phosphate anions ($H_2PO_4^-$) - The ILs were synthesized by treating pyridine with varying moles of 85% phosphoric acid (H_3PO_4) - Biomass samples were pretreated in these ionic liquids at temperatures ranging from 70 °C to 100 °C for 30 to 120 minutes - Post-treatment, lignin was separated using acetone-water anti-solvent mixture, filtered, and then purified by centrifugation and freeze-drying	- The extracted lignin yields were optimal at 73% for wheat straw and 72% for rice husk under the best conditions (100 °C for 2 hours) - The lignin showed reduced intensity in FT-IR peaks related to aromatic rings and phenolic OH groups, indicating successful delignification - HSQC NMR analysis revealed that the lignin structure retained guaiacyl and syringyl fragments, with some condensation observed, reflecting the effectiveness and mildness of the extraction process	144
Various types of biomass, including wheat straw, eucalyptus, and pine	- The extraction employed a combination of 1,4-butanediol (BDO) and *p*-toluenesulfonic acid (pTsOH) in an aqueous solution - Molecular dynamics simulations revealed how lignin dissolved at the molecular level - The conditions included a 70% BDO aqueous solution mixed with 10% pTsOH at temperatures ranging from 90 °C to 150 °C - This approach was optimized to maintain lignin native structure while avoiding excessive condensation	- The extracted lignin retained high levels of β-O-4 linkages, with preservation rates reaching up to 95% - The lignin showed high yields (over 80% from eucalyptus and around 50% from resistant conifer wood) and was found to have a low condensation level, making it suitable for high-value applications - The extracted lignin also demonstrated potential as an effective ingredient in chemical sunscreens, significantly enhancing the sun protection factor (SPF) compared to untreated samples	393
Kenaf fiber biomass sourced from Chuping plantation site in Malaysia	- The lignin extraction involved a two-step process - Kenaf fibers were pretreated with a natural deep eutectic solvent (NADES) consisting of lactic acid and choline chloride at molar ratios of 1 : 12 and 1 : 15 - Fibers were then subjected to acid hydrolysis using 72% sulfuric acid to remove carbohydrates, then the lignin was extracted, filtered, and dried	- The lignin extracted using NADES showed a slight increase in carbon and nitrogen percentages compared to commercial lignin - NADES-extracted lignin exhibited a smoother and wavier surface compared to the irregular texture of commercial lignin - FTIR spectra indicated similar functional groups but with slight variations in intensity and position - XRD analysis revealed a slight decrease in crystallinity after NADES pretreatment	406

Table 6 (*Contd.*)

Biomass used	Extraction methods involved	Properties of extracted lignin	Ref.
		- TGA and DSC analysis showed that NADES-extracted lignin had a different thermal degradation profile compared to commercial lignin, with varying decomposition temperatures and enthalpy values	
Residual LCB from Ocote pine (Pinus montezumae Lamb.) including sawdust and bark sourced from the forest fields of Rancho Peñitas and Guzmán in San Joaquín, Michoacán, Mexico	- The Kraft process was utilized for delignification, employing sodium hydroxide (NaOH) and sodium sulfide (Na_2S) in a 600 mL Parr reactor - The biomass (50 g of sawdust or bark) was digested in a white liquor solution at 170 °C for 50 minutes under pressure (8 bar) - Post-digestion, lignin was recovered through filtration and acidification, then purified by repeated washing with deionized water and dried at 50 °C	- The extracted lignin exhibited characteristic bands for aromatic compounds and phenolic groups, with more intense signals for sawdust lignin - Lignin from both sawdust and bark demonstrated high thermal stability with sawdust lignin showing complete decomposition above 800 °C, whereas bark lignin retained stability due to its higher aromatic content - Sawdust lignin had a higher calorific value (28.75 MJ kg^{-1}) compared to bark lignin (23.61 MJ kg^{-1}), indicating better energy content. Both types showed low ash content and minimal sulfur, making them suitable for biofuel production	408

[a] BDO refers to 1,4-butanediol, *p*TsOH stands for *p*-toluenesulfonic acid. TGA is thermogravimetric analysis, and FTIR represents Fourier-transform infrared spectroscopy. DSC is differential scanning calorimetry. PFA/PAA refers to peracetic and phosphoric acids. MWL is milled wood lignin, ILL is ionic liquid lignin, and EOL is ethanol organosolv lignin. PyFor stands for pyridinium formate, AL is alkaline lignin, and EL is ethanosolv lignin. HEL is hydrotropic extracted lignin, DI is dichloromethane insoluble lignin, and WI is water immersed lignin. DES refers to deep eutectic solvents, ChCl is choline chloride, and HBDs are hydrogen bond donors. NADES are natural deep eutectic solvents, NaOH is sodium hydroxide, and Na_2S is sodium sulfide.

applications.[397,398] These modifications enable lignin to serve as a valuable bio-based polymer or a precursor for carbon materials, expanding its industrial utility.[173,399,400] Optimizing the extraction method is essential to balance lignin recovery efficiency with structural preservation, ensuring its functional adaptability for biofuel production, biopolymer development, and high-value chemical synthesis.

The studies summarized in Table 6 present a variety of methods for isolating lignin from different LCB with a focus on optimizing extraction efficiency, characterizing properties, and assessing the potential applications of the extracted lignins. Different solvents and extraction techniques were employed, yielding lignins with diverse chemical structures and properties. For example, non-wood biomass sources like wheat straw, pine straw, and alfalfa yielded lignin with varying thermal stability, with wheat straw lignin exhibiting the highest thermal stability and flax fiber showing the highest enthalpy values.[396] Studies on Typha capensis demonstrated that various treatments, including milling, ionic liquids, and ethanol organosolv methods, resulted in lignin with different acetyl content and molecular structure.[140] Extraction from *Eucalyptus urophylla* using ionic liquids exhibited a range of lignin molecular weights and thermal stability, with significant changes in β-O-4′ linkages.[132] Additionally, studies on palm biomass such as empty fruit bunches and palm kernel shells used pyridinium formate, achieving over 90% extraction efficiency,[395] while sugarcane bagasse lignins were extracted through alkaline, ethanosolv, and hydrotropic methods, revealing differences in carbon content and higher heating values.[401] Etek lignin, obtained from acidic wood processing byproducts, demonstrated varied pyrolytic properties with a wide range of heating values and stability, showing potential as biofuel feedstock.[402] Furthermore, lignins extracted using deep eutectic solvents from food processing residues showed differing molecular weights and higher heating values, indicating the potential for tailored applications based on residue type.[403] Extraction of lignin from bamboo using nitrile-based ionic liquids (ILs) highlighted the effectiveness of ILs for efficient lignin recovery, with ILs such as [C2CNBzim]Cl achieving high yields and maintaining recycling efficiency.[404] Various studies also examined lignin extraction from softwoods and genetically modified poplars, with methanol treatment yielding high monomeric phenolic products,[405] while kenaf fiber biomass treated with a natural deep eutectic solvent showed alterations in crystallinity and distinct thermal degradation profiles.[406]

5.1. Lignin properties

Lignin plays a crucial role in regulating liquid transport within plants, enabling them to grow tall and compete for sunlight. Unlike cellulose, which forms crystalline structures, the amorphous nature of lignin results in a three-dimensional polymer network. This structure enhances its flexibility and allows it to fill spaces within the cell wall matrix, thereby strengthening plant tissues mechanically. Lignin composition varies depending on its source.[185] In softwoods such as pine and spruce, lignin primarily consists of coniferyl alcohol units, with some *p*-

coumaryl units and minimal sinapyl alcohol content. In contrast, hardwoods like beech, birch, and oak contain higher concentrations of sinapyl alcohol units.[409] Native lignin is insoluble in water, and during the cooking process, its solubilization is essential for separating it from the fiber fraction.[76] Structurally, lignin is a complex organic polymer that contains both polar groups and nonpolar hydrocarbon and benzene rings. It includes various functional groups like hydroxyl, aromatic sites, alcohols, methoxyl, carboxyl, and carbonyl functionalities. These diverse chemical groups enable lignin to interact and react with a wide range of organic compounds. This reactivity makes lignin a highly valuable and versatile precursor for the synthesis of a variety of synthetic polymers, including resins, polyurethanes, and polyesters, which are extensively used in numerous industrial applications.[410] These functionalities facilitate key chemical transformations, including esterification, alkylation, etherification, hydroxypropylation with epoxides, and urethanization *via* isocyanate or non-isocyanate routes.[411] Fig. 20 illustrates these chemical modifications, which diversify functional potential of lignin. Lignin also exhibits high strength, resistance, and rigidity against ultraviolet light, making it well-suited for heat and sound insulation.[412] Its molecular weight and chemical composition are influenced not only by plant species but also by the specific plant part, leading to variations even within the same plant. For example, lignin–carbohydrate complexes extracted from hardwoods and softwoods exhibit molecular weight ranges of 9800–17 600 g mol^{-1} and 10 000–13 000 g mol^{-1}, respectively.[78,413]

The aromatic nature of lignin grants it unique physicochemical properties, including UV-absorbing capabilities that protect plants from harmful solar radiation. Additionally, high resistance of lignin to biodegradation contributes to the longevity of plant-derived materials in natural environments.[414,415] However, this resistance poses challenges for lignin valorization and recycling, as traditional chemical and biological degradation processes are often inefficient and costly. Moreover, the thermal stability of lignin is influenced by several factors, including interunit structures, functional groups, degree of condensation, and molecular weight.[392] It demonstrates moderate stability at elevated temperatures, with decomposition occurring between 200 and 600 °C, peaking around 400 °C. During this process, phenylpropane side chains degrade, releasing compounds such as formic acid, formaldehyde, carbon dioxide, and water.[416] At higher temperatures (500–700 °C), degradation of the lignin backbone intensifies, leading to the release of volatile products like carbon monoxide, carbon dioxide, and hydrogen.[398] Lignin is also recognized for its potential as a renewable carbon source in carbon fiber production. Through pyrolysis at high temperatures, lignin can be converted into carbon fibers suitable for aerospace, automotive, and other high-performance applications.[402,417]

Lignin-based materials exhibit both antioxidant and antimicrobial properties.[418] Studies have shown that syringic acid, a lignin-derived compound, can modulate MMP expression and regulate MMP-1 production *via* the AP-1 mechanism. This process enhances the survival rate of UVB-damaged HaCaT cells, suggesting potential applications in cosmetics.[419] Additionally, silver-infused lignin-based nanoparticles have demonstrated strong antimicrobial properties, effectively neutralizing common pathogens and underscoring lignin potential as an antimicrobial agent.[420] Beyond its bioactive properties, lignin has been explored as a reinforcement material due to its interesting mechanical strength. Özparpucu *et al.*[421] observed that lignin significantly influenced the axial elastic modulus of poplar wood, attributing this enhancement to its aromatic and heterocyclic structure, which strengthened

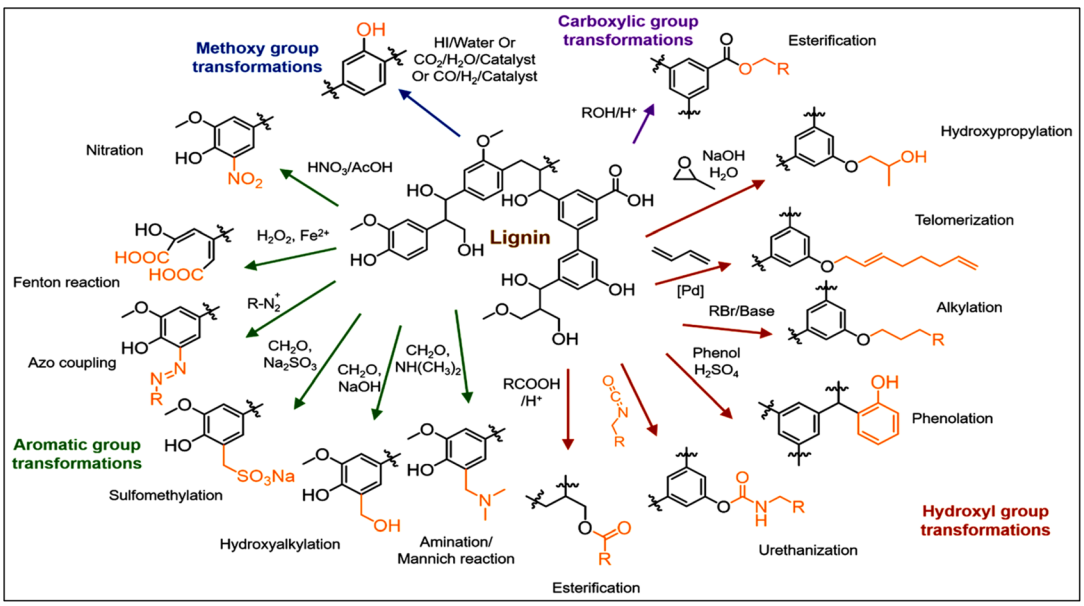

Fig. 20 Overview of chemical transformations for enhancing lignin functionalities. Reproduced with permission from ref. 411 copyright © 2019 MDPI.

wood biomass. Furthermore, Cousins[422] conducted experiments to measure the elastic modulus of two types of lignins (periodate and Klason lignins) at various moisture contents. They found that the Young's modulus of periodate lignin ranged from 3.1×10^9 to 6.7×10^9 Pa, and the shear modulus ranged from 1.2×10^9 to 2.1×10^9 Pa as moisture content decreased. Klason lignin exhibited similar behavior, though its moduli were consistently lower.[422] From a mechanical perspective, lignin plays an important role in reinforcing plant tissues, providing rigidity and structural integrity essential for maintaining upright growth.[423] Its mechanical properties, including Young's modulus, tensile strength, and toughness, vary based on factors such as molecular weight, chemical composition, and degree of polymerization. These properties can be tailored through various processing techniques, including chemical modifications, polymer blending, and controlled extraction methods that alter its molecular structure.[173,174,424] To leverage mechanical benefits of lignin, researchers have developed lignin-based composites by incorporating it into polymeric matrices. These composites exhibited enhanced mechanical properties while offering a more sustainable alternative to traditional petroleum-based materials, contributing to reduced environmental impact.[425,426]

5.2. Lignin (bio)sensing applications

Recent research has increasingly focused on lignin-based composites for advanced (bio)sensing applications, highlighting the potential of this abundant and renewable biopolymer.[427–429] The chemical versatility and structural properties of lignin contribute to enhanced sensitivity, selectivity, and stability in sensing materials.[32,428,429] Studies have demonstrated that integrating lignin into nanostructured materials and hydrogels results in highly effective sensors for detecting environmental pollutants, biological molecules, and hazardous substances.[31,429] These composites benefit from inherent ability of lignin to undergo functionalization, allowing for the incorporation of additional sensing moieties or conductive materials to improve detection limits and response times. Notable advancements include lignin-based electrochemical sensors with enhanced electroactive properties, enabling the detection of trace analytes,[32] as well as lignin-derived photonic sensors that exploit its optical characteristics for highly sensitive biosensing applications.[430,431] The use of lignin in sensor development not only supports the design of sustainable and eco-friendly technologies but also addresses key challenges such as cost-effectiveness and material availability.[32,427,431]

The studies summarized in Table 7 highlight significant advancements in sensor technologies utilizing lignin-based materials, each offering valuable insights into material performance and applications. Lignin-scribed graphene (LSG) combined with nitrogen-doped graphene QDs (N-GQDs) and silver nanoparticles (Ag NPs) demonstrated exceptional sensitivity (1 fM) for detecting Troponin I, emphasizing the potential of hybrid nanocomposites in medical diagnostics.[32] Similarly, carbon-based conductive inks derived from lignin proved effective in detecting uric acid and catechol, showcasing their potential for cost-effective electroanalytical biosensors.[427] In the realm of gas sensing, carbon foams incorporating graphene oxide (GO) and reduced graphene oxide (rGO) exhibited enhanced electrochemical performance for ammonia detection, demonstrating the importance of optimizing additive concentrations and processing methods.[428] For wearable sensor applications, electrospun carbon fibers from *Eucalyptus globulus* lignin responded distinctively to various human motions, suggesting their potential for personalized sensor development.[432] Additionally, lignin-based polyurethane copolymers doped with multiwall carbon nanotubes (MWCNTs) achieved high conductivity with a low percolation threshold, proving valuable for potentiometric chemical sensors.[400] Further advancements include lignin-derived graphene composites integrated with MoS_2 and Ag NPs, achieving remarkable sensitivity for Troponin I detection with a limit as low as 100 attomolar, making them highly promising for biomarker detection.[433] Meanwhile, carbonized lignin screen-printed electrodes with immobilized algae cells demonstrated high sensitivity for atrazine detection, offering a sustainable solution for agricultural monitoring.[429] Lastly, lignin-based phenolic–resin-derived carbon catalysts incorporating CoNi/biochar achieved a low detection limit for 2-nitrophenol, highlighting the effectiveness of combining lignin-derived carbon materials with metal catalysts for electrochemical applications.[434]

Lignin-based materials are emerging as promising candidates for a broad range of applications, including sensing and biosensing. The inherent aromatic structure of lignin provides rigidity to polymeric systems, ensuring excellent thermal and mechanical properties in the resulting materials. Furthermore, the phenolic and aliphatic hydroxyl groups present in lignin offer versatile chemical functionalities, making them suitable for various applications, such as enhancing material properties, enabling functionalization, and improving sensor performance.[174,436]

5.2.1 Environmental sensors. Faria *et al.*[400] modified eucalyptus kraft lignin-based polyurethane by incorporating multiwall carbon nanotubes (MWCNTs) to create a conductive copolymer for use in ion-selective membranes for potentiometric chemical sensor applications. This hybrid material exhibited high stability in aqueous solutions, maintaining a reproducibility of 2% in a 0.1 mmol L^{-1} chromate solution over a three-month period.[400] Similarly, Chokkareddy and coworkers[437] developed an innovative nanocomposite made of multiwalled carbon nanotubes, copper oxide nanoparticles and lignin polymer. This composite was used to modify glassy carbon electrodes for the sensitive detection of chlorogenic acid in both artificial and coffee samples *via* differential pulse voltammetry.[437] Under optimized conditions, the nanocomposite-modified electrode demonstrated high sensitivity and low detection limits. When applied to real coffee samples, the hybrid electrode achieved a recovery rate ranging from 97% to 106%.[437] Stergiou *et al.*[438] introduced lignin-modified glassy carbon electrodes as transducers for ozone detection. Impedimetric and cyclic voltammetric studies confirmed the feasibility of using a polymer degradation-based impedimetric sensor for ozone monitoring, which shows potential for applications in

Table 7 Overview of studies on lignin-based materials for (bio)sensing applications and energy storage devices

Electrode materials	Analytes/measured parameters	Detection limit	Major findings	Ref.
Lignin-scribed graphene (LSG) conjugated with nitrogen-doped graphene QDs (N-GQDs) and lignin-derived silver nanoparticles (Ag NPs)	Troponin I, a cardiac biomarker for acute myocardial infarction	1 fM (30 fg mL^{-1})	- The developed nanocomposite exhibited an optimal conduction mechanism with uniformly distributed Ag NPs and N-GQDs on the LSG surface - It demonstrated high selectivity and sensitivity for Troponin I detection, with the sensor showing excellent linearity, repeatability, and stability - The impedance spectroscopy results indicated a very low detection limit of 1 fM, making this nanocomposite a promising tool for precise and sensitive medical diagnostics	32
Three-dimensional N,S co-doped lignin-based carbon microsphere/graphene composite hydrogel (GH-NSCMS)	Supercapacitor performance metrics; tetracycline for molecularly imprinted electrochemical sensors (MIECS)	Tetracycline: 5×10^{-8} mol L^{-1}	- The GH-NSCMS electrode exhibits a specific capacitance of 434.6 F g^{-1} at 0.5 A g^{-1} and retains 94.15% capacitance after 5000 cycles, demonstrating excellent stability for supercapacitor applications - For tetracycline detection, the MIP electrochemical sensor using GH-NSCMS shows high sensitivity with a wide linear range of 0.1–50 μM and a low detection limit of 5×10^{-8} mol L^{-1}, benefiting from the high conductivity and imprinting accuracy of the composite	31
Carbon-based conductive inks derived from carbonized lignin (Eucalyptus globulus waste) combined with cyclohexanone and cellulose acetate	Uric acid and catechol	0.3 μM for uric acid; 2.01 μM for catechol	- A stable conductive ink was developed with optimal conductivity and rheological properties, featuring an electrochemically active area of 0.1813 cm^2, surpassing that of petroleum-based inks (0.1420 cm^2) - The ink was used to produce screen-printed electrodes that demonstrated effective performance in detecting uric acid and catechol, while also showcasing biocompatibility with laccase enzyme	427
Carbon foams (CFs) produced from lignin–phenol–formaldehyde (LPF) resin with 1%, 2%, and 4% graphene oxide (GO) and reduced graphene oxide (rGO) additives	Ammonia		- The integration of GO and rGO into LPF resin-based carbon foams resulted in significant enhancements in electrochemical properties - Carbon foams with 2% GO (GO_2%) exhibited a 39% and 62% larger electroactive area compared to control and 2% rGO sensors, respectively - The study demonstrated that the thermal decomposition and reduction processes effectively removed oxygen groups from GO, improving the electron transfer and overall electrochemical performance of the sensors	428
Electrospun ultrathin carbon fibers derived from Eucalyptus globulus lignin (EKL) and sugarcane bagasse Kraft lignin (BKL)	Human body motions (finger bending, arm bending, finger pressing)	—	- Carbon fiber-based sensors was developed from EKL and BKL lignins and investigated their chemical structures - EKL, with a slightly linear structure featuring sinapyl and coniferyl alcohols, produced sensors with high signal amplitude ($\Delta R/R_0 \approx 9 \times 10^4$) for finger bending motions - In contrast, BKL, which formed more amorphous carbon and graphite, showed a larger variation in resistance for arm bending ($\Delta R/R_0 \sim 380$) and smaller changes for finger pressing ($\Delta R/R_0 < 10$)	432
		—		400

Table 7 (*Contd.*)

Electrode materials	Analytes/measured parameters	Detection limit	Major findings	Ref.
Modified eucalyptus kraft lignin doped with multiwall carbon nanotubes (MWCNTs) incorporated into a crosslinked elastomeric polyurethane copolymer - The polymer showed improved conductivity without compromising stability or performance, making it suitable for use in potentiometric chemical sensors - The copolymer low glass transition temperature of approximately −49 °C and its stability in various solvents enhanced its suitability for self-plasticizing sensor applications	Potentiometric chemical sensors		- A conductive lignin-based polyurethane copolymer with MWCNTs was fabricated, demonstrating significantly enhanced electrical conductivity while maintaining thermal and viscoelastic properties - The addition of MWCNTs resulted in a very low percolation threshold of 0.18% (w/w), attributed to the oriented distribution of MWCNTs within lignin clusters	
Lignin-derived graphene (3D LSG) integrated with MoS_2 and silver nanoparticles (Ag NPs)	Troponin I (a biomarker for acute myocardial infarction)	100 attomolar	- A lignin-derived graphene-based biosensor was fabricated with enhanced performance by incorporating MoS_2 and Ag NPs - The hybrid material, 3D LSG_MoS_2_Ag NPs-2.0, exhibited improved surface area and sensitivity due to the addition of MoS_2 nanoflowers and Ag NPs - This biosensor demonstrated high analytical performance with a detection limit of 100 attomolar for Troponin I, a sensitivity of 31.45 μA mM^{-1} cm^{-2}, and excellent stability (87%) and reproducibility (relative standard deviation of 3.8%) - The biosensor achieved approximately a 4-fold increase in selectivity and high specificity, making it a promising tool for detecting Troponin I in clinical diagnostics	433
Polyurethane–lignin copolymer blended with multi-walled carbon nanotubes (MWCNTs), using LignoBoost® kraft lignin	Copper ions (Cu^{2+})		- A polyurethane–lignin copolymer doped with MWCNTs successfully synthesized, specifically using LignoBoost® kraft lignin, which contained increased polyphenolic groups from tannins - This copolymer demonstrated enhanced electrical conductivity and was utilized in all-solid-state potentiometric sensors - The sensors showed high selectivity and sensitivity towards Cu^{2+} ions and exhibited long-term stability - Electrical impedance and conductivity measurements confirmed that the interaction between MWCNTs and lignin significantly improved the polymer electrical properties, with a notable percolation threshold of 0.77% MWCNTs in the lignin-based polymer - Compared to technical lignins, LignoBoost® kraft lignin higher polyphenolic content contributed to superior ion–exchange properties and enhanced sensing performance	435 429

Table 7 (*Contd.*)

Electrode materials	Analytes/measured parameters	Detection limit	Major findings	Ref.
Carbonized lignin screen-printed electrodes with immobilized whole cells of *Chlamydomonas reinhardtii* UV180 mutant - The sensor exhibited a working stability of 10 hours, proving effective for sustainable agricultural monitoring	Nanoformulated atrazine encapsulated in zein and chitosan-doped poly-ε-caprolactone (PCL-Ch) nanoparticles	0.9 nM for atrazine-zein and 1.1 nM for atrazine-PCL-Ch	- The biosensor demonstrated a highly sensitive and eco-friendly approach for detecting nanoformulated atrazine with linear dose-response curves in the 0.1 to 5 μM range - It showed no interference from various contaminants and wastewater matrix effects, with recovery rates of 106 ± 8% for atrazine-zein and 93 ± 7% for atrazine-PCL-Ch	
Lignin-based phenolic-resin-derived carbon with CoNi/biochar catalyst (synthesized *via in situ* pyrolysis)	2-Nitrophenol	0.0132 μM	- A CoNi/biochar catalyst was developed from lignin-derived phenolic resin, which featured rough spherical structures and enhanced electron acceptance capabilities due to the incorporation of Co and Ni - The carbon material exhibited strong electrochemical performance with high stability, selectivity, and repeatability for the detection of 2-nitrophenol - The catalyst showed a low detection limit of 0.0132 μM and a linear detection range up to 100 μM, highlighting its effectiveness for electrochemical sensing applications	434

industrial and technical settings.[438] Wang *et al.*[432] developed carbon fibers derived from *Eucalyptus globulus* lignin and sugarcane bagasse kraft lignin to detect specific human body motions. These lignin-based piezoresistive sensors exhibited promising potential for use in wearable electronics applications.[432]

5.2.2 Bioimaging and biomedical applications. Lignin, a polyphenolic compound with intrinsic electron–transfer properties, serves as a high-performance material for bioelectronic interfaces, particularly in biosensing applications. Its redox-active moieties, such as phenolic and methoxyl groups, enable efficient electron transfer, making it suitable for fabricating sensors that detect biomolecules. A key application involves lignin-based electrochemical biosensors, where its conductive properties are utilized in conjunction with enzymatic activity to facilitate redox reactions.[439,440] For example, Jędrzak *et al.*[439] developed a biosensor incorporating a multicomponent material of magnetite, lignin, polydopamine, glucose oxidase, and ferrocene, integrated into a carbon paste electrode (CPE/Fe_2O_4/Lig/PDA/GOx/Fc). The biosensor was characterized using FTIR, TEM, AFM, and zeta potential measurements, and glucose oxidase immobilization was assessed with a Bradford assay. The performance of the biosensor was evaluated alongside photometric methods and three commercial glucometers. Results from testing glucose-based commercial products demonstrated repeatability and highlighted the biosensor potential for accurate glucose detection in real-world applications.[439] In addition, Beaucamp *et al.*[440] developed a third-generation glucose biosensor using glucose oxidase (GOx) immobilized on mesoporous carbon nanostructures, which were derived from a 50% alcell lignin and 50% polylactic acid (PLA) precursor blend. Methylene diphenyl diisocyanate was added to prevent fusion during thermal stabilization.[440] The PLA acted as a sacrificial material, enabling the formation of mesopores (2–4 nm) within larger pores, creating a hierarchical structure ideal for GOx immobilization. The resulting biosensor demonstrated a high surface coverage of 3.0 $\times 10^{-10}$ mol cm^{-2} and fast direct electron transfer of 1.3 s^{-1}. It exhibited strong, selective glucose activity, with a low Michaelis–Menten constant (K_m = 0.600 mM), linear response from 0.15 to 2.7 mM, and high sensitivity (50 μA mM^{-1} cm^{-2}), with a limit of detection of 89 μmol L^{-1}.[440] Tortolini *et al.*[441] designed novel nanoarchitectures based on lignin nanoparticles (LNPs) for eco-friendly electrochemical biosensing. They utilized two types of LNPs namely organosolv (OLNPs) and kraft lignin (KLNPs), synthesized from sulfur-free and sulfur-containing lignin respectively, to modify a gold electrode. Electrochemical analysis using CV and EIS revealed a decrease in faradaic current and an increase in ΔE_p, indicating that the LNPs layer inhibited electron transfer.[441] When the modified electrodes were assembled with concanavalin A (ConA) and glucose oxidase (GOx), they demonstrated glucose sensitivity of (4.53 ± 0.467) μA mM^{-1} cm^2 for OLNPs and (13.74 ± 1.84) μA mM^{-1} cm^2 for KLNPs. The best analytical performance was achieved with a three-layered Au(KLNPs/ConA/GOx)$_3$ electrode.[441] Moreover, the polyphenolic structure of lignin enhances its ability to chelate metals, making it highly valuable

in biosensing applications. The phenolic hydroxyl groups in lignin can bind with metal ions, forming stable complexes that enable the detection and quantification of specific metals in biological samples. This metal-binding capacity allows lignin to be utilized in the development of sensitive, selective biosensors for environmental monitoring, medical diagnostics, and food safety, offering an eco-friendly alternative to synthetic chelating agents.[431,442,443] Xu *et al.*[442] developed lignin–sulfonate/graphene QDs core/shell hybrids for label-free, sensitive, and selective detection of Fe^{3+}. The resulting sensor demonstrated excellent sensitivity and selectivity towards Fe^{3+} in both artificial and lake water samples, achieving a detection limit as low as 0.5 nM.[442] Moreover, lignin-based sensors have also demonstrated significant potential in disease diagnosis, particularly due to their ability to interact with biological markers and metals in complex biological systems. These sensors can be engineered to detect specific disease-related biomarkers, offering a promising tool for early detection and monitoring.[444] Rai *et al.*[444] synthesized water-soluble reduced fluorescent carbon dots using lignosulfonate lignin as a carbon source, aimed at curcumin nano-carrier and bioimaging applications. This research highlights significant potential of lignin-based materials for cancer diagnosis and treatment.[444] Furthermore, interesting properties of lignin make it an excellent candidate for the development of fluorescent nanocolorants, which can be used in live cell imaging. These lignin-based nanocolorants offer non-toxic, biodegradable alternatives to traditional fluorescent dyes, enabling real-time tracking of cellular processes with minimal impact on cell viability, thus advancing research in diagnostics and cellular biology.[445] Pillai *et al.*[445] performed a green synthesis of lignin-based fluorescent nanocolorants for live cell imaging. These non-toxic and efficient materials exhibited high fluorescent intensity, proving effective for live cell fluorescent imaging, particularly with L929 cells.[445]

5.2.3 Stress/strain and wearable sensors. Nguyen *et al.*[446] synthesized lignin-based renewable shape-memory materials for switchable electrical conductivity in stress/strain-sensing applications, achieving excellent results in devices for detecting human motion and monitoring stress history.[446] Moreover, Yang *et al.*[447] developed a lignin-based hydrogel with enhanced flexibility, tensile strain ($\geq$350%), compressive strain ($\approx$95%), and fatigue resistance (up to 10 000 cycles under 50% strain, and 200–800 cycles under 95% compressive strain). The improved properties of lignin-based hydrogel were achieved by incorporating glycerol and lithium chloride, which facilitated dynamic hydrogen and lithium ion bonds and reduced covalent cross-linking between lignin and other monomers.[447] These modifications also enhanced moisture retention and freeze resistance, enabling effective sensing performance at -40 ± 1 °C. The hydrogel was used to 3D print wearable tensile strain sensors and ripple-shaped 3×3 matrix hydrogel pressure sensors, demonstrating uniform stress distribution and superior performance in controlling bionic hand movements. These advancements highlight the potential of lignin-based hydrogels for applications in human–machine interfaces.[447] Lignin, when combined with other plant-derived biopolymers such as cellulose, can significantly enhance its mechanical and functional properties, making it an interesting material for strain sensor applications. The synergistic effects of lignin and cellulose can improve the overall strength, flexibility, and durability of the composite materials, enabling them to respond sensitively to changes in strain or deformation. These reinforced materials exhibit excellent mechanical properties like high tensile strength, elasticity, and stretchability, which are essential for real-time monitoring of movements.[332,448] Huang *et al.*[332] developed a hydrogel by incorporating lignin, trivalent iron ions, and nanocellulose into the precursor fluid, enabling gelation without the need for external heating or UV radiation. The study found that the gelation time was positively correlated with the lignin content, with rapid gel formation occurring in 63 s when the lignin content was 8 wt%.[332] The combination of lignosulfonate and nanocellulose introduced both non-covalent and covalent bonds, enhancing the hydrogel tensile strength (227 kPa) and elongation at break (515%). This hydrogel was also used as a strain sensor, capable of monitoring human joint movements, highlighting its potential for practical applications in sensing technologies.[332] Similarly, Zhou *et al.*[448] successfully developed a multifunctional ion-conductive hydrogel with remarkable mechanical properties and ionic conductivity, addressing the challenge of combining high mechanical strength with efficient electrical conductivity [448] The hydrogel, designed by integrating lignin-containing cellulose nanofibers, polyvinyl alcohol chains, ethylene glycol, and aluminum chloride, exhibited high mechanical performance, including tensile strength of 1.28 MPa, strain capacity of 794.94%, toughness of 6.32 MJ m^{-3}, and fatigue resistance. It also exhibited excellent sensing stability (300 cycles at 80% strain), high ionic conductivity (0.82 S m^{-1}), quick response (300 ms), freeze tolerance (−24 °C), and long-term solvent retention (180 days), making it ideal for wearable sensors.[448]

5.2.4 Humidity and chemical sensors. Rich in phenolic and aliphatic hydroxyl groups, lignin exhibits strong hydrogen bonding and moisture absorption capabilities. Its amorphous structure and natural hydrophilicity allow it to swell or change conductivity in response to humidity variations. Additionally, lignin can be processed into thin films or composites with conductive materials, enhancing sensitivity and stability.[449] Chen *et al.*[449] developed an environmental humidity sensor by combining lignosulfonate derived from biomass with graphene oxide. The sensor exhibited a maximum response of 298% at 97% relative humidity when using a 3 wt% thin film. This approach addresses the growing demand for low-cost, sustainable, and easily producible electrodes for portable point-of-care testing devices.[449] Moreover, incorporating biopolymers of varying size and molecular weight into lignin matrices significantly affects composite properties. Gigli *et al.*[450] demonstrated that combining chitosan with lignin notably improved the electrochemical responsiveness, structural organization, and molecular interactions of composite nanoparticles, enhancing their suitability for sensing applications. The molecular weight of chitosan played a crucial role: low- and medium-molecular-weight chitosan integrated efficiently within kraft lignin (KL) nanoparticles, forming compact aggregates with reduced energy gaps between the highest occupied molecular orbital

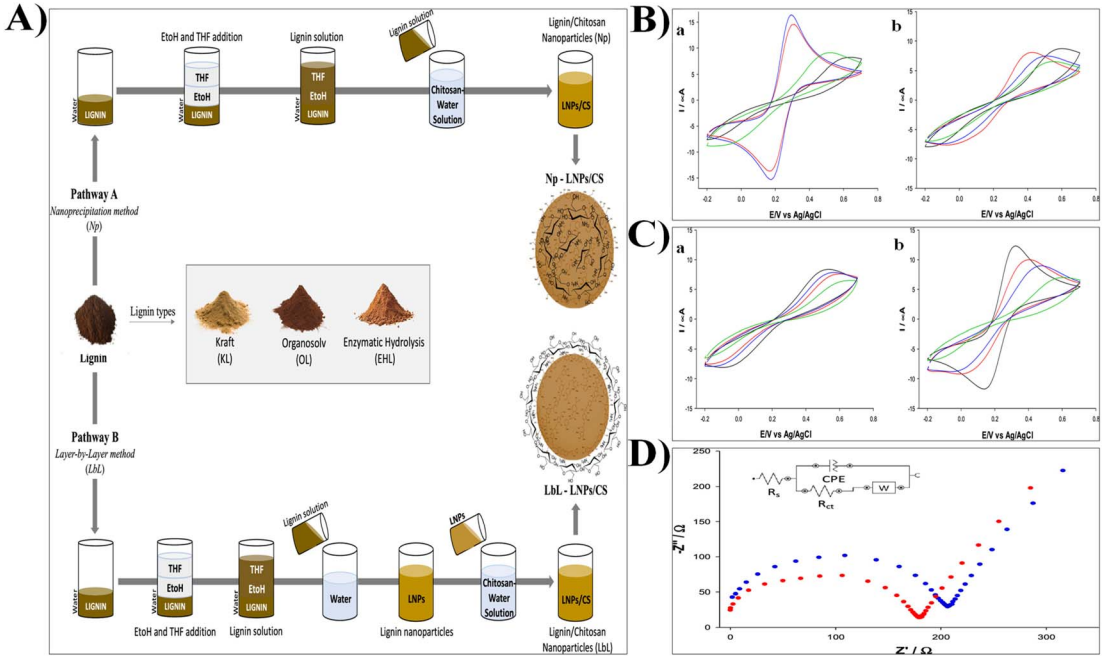

Fig. 21 (A) Schematic representation of the synthesis of LNPs/CS using two methods: pathway A illustrates the nanoprecipitation method, while Pathway B depicts the layer-by-layer (LbL) assembly method. (B) Cyclic voltammograms (CVs) of various KLNP platforms: KLNPs/GCE (black), KLNPs/CS1/GCE (red), KLNPs/CS2/GCE (blue), and KLNPs/CS3/GCE (green). Redox probe: 5 mM $[Fe(CN)_6]^{3-/4-}$ in 0.1 M KCl solution, scan rate: 50 mV s^{-1}. (C) (a) CVs of OLNP platforms synthesized by the nanoprecipitation method: OLNPs/GCE (black), OLNPs/CS1/GCE (red), OLNPs/CS2/GCE (blue), and OLNPs/CS3/GCE (green). (b) CVs of EHLNP platforms synthesized by the nanoprecipitation method: EHLNPs/GCE (black), EHLNPs/CS1/GCE (red), EHLNPs/CS2/GCE (blue), and EHLNPs/CS3/GCE (green). Redox probe: 5 mM $[Fe(CN)_6]^{3-/4-}$ in 0.1 M KCl solution, scan rate: 50 mV s^{-1}. (D) Nyquist plots comparing Np-KLNPs/CS2/GCE (red) and Np-OLNPs/CS3/GCE (blue), measured in 5 mM $[Fe(CN)_6]^{3-/4-}$ in 0.1 M KCl solution. The inset shows the equivalent circuit used for fitting the experimental data. Reproduced with permission from ref. 450, copyright © 2022 American Chemical Society.

(HOMO) and the lowest unoccupied molecular orbital (LUMO), which facilitated improved electron transfer and enhanced electrochemical reversibility.[450] In contrast, high-molecular-weight chitosan caused steric hindrance, disrupting aggregate formation and reducing performance. The type of lignin also influenced results; KL, rich in guaiacyl units, synergized well with chitosan to form stable, electroactive nanostructures, while lignins with higher p-hydroxyphenyl content (like enzymatic hydrolysis lignin, EHL) formed weaker interactions, lowering sensing efficiency. Additionally, nanoprecipitation promoted better aggregation and molecular interactions than layer-by-layer assembly, yielding composites with superior electrochemical properties. Overall, tailoring chitosan molecular weight and lignin type produced eco-friendly, highly responsive composites optimized for advanced electrochemical sensing.[450] In this study, Gigli *et al.*,[450] investigated lignin–chitosan nanoparticles (LNPs/CS) synthesized through layer-by-layer and nanoprecipitation methods (Fig. 21A). The electrochemical responsiveness of the LNPs/CS was evaluated using CV (Fig. 21B and C) and EIS (Fig. 21D). The electrochemical reversibility was influenced by the preparation method, chitosan molecular weight, and lignin type. Nanoprecipitation with Kraft lignin produced the most responsive nanodevice, suggesting effective interactions between the biopolymers.[450] The steric hindrance of chitosan was found to affect reversibility, with low-to-medium molecular weight chitosan yielding the best results. Field emission scanning electron microscopy and X-ray analyses revealed the distribution of chitosan within the nanoparticles, influencing their aggregation.[450] The interaction between lignin and chitosan varied, with Kraft lignin showing positive effects and enzymatic hydrolysis lignin demonstrating a detrimental impact, likely due to differences in their interaction networks. The LNPs/CS, prepared sustainably and easily, exhibited superior electrochemical efficiency, indicating the potential of this eco-friendly platform design for further applications.[450] In addition, lignin-based materials have gained attention as effective components for fiber-optic humidity sensors by using lignin-based hydrogels or thin films integrated with optical fibers. These sensors take advantage of lig natural hygroscopic properties, which allow it to reversibly absorb and release water molecules, leading to physical and optical changes, primarily swelling and changes in refractive index within the lignin matrix.[451] Such changes affect light propagation in the fiber, including variations in intensity, phase, or wavelength, thereby converting humidity fluctuations into measurable optical signals. Upon moisture exposure, the lignin layer swells and alters its refractive index, impacting evanescent field interactions or light coupling in fiber configurations like Bragg gratings or tapered fibers, producing detectable shifts in transmitted or reflected light. This reversible hydration process ensures consistent, repeatable sensor performance across multiple humidity cycles, enabling precise, real-time

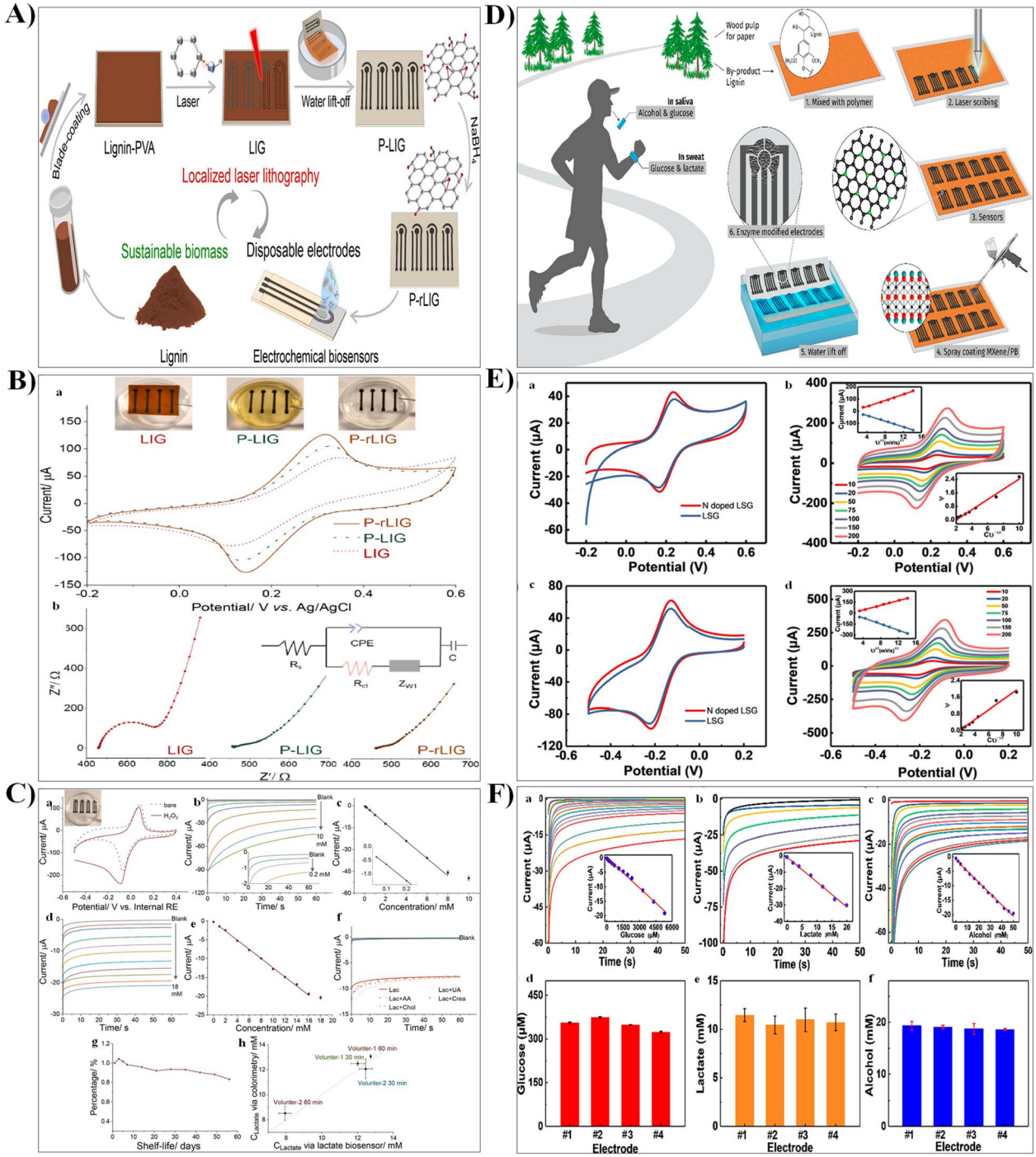

Fig. 22 (A) A sustainable approach converting lignin into graphene-based disposable electrodes for electrochemical biosensors. (B) Electrochemical kinetics evaluation: (a) cyclic voltammograms of LIG, P-LIG, and P-rLIG electrodes in $[Fe(CN)_6]^{3-/4-}$; (b) EIS of LIG, P-LIG, and P-rLIG electrodes in $[Fe(CN)_6]^{3-/4-}$. (C) Performance of electrochemical lactate biosensors: (a) cyclic voltammograms of PB/P-rLIG electrode in H_2O_2; (b) amperometric response to H_2O_2; (c) calibration curve for H_2O_2; (d) amperometric response to lactate; (e) calibration curve for lactate; (f) interference study; (g) shelf-life study; (h) correlation with standard assay for real sweat sample analysis. Reproduced with permission from ref. 453, copyright © 2022 Elsevier. (D) Schematic representation of the direct-write laser scribing process for N-LSG: (1) preparation of lignin/PVA/urea film on a substrate using the doctor blading method, (2) laser scribing to create N-LSG from the film, (3) patterned N-LSG electrodes, (4) modification of the electrodes with $Ti_3C_2T_x$/PB *via* spray coating, (5) water lift-off to remove uncarbonized film, and (6) enzyme functionalization of N-LSG electrodes. (E) Cyclic voltammetry (CV) profiles of LSG4.8 and N-LSG4.8 electrodes: (a) 5×10^{-3} M $[Fe(CN)_6]^{4-}$ and (c) 5×10^{-3} M $[Ru(NH_3)_6]^{3+}$ at a scan rate of 10 mV s^{-1}. (b and d) CVs of N-LSG4.8 at varying scan rates, with insets showing peak current (I_p) *vs.* $\nu^{1/2}$ (upper left) and Nicholson's kinetic parameter Ψ *vs.* $C\nu^{-1/2}$ (lower right). (F) Chronoamperometry plots for (a) glucose sensor (0–5.3 mM glucose in artificial sweat), (b) lactate sensor (0–20 mM lactate in artificial sweat), and (c) alcohol sensor (0–50 mM alcohol in artificial sweat), with insets showing calibration curves at 40 seconds post-bias application. (d–f) Reproducibility verification for glucose, lactate, and alcohol sensors in artificial sweat containing 350 μM glucose, 10 mM lactate, and 20 mM alcohol. Reproduced with permission from ref. 454, copyright © 2020 American Chemical Society.

monitoring.[451] Fu *et al.*[451] employed a combination of recyclable acid hydrotrope (*p*-toluenesulfonic acid) and ultrasonic treatment to extract lignin-containing fibers from poplar wood. These fibers were used to produce reinforced polyvinyl alcohol hydrogels through a dissolution-regeneration process in $LiBr \cdot 3H_2O$ solution.[451] The resulting hydrogel, coated onto the end face of a single-mode fiber, was used to construct a fiber-optic relative humidity sensor. This sensor demonstrated high sensitivity (4.7 dB) and excellent repeatability ($R^2 = 0.98$) within the 45% to 80% humidity range.[451]

5.2.5 Biochemical sensing. Jędrzak *et al.*[452] developed an enzymatic biosensor by immobilizing glucose oxidase on a silica–lignin system-based carbon paste electrode to study glucose oxidation electrochemically. This biosensor exhibited high sensitivity and selectivity, with a linear response range and a low detection limit for glucose. Additionally, it was employed in immunosensing applications to detect HIV p17 peptide with notable sensitivity and selectivity.[452] Meng *et al.*[453] introduced an eco-friendly approach for creating graphene electrodes for electrochemical lactate biosensors, utilizing biomass lignin conversion, laser lithography, water lift-off, and $NaBH_4$ treatment (Fig. 22A). Laser lithography effectively transformed lignin into porous laser-induced graphene (LIG), which was optimized for conductivity and substrate attachment. Water-based patterning enabled the creation of porous LIG (P-LIG), which was further reduced to P-rLIG with $NaBH_4$. Electrochemical analyses *via* CV and EIS showed varying peak currents and separations.[453] The P-LIG electrode exhibited enhanced electrochemical kinetics due to the removal of insulating salts and the exposure of pores. The P-rLIG electrodes displayed the highest current density and lowest peak separation, indicating improved conductivity and electron transfer, making them ideal for biosensors (Fig. 22B). These electrodes allowed the fabrication of disposable lactate biosensors with excellent analytical performance, making them promising candidates for sustainable biosensor manufacturing (Fig. 22C).[453] Lei *et al.*[454] developed a novel approach for creating nitrogen-doped laser-scribed graphene (N-LSG) electrodes from a lignin-based precursor, as illustrated in Fig. 22D, using a CO_2 laser scribing process to produce highly conductive, porous electrodes. These N-LSG electrodes exhibited enhanced electrochemical activity, with a conductivity of 2.8 Ω per square and improved electron transfer rates, as demonstrated through CV with redox mediators $[Fe(CN)_6]^{4-}$ and $[Ru(NH_3)_6]^{3+}$ (Fig. 22E).[454] Further functionalization with MXene/Prussian blue (Ti_3C_2Tx/PB) composites enabled the fabrication of biosensors for detecting glucose, lactate, and alcohol. The glucose sensor showed a sensitivity of 49.2 μA mM^{-1} cm^{-2} and a detection limit of 0.3 μM, while the lactate sensor had a sensitivity of 21.6 μA mM^{-1} cm^{-2} and a detection limit of 0.5 μM. The alcohol sensor exhibited a sensitivity of 5.78 μA mM^{-1} cm^{-2} (Fig. 22F). The sensors displayed high reproducibility, with relative standard deviations (RSDs) of 3.4%, 5.7%, and 5.4% for glucose, lactate, and alcohol, respectively (Fig. 22F). These findings underscore the potential of lignin-based sensors for low-cost, high-performance, and flexible biosensing applications.[454]

Compared to synthetic polymers traditionally used in sensor design, such as PANI, PPy, and poly(ethylene glycol) (PEG), lignin offers a more sustainable, cost-effective alternative, although its performance can vary depending on the specific sensor application and architecture.[443,449,455,456] Synthetic materials are known for their consistent mechanical properties, superior conductivity, and batch-to-batch reproducibility. For instance, conducting polymers like PANI and PPy, for instance, are prized for their tunable electrical conductivity and processability, allowing for precise control over sensor performance and enabling highly sensitive detection, often at the nanomolar level. However, these synthetic platforms require complex and often expensive synthesis processes, involve toxic reagents, and present challenges related to environmental disposal.[457,458] In contrast, lignin, a byproduct of the pulp and paper industry, is widely available, inexpensive, and contributes to the circular bioeconomy. Despite its heterogeneous structure, which can introduce variability in biosensor performance, advances in lignin purification and fractionation have considerably improved its consistency and reliability.[406,408,418,451] Moreover, the natural compatibility of lignin with a variety of nanomaterials, including carbon nanotubes, graphene oxide, and metal oxides, has facilitated the development of hybrid sensor interfaces that can compete with or even outperform synthetic materials in certain applications, especially where biocompatibility, environmental sustainability, and cost-effectiveness are key priorities.[400,439,454]

6. Challenges and future avenues for the use of lignocellulosic biomass and its main biopolymers for the development of high-performance sensors

Sensors have garnered significant attention for their ability to detect a wide spectrum of analytes with remarkable sensitivity and selectivity. Their applicability spans wide range of areas such as environmental monitoring, biomedical diagnostics, and industrial processes, where rapid, on-site detection of pollutants, pathogens, and biomarkers is indispensable. LCB, composed of cellulose, hemicellulose, and lignin, is an eco-friendly and sustainable material for electrode modification, offering compelling prospects for enhancing electrochemical sensor performance. Despite its potential, the practical utilization of LCB in electrochemical sensing is hindered by technical and environmental challenges that require innovative solutions to unlock its full capabilities. Cellulose, the most abundant constituent of LCB, is a structurally robust polysaccharide characterized by its highly crystalline fibrous architecture. This structure provides a high surface area and excellent mechanical performance for analyte adsorption, an essential attribute for improving sensor sensitivity. Additionally, cellulose ability to form stable films and scaffolds makes it an appealing material for electrochemical applications. However, its inherent electrical insulation requires integration with electrically

conductive materials, such as carbon-based materials (*e.g.*, carbon nanotubes, graphene), metal nanoparticles (*e.g.*, silver and gold nanoparticles), and conductive polymers (*e.g.*, polypyrrole, poly(3,4-ethylenedioxythiophene), and polyaniline) to facilitate electron transfer and enhance electrochemical responsiveness. Moreover, achieving uniform dispersion of these conductive nanomaterials within the cellulose matrix is crucial for maintaining consistent sensor performance and preventing aggregation, which could compromise the electrochemical performance of the sensor. Hemicellulose, another major component of LCB, is a heterogeneous group of polysaccharides that enhance the mechanical flexibility of plant cell walls. Its functional groups provide interactive sites for analytes, which augments its potential for improving electrochemical sensor performance. However, like cellulose, hemicellulose suffers from poor intrinsic electrical conductivity, meaning that chemical modifications such as grafting or blending with conductive materials are often necessary to improve its electrochemical properties. Additionally, hemicellulose stability under harsh environmental conditions remains a challenge, as it is prone to hydrolysis and degradation, limiting the operational lifespan of hemicellulose-based sensors. Lignin, a complex aromatic polymer within LCB, provides structural integrity and hydrophobicity to plant cell walls. Its chemically rich composition, including phenolic and methoxy groups, imparts a high degree of reactivity that can be used to detect analytes such as heavy metals and organic pollutants through oxidation and reduction reactions. Despite its potential, the poor solubility and hydrophobic nature of lignin complicate its integration into electrochemical sensors, requiring chemical modifications, such as functionalization, to enhance its dispersion and electrochemical properties. These modifications, however, often increase processing complexity. Furthermore, the susceptibility of lignin to microbial degradation presents a challenge to its long-term stability in sensor applications.

Stability and reproducibility in the fabrication of sensors based on LCB or their main biopolymers are significant challenges, particularly when scaling up for industrial or large-scale applications. These sensors, which rely on the varying properties of the biomaterials composing LCB, must maintain consistent performance over time and across production batches. Variations in biomass composition, environmental conditions, and fabrication methods can result in discrepancies in sensor reliability, affecting their efficiency and long-term viability. Furthermore, the hydrophilic nature of these materials makes them susceptible to moisture absorption, which can adversely impact sensor performance, especially in humid or fluctuating environments. Additionally, the biodegradability of several LCB components, under microbial activity or exposure to aggressive chemicals, presents challenges to their long-term durability in sensor applications. Strategies such as cross-linking, surface functionalization, and the application of protective coatings have been explored to address these limitations, but these solutions often add complexity and increase production costs, creating barriers to commercial scalability.

For biopolymer-based electrochemical sensors to be effectively used in practical applications, such as monitoring trace pollutants in environmental systems or detecting biomarkers in clinical diagnostics, their design and performance must meet several critical criteria. One of the primary goals is achieving low detection limits, ensuring that the sensor can identify even the smallest concentrations of target analytes. Additionally, rapid response times are important for real-time monitoring, as they enable immediate analysis and facilitate quick decision-making. However, these performance metrics alone are not sufficient. High selectivity is another key requirement, particularly when sensors are deployed in complex matrices, such as environmental samples (*e.g.*, water or air) or biological fluids (*e.g.*, blood or urine), which may contain interfering substances. To meet these demanding performance standards, optimizing the functionalization of LCB-based electrochemical sensors is essential. Functionalizing these biomaterials by introducing specific chemical groups or incorporating nanoparticles can enhance their electrical conductivity, stability, and sensitivity, making them better suited to detect target analytes even in the presence of other substances. By fine-tuning this functionalization, it is possible to improve sensor selectivity and minimize false positives or negatives, which is especially important when dealing with complex sample matrices that contain a wide range of chemicals. Moreover, for these sensors to be practically viable, particularly in real-world applications, miniaturization and portability are necessary. Compact devices that can be easily transported and deployed in various settings, such as field monitoring of air quality or on-site diagnostics in healthcare, are in high demand. Miniaturization allows these sensors to be integrated into handheld or wearable devices, enhancing their practicality and convenience for users. The portability of these sensors also ensures they can be used for continuous, long-term monitoring without requiring extensive infrastructure, making them ideal for applications in remote areas or dynamic environments. However, the design of these portable sensors must not compromise their sensitivity, selectivity, or response time; these aspects should remain consistent even as the device becomes more compact. The integration of advanced sensitive materials and conductive polymers with lignocellulosic substrates has shown promise in achieving these objectives. These materials can enhance the performance of LCB-based electrochemical sensors by improving electron transfer rates, enabling faster and more reliable interactions with target analytes.

7. Conclusion

Lignocellulosic biomass (LCB) is a next-generation, versatile, and renewable material with significant potential for (bio) sensing and energy-related applications. This review provides an overview of LCB, discussing its macromolecular structure, types, and sources, along with the characteristics and physicochemical properties of its major macromolecular components (cellulose, hemicellulose, and lignin). It also highlights the pretreatment methods commonly used to enhance biomass fractionation and extract its biopolymers. Despite its

remarkable properties, the potential of LCB as electrode modifiers for (bio)sensing applications remains underutilized. While some studies have explored the use of hemicellulose in sensor technology and energy-related applications, cellulose and lignin have attracted more attention, with numerous efforts focused on fabricating sensors and supercapacitors based on these components. Cellulose and lignin-based materials offer a versatile platform for developing analytical devices, demonstrating great promise in areas such as health diagnostics, environmental monitoring, food quality control, forensic analysis and physical sensing. Numerous studies have explored the potential of LCB and its structural biopolymers for developing electrochemical sensors. These studies successfully demonstrated how LCB-derived materials can enhance the electrochemical properties of sensors, improving their sensitivity, selectivity, and stability in various detection applications.

Data availability

This is a review and does not include any original data. All the data discussed and analyzed in this review are sourced from previously published studies, which are properly cited throughout this work. As a result, no new data were generated or analyzed for this work. The referenced publications serve as the source for all data presented. For further details, readers are encouraged to consult the original sources listed in the reference section.

Author contributions

Arnaud Kamdem Tamo: conceptualization, methodology, investigation, data curation, funding acquisition, writing – original draft, writing – review & editing; Ingo Doench: investigation, data curation, writing – review & editing; Gullit Deffo: investigation, data curation, writing – review & editing; Sherman Lesly Zambou Jiokeng: investigation, data curation, writing – review & editing; Giscard Doungmo: investigation, data curation, writing – review & editing; Cyrille Ghislain Fotsop: data curation, writing – review & editing; Ranil Clément Tonleu Temgoua: data curation, writing – review & editing; Alexandra Montembault: methodology, writing – review & editing, funding acquisition; Anatoli Serghei: methodology, writing – review & editing, funding acquisition; Evangéline Njanja: methodology, writing – review & editing; Ignas Kenfack Tonle: methodology, writing – review & editing; Anayancy Osorio-Madrazo: conceptualization, investigation, funding acquisition, supervision, methodology, writing – original draft, writing – review & editing.

Conflicts of interest

There are no conflicts to declare.

Acknowledgements

The Emmy Noether Programme of the German Research Foundation (DFG) (Grant Number: OS 497/6-1, AOBJ: 660891), the Walter Benjamin Programme of the German Research Foundation (DFG) (Grant Number: KA 6604/2-1, AOBJ: 708768), and the German Academic Exchange Service (DAAD) are gratefully acknowledged for their financial support. We thank the Open Access Publishing Fund of the University of Bayreuth for funding.

References

1 C. Wang, T. He, H. Zhou, Z. Zhang and C. Lee, *Bioelectron. Med.*, 2023, **9**, 17.
2 M. Javaid, A. Haleem, R. P. Singh, S. Rab and R. Suman, *Sens. Int.*, 2021, **2**, 100110.
3 A. P. F. Turner, *Chem. Soc. Rev.*, 2013, **42**, 3184.
4 E. Aparicio-Martínez, V. Osuna, R. B. Dominguez, A. Márquez-Lucero, E. A. Zaragoza-Contreras and A. Vega-Rios, *J. Nanomater.*, 2018, **2018**, 1–9.
5 C. Suh and Y.-B. Ko, *IEEE Trans. Consum. Electron.*, 2008, **54**, 1177–1184.
6 V. Veeramani, M. Sivakumar, S.-M. Chen, R. Madhu, H. R. Alamri, Z. A. Alothman, Md. S. A. Hossain, C.-K. Chen, Y. Yamauchi, N. Miyamoto and K. C.-W. Wu, *RSC Adv.*, 2017, **7**, 45668–45675.
7 M. C. Deussi Ngaha, V. Kougoum Tchieda, A. K. Tamo, G. Doungmo, E. Njanja and I. Kenfack Tonle, *Electroanalysis*, 2022, **34**, 1789–1801.
8 A. De La Escosura-Muñiz and A. Merkoçi, *ACS Nano*, 2012, **6**, 7556–7583.
9 G. Deffo, A. K. Tamo, C. G. Fotsop, H. H. B. Tchoumi, D. E. N. Talla, C. G. Wabo, M. C. N. Deussi, R. C. T. Temgoua, G. Doungmo, E. Njanja, I. K. Tonle, P. Puzari, C. Birkemeyer and E. Ngameni, *Coord. Chem. Rev.*, 2025, **536**, 216680.
10 J. Lei and H. Ju, *Chem. Soc. Rev.*, 2012, **41**, 2122.
11 V. Naresh and N. Lee, *Sensors*, 2021, **21**, 1109.
12 H. Golmohammadi, E. Morales-Narváez, T. Naghdi and A. Merkoçi, *Chem. Mater.*, 2017, **29**, 5426–5446.
13 D. Quesada-González and A. Merkoçi, *Biosens. Bioelectron.*, 2015, **73**, 47–63.
14 G. Deffo, R. Hazarika, M. C. Deussi Ngaha, M. Basumatary, S. Kalita, N. Hussain, E. Njanja, P. Puzari and E. Ngameni, *Anal. Methods*, 2023, **15**, 2456–2466.
15 A. V. Somba, T. Kamgaing, C. G. Fotsop, G. Deffo, B. W. Nkuigoua, R. F. T. Tagne, K. Y. Tajeu, R. C. T. Temgoua, E. Njanja and I. K. Tonle, *ChemistrySelect*, 2024, **9**, e202303250.
16 J. Rao, H. Gao, Y. Guan, W. Li and Q. Liu, *Carbohydr. Polym.*, 2019, **208**, 513–520.
17 J.-W. Han, B. Kim, J. Li and M. Meyyappan, *J. Phys. Chem. C*, 2012, **116**, 22094–22097.
18 J. Hu, Y. Wu, Q. Yang, Q. Zhou, L. Hui, Z. Liu, F. Xu and D. Ding, *Carbohydr. Polym.*, 2022, **275**, 118697.
19 X. Gong, C. Fu, N. Alam, Y. Ni, L. Chen, L. Huang and H.-C. Hu, *Ind. Crops Prod.*, 2022, **176**, 114412.
20 Q. Zhang, C. An, S. Fan, S. Shi, R. Zhang, J. Zhang, Q. Li, D. Zhang, X. Hu and J. Liu, *Nanotechnology*, 2018, **29**, 285501.

21 H. Abdali, B. Heli and A. Ajji, *Sensors*, 2019, **19**, 5215.
22 E. Núñez-Carmona, A. Bertuna, M. Abbatangelo, V. Sberveglieri, E. Comini and G. Sberveglieri, *Mater. Lett.*, 2019, **237**, 69–71.
23 C. I. L. Justino, A. C. Duarte and T. A. P. Rocha-Santos, *TrAC, Trends Anal. Chem.*, 2016, **85**, 36–60.
24 V. Mani, B. Devadas and S.-M. Chen, *Biosens. Bioelectron.*, 2013, **41**, 309–315.
25 R. Devasenathipathy, V. Mani, S.-M. Chen, S.-T. Huang, T.-T. Huang, C.-M. Lin, K.-Y. Hwa, T.-Y. Chen and B.-J. Chen, *Enzyme Microb. Technol.*, 2015, **78**, 40–45.
26 I. K. Tonle, E. Ngameni, F. M. M. Tchieno and A. Walcarius, *J. Solid State Electrochem.*, 2015, **19**, 1949–1973.
27 V. S. Bhat, S. Supriya and G. Hegde, *J. Electrochem. Soc.*, 2020, **167**, 037526.
28 E. Njanja, S. F. Mbokou, M. Pontie, M. Nacef and I. K. Tonle, *SN Appl. Sci.*, 2019, **1**, 513.
29 S. F. Mbokou, M. Pontié, J.-P. Bouchara, F. M. M. Tchieno, E. Njanja, A. Mogni, P. Y. Pontalier and I. K. Tonle, *Int. J. Electrochem.*, 2016, **2016**, 1–10.
30 W. S. Thet Tun, A. Saenchoopa, S. Daduang, J. Daduang, S. Kulchat and R. Patramanon, *RSC Adv.*, 2023, **13**, 9603–9614.
31 L. Cui, H. Xu, Y. An, M. Xu, Z. Lei and X. Jin, *Adv. Powder Technol.*, 2022, **33**, 103571.
32 M. Vasudevan, S. Remesh, V. Perumal, P. B. Raja, M. N. M. Ibrahim, S. C. B. Gopinath, H.-L. Lee, S. Karuppanan, M. Ovinis, N. Arumugam and R. S. Kumar, *Microchem. J.*, 2023, **195**, 109405.
33 Z. Li, M. Wang, L. Chen, H. Ji and H.-Y. Yu, *Sustainable Mater. Technol.*, 2023, **36**, e00649.
34 F. P. Tchoumi, A. K. Tamo, G. Doungmo, C. G. Fotsop, J. C. Kemmegne-Mbouguen and E. Ngameni, *J. Appl. Electrochem.*, 2024, **54**, 1901–1918.
35 C. N. Pecheu, S. L. Z. Jiokeng, A. K. Tamo, G. Doungmo, I. Doench, A. Osorio-Madrazo, I. K. Tonle and E. Ngameni, *Nanomaterials*, 2022, **12**, 2928.
36 J. J. K. Ngouoko, K. Y. Tajeu, C. G. Fotsop, A. K. Tamo, G. Doungmo, R. C. T. Temgoua, T. Kamgaing and I. K. Tonle, *Crystals*, 2022, **12**, 1189.
37 J. J. K. Ngouoko, K. Y. Tajeu, R. C. T. Temgoua, G. Doungmo, I. Doench, A. K. Tamo, T. Kamgaing, A. Osorio-Madrazo and I. K. Tonle, *Materials*, 2022, **15**, 4262.
38 D. V. T. Ebunang, K. Y. Tajeu, C. N. Pecheu, S. L. Z. Jiokeng, A. K. Tamo, I. Doench, A. Osorio-Madrazo, I. K. Tonle and E. Ngameni, *Sensors*, 2022, **22**, 6173.
39 R. Sabo, A. Yermakov, C. T. Law and R. Elhajjar, *J. Renewable Mater.*, 2016, **4**, 297–312.
40 M. Moyo, J. O. Okonkwo and N. M. Agyei, *Enzyme Microb. Technol.*, 2014, **56**, 28–34.
41 G. Kenne Dedzo, C. Péguy Nanseu-Njiki and E. Ngameni, *Talanta*, 2012, **99**, 478–486.
42 M. Moyo, J. O. Okonkwo and N. M. Agyei, *Electroanalysis*, 2013, **25**, 1946–1954.
43 S. Behera, R. Arora, N. Nandhagopal and S. Kumar, *Renewable Sustainable Energy Rev.*, 2014, **36**, 91–106.
44 J. Cai, Y. He, X. Yu, S. W. Banks, Y. Yang, X. Zhang, Y. Yu, R. Liu and A. V. Bridgwater, *Renewable Sustainable Energy Rev.*, 2017, **76**, 309–322.
45 L. G. Djemmoe, T. E. Njanja, M. C. Ngaha Deussi and K. I. Tonle, *C. R. Chim.*, 2016, **19**, 841–849.
46 C. P. Nanseu-Njiki, G. K. Dedzo and E. Ngameni, *J. Hazard. Mater.*, 2010, **179**, 63–71.
47 X. Ren, D. Chen, X. Meng, F. Tang, A. Du and L. Zhang, *Colloids Surf., B*, 2009, **72**, 188–192.
48 J. Wan, X. Yan, J. Ding and R. Ren, *Sens. Actuators, B*, 2010, **146**, 221–225.
49 N. Tripathi, C. D. Hills, R. S. Singh and C. J. Atkinson, *npj Clim. Atmos. Sci.*, 2019, **2**, 35.
50 S. K. Tiwari, M. Bystrzejewski, A. De Adhikari, A. Huczko and N. Wang, *Prog. Energy Combust. Sci.*, 2022, **92**, 101023.
51 K. Radotić, D. Djikanović, J. Simonović Radosavljević, N. Jović-Jovičić and Z. Mojović, *J. Electroanal. Chem.*, 2020, **862**, 114010.
52 T. Sha, X. Li, J. Liu, M. Sun, N. Wang, X. Bo, Y. Guo, Z. Hu and M. Zhou, *Sens. Actuators, B*, 2018, **277**, 195–204.
53 X. Li, H. Li, T. Liu, Y. Hei, M. Hassan, S. Zhang, J. Lin, T. Wang, X. Bo, H.-L. Wang, H. Li and M. Zhou, *Sens. Actuators, B*, 2018, **255**, 3248–3256.
54 F. Yang, W. Fu, J. Liu, W. Ding and W. Sun, *Int. J. Electrochem. Sci.*, 2023, **18**, 100364.
55 A. Demirbas, in *Biorefineries Green Energy and Technology*, Springer, London, 2010, pp. 115–133.
56 A. K. Tamo, *J. Mater. Chem. B*, 2024, **12**, 7692–7759.
57 F. H. Isikgor and C. R. Becer, *Polym. Chem.*, 2015, **6**, 4497–4559.
58 M. Mujtaba, L. Fernandes Fraceto, M. Fazeli, S. Mukherjee, S. M. Savassa, G. Araujo De Medeiros, A. Do Espírito Santo Pereira, S. D. Mancini, J. Lipponen and F. Vilaplana, *J. Cleaner Prod.*, 2023, **402**, 136815.
59 R. S. Abolore, S. Jaiswal and A. K. Jaiswal, *Carbohydr. Polym. Technol. Appl.*, 2024, **7**, 100396.
60 G. F. K. Nindjio, R. F. T. Tagne, S. L. Z. Jiokeng, C. G. Fotsop, A. Bopda, G. Doungmo, R. C. T. Temgoua, I. Doench, E. T. Njoyim, A. K. Tamo, A. Osorio-Madrazo and I. K. Tonle, *Polymers*, 2022, **14**, 3776.
61 A. K. Tamo, L. D. W. Djouonkep and N. B. S. Selabi, *Int. J. Biol. Macromol.*, 2024, **270**, 132123.
62 L. F. Ballesteros, M. Michelin, A. A. Vicente, J. A. Teixeira and M. Â. Cerqueira, *Lignocellulosic Materials and Their Use in Bio-Based Packaging*, Springer International Publishing, Cham, 2018.
63 D. Carpenter, T. L. Westover, S. Czernik and W. Jablonski, *Green Chem.*, 2014, **16**, 384–406.
64 G. Izydorczyk, D. Skrzypczak, M. Mironiuk, K. Mikula, M. Samoraj, F. Gil, R. Taf, K. Moustakas and K. Chojnacka, *Sci. Total Environ.*, 2024, **923**, 171343.
65 T. Damm, U. Commandeur, R. Fischer, B. Usadel and H. Klose, *Process Biochem.*, 2016, **51**, 288–296.
66 W. Li, L. Zhu, Y. Xu, G. Wang, T. Xu and C. Si, *Adv. Mater.*, 2024, 2415761.
67 M. B. Figueirêdo, I. Hita, P. J. Deuss, R. H. Venderbosch and H. J. Heeres, *Green Chem.*, 2022, **24**, 4680–4702.

68 A. Zoghlami and G. Paës, *Front. Chem.*, 2019, **7**, 874.
69 Y.-H. P. Zhang, *J. Ind. Microbiol. Biotechnol.*, 2008, **35**, 367–375.
70 L.-Z. Huang, M.-G. Ma, X.-X. Ji, S.-E. Choi and C. Si, *Front. Bioeng. Biotechnol.*, 2021, **9**, 690773.
71 J. Berglund, D. Mikkelsen, B. M. Flanagan, S. Dhital, S. Gaunitz, G. Henriksson, M. E. Lindström, G. E. Yakubov, M. J. Gidley and F. Vilaplana, *Nat. Commun.*, 2020, **11**, 4692.
72 M. F. Qaseem, H. Shaheen and A.-M. Wu, *Renewable Sustainable Energy Rev.*, 2021, **144**, 110996.
73 R. Figueiredo, P. Araújo, J. P. P. Llerena and P. Mazzafera, *Food Energy Secur.*, 2019, **8**, e00163.
74 J. Rao, Z. Lv, G. Chen and F. Peng, *Prog. Polym. Sci.*, 2023, **140**, 101675.
75 E. Ahmad and K. K. Pant, in *Waste Biorefinery*, Elsevier, 2018, pp. 409–444.
76 O. Y. Abdelaziz, D. P. Brink, J. Prothmann, K. Ravi, M. Sun, J. García-Hidalgo, M. Sandahl, C. P. Hulteberg, C. Turner, G. Lidén and M. F. Gorwa-Grauslund, *Biotechnol. Adv.*, 2016, **34**, 1318–1346.
77 M. H. Tanis, O. Wallberg, M. Galbe and B. Al-Rudainy, *Molecules*, 2023, **29**, 98.
78 D. Tarasov, M. Leitch and P. Fatehi, *Biotechnol. Biofuels*, 2018, **11**, 269.
79 D. L. Lynch and C. C. Lynch, *Nature*, 1958, **181**, 1478–1479.
80 S. Lee, M. Kang, J.-H. Bae, J.-H. Sohn and B. H. Sung, *Front. Bioeng. Biotechnol.*, 2019, **7**, 209.
81 B. Lü, Q. Gao, P. Li, J. Rao, Z. Lv, M. Shi, Y. Hu, X. Hao, G. Chen, M. Yin and F. Peng, *Cell Rep. Phys. Sci.*, 2022, **3**, 101015.
82 M. M. Alam, A. Greco, Z. Rajabimashhadi and C. Esposito Corcione, *Cleaner Mater.*, 2024, **13**, 100253.
83 M. Martín, M. Taifouris and G. Galán, *Bioresour. Technol.*, 2023, **385**, 129397.
84 G. Velvizhi, P. J. Jacqueline, N. P. Shetti, L. K, G. Mohanakrishna and T. M. Aminabhavi, *J. Environ. Manage.*, 2023, **345**, 118527.
85 M. K. Awasthi, T. Sar, S. C. Gowd, K. Rajendran, V. Kumar, S. Sarsaiya, Y. Li, R. Sindhu, P. Binod, Z. Zhang, A. Pandey and M. J. Taherzadeh, *Fuel*, 2023, **342**, 127790.
86 T. Raj, K. Chandrasekhar, A. Naresh Kumar and S.-H. Kim, *Renewable Sustainable Energy Rev.*, 2022, **158**, 112130.
87 V. B. Agbor, N. Cicek, R. Sparling, A. Berlin and D. B. Levin, *Biotechnol. Adv.*, 2011, **29**, 675–685.
88 R. Huang, R. Su, W. Qi and Z. He, *Bioenergy Res.*, 2011, **4**, 225–245.
89 C. Veluchamy, A. S. Kalamdhad and B. H. Gilroyed, in *Handbook of Environmental Materials Management*, ed. C. M. Hussain, Springer International Publishing, Cham, 2018, pp. 1–19.
90 A. K. Kumar and S. Sharma, *Bioresour. Bioprocess.*, 2017, **4**, 7.
91 H. Rezaei, M. Tajilrou, J. S. Lee, K. Singaraveloo, A. Lau and S. Sokhansanj, *Particuology*, 2024, **86**, 182–187.
92 V. Dhyani and T. Bhaskar, *Renewable Energy*, 2018, **129**, 695–716.
93 J. S. Kim, Y. Y. Lee and T. H. Kim, *Bioresour. Technol.*, 2016, **199**, 42–48.
94 X. Chen, R. Zhai, K. Shi, Y. Yuan, B. E. Dale, Z. Gao and M. Jin, *Ind. Crops Prod.*, 2018, **124**, 719–725.
95 R. Kataria, R. Ruhal, R. Babu and S. Ghosh, *Chem. Eng. J.*, 2013, **230**, 36–47.
96 C. Arce and L. Kratky, *iScience*, 2022, **25**, 104610.
97 D. Fougere, K. Clarke, Y. Zhao and K. Li, *Biomass Bioenergy*, 2015, **80**, 17–29.
98 Y. Su, X. Yu, Y. Sun, G. Wang, H. Chen and G. Chen, *Sci. Rep.*, 2018, **8**, 5385.
99 A. Anu, R. C. Kuhad, A. Rapoport, V. Kumar, D. Singh, V. Kumar, S. K. Tiwari, S. Ahlawat and B. Singh, *Crit. Rev. Environ. Sci. Technol.*, 2024, **54**, 771–796.
100 M. Si, D. Liu, M. Liu, X. Yan, C. Gao, L. Chai and Y. Shi, *Bioresour. Technol.*, 2019, **272**, 275–280.
101 Z. Wu, K. Peng, Y. Zhang, M. Wang, C. Yong, L. Chen, P. Qu, H. Huang, E. Sun and M. Pan, *Mater. Today Bio*, 2022, **16**, 100445.
102 S. Chen, X. Zhang, D. Singh, H. Yu and X. Yang, *Biofuels*, 2010, **1**, 177–199.
103 M. Taylor, H. Alabdrabalameer and V. Skoulou, *Sustainability*, 2019, **11**, 3604.
104 A. Singhal, C. Roslander, A. Goel, A. Ismailov, B. Erdei, O. Wallberg, J. Konttinen and T. Joronen, *Chem. Eng. J.*, 2024, **489**, 151298.
105 Y. Liang, D. Tong, K. Hou, Z. Li, L. Zhang, L. Shao, Z. Wu, Y. Huang and P. Zhan, *Biomass Convers. Biorefin.*, 2025, DOI: 10.1007/s13399-025-06793-1.
106 A. O. Campos, E. A. Asevedo, P. F. Souza Filho and E. S. D. Santos, *Biomass*, 2024, **4**, 92–106.
107 C.-Y. Ma, L.-H. Xu, Q. Sun, X.-J. Shen, J.-L. Wen and T.-Q. Yuan, *Chem. Eng. J.*, 2022, **450**, 138315.
108 Y. Feng, L. Tao, Y. He, Q. Jin, C. Kuai, Y. Zheng, M. Li, Q. Hou, Z. Zheng, F. Lin and H. Huang, *J. Mater. Chem. A*, 2019, **7**, 26954–26965.
109 A. K. Tamo, I. Doench, A. Morales Helguera, D. Hoenders, A. Walther and A. Osorio-Madrazo, *Polymers*, 2020, **12**, 1522.
110 E. B. Moya, B. Syhler, G. Dragone and S. I. Mussatto, *Enzyme Microb. Technol.*, 2024, **175**, 110403.
111 S. Meenakshisundaram, A. Fayeulle, E. Léonard, C. Ceballos, X. Liu and A. Pauss, *Appl. Microbiol.*, 2022, **2**, 716–734.
112 X. Li, Y. Shi, W. Kong, J. Wei, W. Song and S. Wang, *Energy Rep.*, 2022, **8**, 696–709.
113 P. Nargotra, V. Sharma, Y.-C. Lee, Y.-H. Tsai, Y.-C. Liu, C.-J. Shieh, M.-L. Tsai, C.-D. Dong and C.-H. Kuo, *Catalysts*, 2022, **13**, 83.
114 *Microbial Enzymes in Bioconversions of Biomass*, ed. V. K. Gupta, Springer International Publishing : Imprint: Springer, Cham, 1st edn, 2016.
115 C. Dupont, R. Chiriac, G. Gauthier and F. Toche, *Fuel*, 2014, **115**, 644–651.
116 C. Mayer-Laigle, N. Blanc, R. K. Rajaonarivony and X. Rouau, *Bioengineering*, 2018, **5**, 41.

117 D. E. Priyanto, S. Ueno, K. Hashida and H. Kasai, *Adv. Powder Technol.*, 2017, **28**, 1660–1667.
118 J. S. Tumuluru and D. J. Heikkila, *Bioengineering*, 2019, **6**, 12.
119 P. Karinkanta, A. Ämmälä, M. Illikainen and J. Niinimäki, *Biomass Bioenergy*, 2018, **113**, 31–44.
120 Z. Cui, J. Lin, C. Zhan, J. Wu, S. Shen, J. Si and Q. Wang, *J. Biomater. Sci., Polym. Ed.*, 2020, **31**, 561–577.
121 J.-A. Choi, J.-H. Hwang, B. A. Dempsey, R. A. I. Abou-Shanab, B. Min, H. Song, D. S. Lee, J. R. Kim, Y. Cho, S. Hong and B.-H. Jeon, *Energy Environ. Sci.*, 2011, **4**, 3513.
122 X. Liu, H. Sun, T. Mu, M. L. Fauconnier and M. Li, *Food Chem.*, 2023, **413**, 135675.
123 Z. Pang, P. Wang and C. Dong, *Cellulose*, 2018, **25**, 7053–7064.
124 L. Desrochers, D. Puttock and M. Ryans, *Biomass Bioenergy*, 1993, **5**, 401–411.
125 J. Viell, H. Wulfhorst, T. Schmidt, U. Commandeur, R. Fischer, A. Spiess and W. Marquardt, *Bioresour. Technol.*, 2013, **146**, 144–151.
126 W. Stelte, A. R. Sanadi, L. Shang, J. K. Holm, J. Ahrenfeldt and U. B. Henriksen, *BioResources*, 2012, **7**, 4451–4490.
127 P. Basu, *Biomass Gasification, Pyrolysis, and Torrefaction: Practical Design and Theory*, Academic Press Is and Imprint of Elsevier, London, United Kingdom ; San Diego, CA, United States, 3rd edn, 2018.
128 T. G. Bridgeman, J. M. Jones, I. Shield and P. T. Williams, *Fuel*, 2008, **87**, 844–856.
129 J. M. C. Ribeiro, R. Godina, J. C. D. O. Matias and L. J. R. Nunes, *Sustainability*, 2018, **10**, 2323.
130 M. Phanphanich and S. Mani, *Bioresour. Technol.*, 2011, **102**, 1246–1253.
131 E. Calcio Gaudino, G. Cravotto, M. Manzoli and S. Tabasso, *Green Chem.*, 2019, **21**, 1202–1235.
132 Y.-C. Sun, X.-N. Liu, T.-T. Wang, B.-L. Xue and R.-C. Sun, *ACS Sustainable Chem. Eng.*, 2019, **7**, 13062–13072.
133 A. Duque, P. Manzanares and M. Ballesteros, *Renewable Energy*, 2017, **114**, 1427–1441.
134 D. Konan, E. Koffi, A. Ndao, E. C. Peterson, D. Rodrigue and K. Adjallé, *Energies*, 2022, **15**, 3002.
135 Y.-S. Cheng, Y. Zheng, C. W. Yu, T. M. Dooley, B. M. Jenkins and J. S. VanderGheynst, *Appl. Biochem. Biotechnol.*, 2010, **162**, 1768–1784.
136 H. Xu, B. Li and X. Mu, *Ind. Eng. Chem. Res.*, 2016, **55**, 8691–8705.
137 A. Shahbazi and B. Zhang, in *Bioalcohol Production*, Elsevier, 2010, pp. 143–158.
138 R. Harun and M. K. Danquah, *Process Biochem.*, 2011, **46**, 304–309.
139 M. H. Rubiyah, K. Melethil, S. Varghese, M. Kurian, S. Babu, L. Jojo and B. Thomas, *Carbohydr. Polym. Technol. Appl.*, 2023, **6**, 100374.
140 I. G. Audu, N. Brosse, H. Winter, A. Hoffmann, M. Bremer, S. Fischer and M.-P. Laborie, *Polymers*, 2018, **10**, 619.
141 B.-W. Koo, H.-Y. Kim, N. Park, S.-M. Lee, H. Yeo and I.-G. Choi, *Biomass Bioenergy*, 2011, **35**, 1833–1840.
142 V. A. Barbash, O. V. Yaschenko and O. M. Shniruk, *Nanoscale Res. Lett.*, 2017, **12**, 241.
143 A. Brandt, J. Gräsvik, J. P. Hallett and T. Welton, *Green Chem.*, 2013, **15**, 550.
144 A. M. Asim, M. Uroos and N. Muhammad, *RSC Adv.*, 2020, **10**, 44003–44014.
145 H. Abushammala, J. F. Pontes, G. H. Gomes, A. Osorio-Madrazo, R. M. S. M. Thiré, F. V. Pereira and M.-P. G. Laborie, *Holzforschung*, 2015, **69**, 1059–1067.
146 Z. Zhou, D. Ouyang, D. Liu and X. Zhao, *Bioresour. Technol.*, 2023, **367**, 128208.
147 Z. Yuan, G. E. Klinger, S. Nikafshar, Y. Cui, Z. Fang, M. Alherech, S. Goes, C. Anson, S. K. Singh, B. Bals, D. B. Hodge, M. Nejad, S. S. Stahl and E. L. Hegg, *ACS Sustainable Chem. Eng.*, 2021, **9**, 1118–1127.
148 C. G. Fotsop, D. R. Tchuifon Tchuifon, P. A. N. Kouteu, K. L. T. Nguena, A. K. Tamo, D. N. Dongmo, S. G. M. Mafo, F. H. K. Djioko, R. M. Mouangue and I. K. Tonle, *Biomass Convers. Biorefin.*, 2024, DOI: **10.1007/s13399-024-05331-9**.
149 D. Z. Haddis, M. Chae, J. Asomaning and D. C. Bressler, *Carbohydr. Polym.*, 2024, **323**, 121460.
150 K. C. Badgujar, R. Dange and B. M. Bhanage, *J. Indian Chem. Soc.*, 2021, **98**, 100018.
151 A. Demirbaş, *Energy Convers. Manage.*, 2001, **42**, 279–294.
152 H. Lv, L. Yan, M. Zhang, Z. Geng, M. Ren and Y. Sun, *Chem. Eng. Technol.*, 2013, **36**, 1899–1906.
153 F. Teymouri, L. Laureano-Perez, H. Alizadeh and B. E. Dale, *Bioresour. Technol.*, 2005, **96**, 2014–2018.
154 M. T. Holtzapple, J. E. Lundeen, R. Sturgis, J. E. Lewis and B. E. Dale, *Appl. Biochem. Biotechnol.*, 1992, **34–35**, 5–21.
155 A. Kallioinen, A. Vaari, M. Rättö, J. Konn, M. Siika-aho and L. Viikari, *J. Biotechnol.*, 2003, **103**, 67–76.
156 L. Lin, R. Yan, Y. Liu and W. Jiang, *Bioresour. Technol.*, 2010, **101**, 8217–8223.
157 H. Yu, G. Guo, X. Zhang, K. Yan and C. Xu, *Bioresour. Technol.*, 2009, **100**, 5170–5175.
158 J. S. Schilling, J. Ai, R. A. Blanchette, S. M. Duncan, T. R. Filley and U. W. Tschirner, *Bioresour. Technol.*, 2012, **116**, 147–154.
159 Q. Guo, X. Chen and H. Liu, *Fuel*, 2012, **94**, 551–555.
160 D. Gera, M. P. Mathur, M. C. Freeman and A. Robinson, *Energy Fuels*, 2002, **16**, 1523–1532.
161 Z. Wang, C. J. Lim, J. R. Grace, H. Li and M. R. Parise, *Bioresour. Technol.*, 2017, **244**, 281–288.
162 B. C. Vidal, B. S. Dien, K. C. Ting and V. Singh, *Appl. Biochem. Biotechnol.*, 2011, **164**, 1405–1421.
163 *Engineering and Science of Biomass Feedstock Production and Provision*, ed. Y. Shastri, A. Hansen, L. Rodríguez and K. C. Ting, Springer New York, New York, NY, 2014.
164 P. S. Lam, S. Sokhansanj, X. Bi, C. J. Lim, L. J. Naimi, M. Hoque, S. Mani, A. R. Womac, S. Narayan and X. P. Ye, *Appl. Eng. Agric.*, 2008, **24**, 351–358.
165 H. Rezaei, C. J. Lim, A. Lau and S. Sokhansanj, *Powder Technol.*, 2016, **301**, 737–746.
166 Z. Liu, B. Mi, Z. Jiang, B. Fei, Z. Cai and X. Liu, *Renewable Energy*, 2016, **86**, 1–7.

167 *The Handbook of Biomass Combustion and Co-firing*, ed. J. Koppejan and S. Van Loo, Routledge, 0 edn, 2012.
168 J. Shankar Tumuluru, S. Sokhansanj, J. R. Hess, C. T. Wright and R. D. Boardman, *Ind. Biotechnol.*, 2011, **7**, 384–401.
169 S. Basu, U. S. Shivhare and A. S. Mujumdar, *Drying Technol.*, 2006, **24**, 917–930.
170 E. E. Thybring, S. V. Glass and S. L. Zelinka, *Forests*, 2019, **10**, 704.
171 A. K. Tamo, I. Doench, L. Walter, A. Montembault, G. Sudre, L. David, A. Morales-Helguera, M. Selig, B. Rolauffs, A. Bernstein, D. Hoenders, A. Walther and A. Osorio-Madrazo, *Polymers*, 2021, **13**, 1663.
172 S. Marquez-Bravo, I. Doench, P. Molina, F. E. Bentley, A. K. Tamo, R. Passieux, F. Lossada, L. David and A. Osorio-Madrazo, *Polymers*, 2021, **13**, 1563.
173 C. Lai, Z. Zhou, L. Zhang, X. Wang, Q. Zhou, Y. Zhao, Y. Wang, X.-F. Wu, Z. Zhu and H. Fong, *J. Power Sources*, 2014, **247**, 134–141.
174 M. E. Jawerth, C. J. Brett, C. Terrier, P. T. Larsson, M. Lawoko, S. V. Roth, S. Lundmark and M. Johansson, *ACS Appl. Polym. Mater.*, 2020, **2**, 668–676.
175 P. E. Mason, L. I. Darvell, J. M. Jones and A. Williams, *Energy Fuels*, 2016, **30**, 2158–2163.
176 S. V. Vassilev, D. Baxter, L. K. Andersen and C. G. Vassileva, *Fuel*, 2010, **89**, 913–933.
177 S. V. Vassilev, C. G. Vassileva, Y.-C. Song, W.-Y. Li and J. Feng, *Fuel*, 2017, **208**, 377–409.
178 O. Olatunji, S. Akinlabi, A. Oluseyi, M. Peter and N. Madushele, *IOP Conf. Ser.:Mater. Sci. Eng.*, 2018, **413**, 012054.
179 D. K. Sarkar, *Thermal Power Plant: Design and Operation*, Elsevier, Amsterdam, 2015.
180 A. I. Lawal, A. E. Aladejare, M. Onifade, S. Bada and M. A. Idris, *Int. J. Coal Sci. Technol.*, 2021, **8**, 124–140.
181 A. Bichot, M. Lerosty, L. Geirnaert, V. Méchin, H. Carrère, N. Bernet, J.-P. Delgenès and D. García-Bernet, *Molecules*, 2019, **24**, 3885.
182 M. C. D. Ngaha, E. Njanja, G. Doungmo, A. K. Tamo and I. K. Tonle, *Int. J. Biomater.*, 2019, **2019**, 1–18.
183 L. D. W. Djouonkep, A. K. Tamo, I. Doench, N. B. S. Selabi, E. M. Ilunga, A. R. K. Lenwoue, M. Gauthier, Z. Cheng and A. Osorio-Madrazo, *Molecules*, 2022, **27**, 325.
184 L. Djouonkep, A. Tchameni, N. Selabi, A. K. Tamo, I. Doench, Z. Cheng, M. Gauthier, B. Xie and A. Osorio-Madrazo, *Int. J. Mol. Sci.*, 2022, **23**, 8967.
185 Z. Sun, B. Fridrich, A. De Santi, S. Elangovan and K. Barta, *Chem. Rev.*, 2018, **118**, 614–678.
186 D. Kim, J. M. Kim, Y. Jeon, J. Lee, J. Oh, W. Hooch Antink, D. Kim and Y. Piao, *Sens. Actuators, B*, 2018, **259**, 50–58.
187 J. Poisson and K. Zhang, *Acc. Mater. Res.*, 2024, **5**, 920–932.
188 D. O. Dorohoi, M. Postolache, C. D. Nechifor, D. G. Dimitriu, R. M. Albu, I. Stoica and A. I. Barzic, *Molecules*, 2023, **28**, 2955.
189 H. Liu, J. Ding, K. Zhang and L. Ding, *TrAC, Trends Anal. Chem.*, 2019, **118**, 315–337.
190 Y. Shi, W. Li, X. Hu, X. Zhang, X. Huang, Z. Li, X. Zhai, T. Shen, J. Shi, Y. He and X. Zou, *Food Chem.*, 2024, **434**, 137260.
191 S. Long, Y. Feng, F. He, J. Zhao, T. Bai, H. Lin, W. Cai, C. Mao, Y. Chen, L. Gan, J. Liu, M. Ye, X. Zeng and M. Long, *Nano Energy*, 2021, **85**, 105973.
192 L. Durai, A. Gopalakrishnan and S. Badhulika, *Anal. Chim. Acta*, 2021, **1169**, 338598.
193 Z. Deng, Z. Wu, H. Rokni, Z. Yin, J. Lin, H. Zhang and S. Cheraghi, *Chemosphere*, 2022, **309**, 136568.
194 W. Hu, S. Chen, L. Liu, B. Ding and H. Wang, *Sens. Actuators, B*, 2011, **157**, 554–559.
195 C. Hu, X. Bai, Y. Wang, W. Jin, X. Zhang and S. Hu, *Anal. Chem.*, 2012, **84**, 3745–3750.
196 Ş. F. Küçükayar, V. Şimşek, M. O. Caglayan, Z. Üstündağ and S. Şahin, *Microchem. J.*, 2023, **193**, 109023.
197 X. Cui, Y. Zhang, Z. Chen, H. Xiao, R. Xiong and C. Huang, *Int. J. Biol. Macromol.*, 2023, **252**, 126431.
198 I. K. Tonle, S. Letaief, E. Ngameni, A. Walcarius and C. Detellier, *Electroanalysis*, 2011, **23**, 245–252.
199 T. B. Tran, S. J. Son and J. Min, *BioChip J.*, 2016, **10**, 318–330.
200 N. Reta, C. P. Saint, A. Michelmore, B. Prieto-Simon and N. H. Voelcker, *ACS Appl. Mater. Interfaces*, 2018, **10**, 6055–6072.
201 C. B. Njine-Bememba, G. K. Dedzo, C. P. Nanseu-Njiki and E. Ngameni, *Holzforschung*, 2015, **69**, 347–356.
202 B. Ngouné, M. Pengou, C. P. Nanseu-Njiki and E. Ngameni, *Corros. Eng., Sci. Technol.*, 2020, **55**, 138–144.
203 B. Ngouné, M. Pengou, A. M. Nouteza, C. P. Nanseu-Njiki and E. Ngameni, *ACS Omega*, 2019, **4**, 9081–9091.
204 C.-M. Kuan, R. L. York and C.-M. Cheng, *Sci. Rep.*, 2015, **5**, 18570.
205 Y. Zhang, F. Wen, Z. Huang, J. Tan, Z. Zhou, K. Yuan and H. Wang, *J. Electroanal. Chem.*, 2017, **806**, 150–157.
206 D. Chen, H. Zhou, H. Li, J. Chen, S. Li and F. Zheng, *Sci. Rep.*, 2017, **7**, 14985.
207 M. Li, Y. Qi, Y. Ding, Q. Zhao, J. Fei and J. Zhou, *Sens. Actuators, B*, 2012, **168**, 329–335.
208 S. Yallappa, M. Shivakumar, K. L. Nagashree, M. S. Dharmaprakash, A. Vinu and G. Hegde, *J. Electrochem. Soc.*, 2018, **165**, H614–H619.
209 J. J. Arroyo-Gómez, D. Villarroel-Rocha, K. C. De Freitas-Araújo, C. A. Martínez-Huitle and K. Sapag, *J. Electroanal. Chem.*, 2018, **822**, 171–176.
210 N. Jayarambabu, N. V. S. S. Seshagiri Rao, M. K. C. Sivalenka, K. Saraswathi, B. S. Naick, N. Anitha and T. V. Rao, *Diamond Relat. Mater.*, 2024, **144**, 110959.
211 B. Zhang, X. Li, Z. Wang, H. Ren, J. Wang, Q. Chen, Y. Cai, K. Quan, M. Liu, M. Pan and G. Fang, *Talanta*, 2024, **277**, 126395.
212 O. Fatibello-Filho, *Talanta*, 2001, **55**, 685–692.
213 I. Cruz Vieira, *Talanta*, 2000, **52**, 681–689.
214 O. Fatibello-Filho and I. Cruz Vieira, *Fresenius' J. Anal. Chem.*, 2000, **368**, 338–343.
215 S. Liu, T. Han, Z. Wang, T. Fei and T. Zhang, *Electroanalysis*, 2019, **31**, 527–534.

216 A. N. Vu, L. H. Nguyen, H.-C. V. Tran, K. Yoshimura, T. D. Tran, H. Van Le and N.-U. T. Nguyen, *RSC Adv.*, 2024, **14**, 2048–2060.
217 V. P. Kalpana and V. T. Perarasu, *J. Mol. Struct.*, 2020, **1217**, 128350.
218 B. Chieng, S. Lee, N. Ibrahim, Y. Then and Y. Loo, *Polymers*, 2017, **9**, 355.
219 A. M. Dube, B. J. Daba and M. D. Muleta, *J. Exp. Nanosci.*, 2023, **18**, 2199989.
220 E. Galiwango, N. S. Abdel Rahman, A. H. Al-Marzouqi, M. M. Abu-Omar and A. A. Khaleel, *Heliyon*, 2019, **5**, e02937.
221 Q. He, Y. Bai, Y. Lu, B. Cui, Z. Huang, Q. Yang, D. Jiang and D. Shao, *Biomass Convers. Biorefin.*, 2024, 27745–27754.
222 M. Raza, J. Mustafa, A. H. Al-Marzouqi and B. Abu-Jdayil, *Int. J. Thermofluids*, 2024, **21**, 100548.
223 M. Raza, B. Abu-Jdayil, F. Banat and A. H. Al-Marzouqi, *ACS Omega*, 2022, **7**, 25366–25379.
224 J. Mao, H. Abushammala, H. Hettegger, T. Rosenau and M.-P. Laborie, *Polymers*, 2017, **9**, 473.
225 P. Mali and A. P. Sherje, *Carbohydr. Polym.*, 2022, **275**, 118668.
226 J. Mao, A. Osorio-Madrazo and M.-P. Laborie, *Cellulose*, 2013, **20**, 1829–1840.
227 K. Zhang, A. Barhoum, C. Xiaoqing, H. Li and P. Samyn, in *Handbook of Nanofibers*, ed. A. Barhoum, M. Bechelany and A. S. H. Makhlouf, Springer International Publishing, Cham, 2019, pp. 409–449.
228 N. Carter, I. Grant, M. Dewey, M. Bourque and D. J. Neivandt, *Front. Nanotechnol.*, 2021, **3**, 729743.
229 M. Faisal, M. Žmirić, N. Kim, S. Bruun, L. Mariniello, M. Famiglietti, H. Bordallo, J. Kirkensgaard, B. Jørgensen, P. Ulvskov, K. Hebelstrup and A. Blennow, *Coatings*, 2023, **13**, 1573.
230 H. Koga, K. Nagashima, Y. Huang, G. Zhang, C. Wang, T. Takahashi, A. Inoue, H. Yan, M. Kanai, Y. He, K. Uetani, M. Nogi and T. Yanagida, *ACS Appl. Mater. Interfaces*, 2019, **11**, 15044–15050.
231 N. Forsman, A. Lozhechnikova, A. Khakalo, L.-S. Johansson, J. Vartiainen and M. Österberg, *Carbohydr. Polym.*, 2017, **173**, 392–402.
232 M. P. Arrieta, E. Fortunati, N. Burgos, M. A. Peltzer, J. López and L. Peponi, in *Multifunctional Polymeric Nanocomposites Based on Cellulosic Reinforcements*, Elsevier, 2016, pp. 205–252.
233 A. K. Tamo, T. A. Tran, I. Doench, S. Jahangir, A. Lall, L. David, C. Peniche-Covas, A. Walther and A. Osorio-Madrazo, *Materials*, 2022, **15**, 6039.
234 D. Srivastava, M. S. Kuklin, J. Ahopelto and A. J. Karttunen, *Carbohydr. Polym.*, 2020, **243**, 116440.
235 S. Jackson and J. Chen, *AATCC J. Res.*, 2024, **11**, 151–170.
236 Y. El-Ghoul, A. S. Altuwayjiri and G. A. Alharbi, *RSC Adv.*, 2024, **14**, 26183–26197.
237 C. Trilokesh and K. B. Uppuluri, *Sci. Rep.*, 2019, **9**, 16709.
238 V. U. Siddiqui, T. M. Almehjani, S. M. Sapuan, T. Jamal, R. A. Ilyas, S. M. Eldin, A. Khan and Y. Jameel, *J. Nat. Fibers*, 2024, **21**, 2299943.
239 A. S. Hozman-Manrique, A. J. Garcia-Brand, M. Hernández-Carrión and A. Porras, *Polymers*, 2023, **15**, 664.
240 A. Osorio-Madrazo and M. Laborie, in *Biopolymer Nanocomposites*, ed. A. Dufresne, S. Thomas and L. A. Pothen, Wiley, 1st edn, 2013, pp. 411–436.
241 Z. Lu, H. Zhang, M. Toivakka and C. Xu, *Int. J. Biol. Macromol.*, 2024, **267**, 131490.
242 Z. Tang, X. Lin, M. Yu, A. K. Mondal and H. Wu, *Int. J. Biol. Macromol.*, 2024, **259**, 129081.
243 K. S. Kontturi, K.-Y. Lee, M. P. Jones, W. W. Sampson, A. Bismarck and E. Kontturi, *Cellulose*, 2021, **28**, 6619–6628.
244 M. Eichers, D. Bajwa, J. Shojaeiarani and S. Bajwa, *Ind. Crops Prod.*, 2022, **183**, 114981.
245 J. Yang, C.-R. Han, J.-F. Duan, M.-G. Ma, X.-M. Zhang, F. Xu and R.-C. Sun, *Cellulose*, 2013, **20**, 227–237.
246 P. Samyn, A. Meftahi, S. A. Geravand, M. E. M. Heravi, H. Najarzadeh, M. S. K. Sabery and A. Barhoum, *Int. J. Biol. Macromol.*, 2023, **231**, 123316.
247 M. Kaczmarek and A. M. Białkowska, *J. Nanobiotechnol.*, 2025, **23**, 82.
248 L. Solhi, V. Guccini, K. Heise, I. Solala, E. Niinivaara, W. Xu, K. Mihhels, M. Kröger, Z. Meng, J. Wohlert, H. Tao, E. D. Cranston and E. Kontturi, *Chem. Rev.*, 2023, **123**, 1925–2015.
249 C. Salas, T. Nypelö, C. Rodriguez-Abreu, C. Carrillo and O. J. Rojas, *Curr. Opin. Colloid Interface Sci.*, 2014, **19**, 383–396.
250 T. Agarwal, S. N. G. H. Narayana, K. Pal, K. Pramanik, S. Giri and I. Banerjee, *Int. J. Biol. Macromol.*, 2015, **75**, 409–417.
251 I. Doench, T. Tran, L. David, A. Montembault, E. Viguier, C. Gorzelanny, G. Sudre, T. Cachon, M. Louback-Mohamed, N. Horbelt, C. Peniche-Covas and A. Osorio-Madrazo, *Biomimetics*, 2019, **4**, 19.
252 A. Osorio-Madrazo, M. Eder, M. Rueggeberg, J. K. Pandey, M. J. Harrington, Y. Nishiyama, J.-L. Putaux, C. Rochas and I. Burgert, *Biomacromolecules*, 2012, **13**, 850–856.
253 I. Doench, M. Torres-Ramos, A. Montembault, P. Nunes De Oliveira, C. Halimi, E. Viguier, L. Heux, R. Siadous, R. Thiré and A. Osorio-Madrazo, *Polymers*, 2018, **10**, 1202.
254 M. Wohlert, T. Benselfelt, L. Wågberg, I. Furó, L. A. Berglund and J. Wohlert, *Cellulose*, 2022, **29**, 1–23.
255 M. Jakob, A. R. Mahendran, W. Gindl-Altmutter, P. Bliem, J. Konnerth, U. Müller and S. Veigel, *Prog. Mater. Sci.*, 2022, **125**, 100916.
256 K. Hou, Y. Li, Y. Liu, R. Zhang, B. S. Hsiao and M. Zhu, *Polymer*, 2017, **123**, 55–64.
257 M. A. Hubbe, P. Tayeb, M. Joyce, P. Tyagi, M. Kehoe, K. Dimic-Misic and L. Pal, *BioResources*, 2017, **12**, 9556–9661.
258 M. Börjesson and G. Westman, in *Cellulose - Fundamental Aspects and Current Trends*, ed. M. Poletto and H. L. Ornaghi, InTech, 2015.
259 D. Tahir, M. R. A. Karim, H. Hu, S. Naseem, M. Rehan, M. Ahmad and M. Zhang, *Polymers*, 2022, **14**, 4468.
260 D. Srivastava, J. Ahopelto and A. J. Karttunen, *Molecules*, 2022, **27**, 6240.

261 A. D. French, in *Encyclopedia of Biophysics*, ed. G. C. K. Roberts, Springer Berlin Heidelberg, Berlin, Heidelberg, 2013, pp. 248–253.
262 D. K. Patel, S. D. Dutta and K.-T. Lim, *RSC Adv.*, 2019, **9**, 19143–19162.
263 E. M. Debzi, H. Chanzy, J. Sugiyama, P. Tekely and G. Excoffier, *Macromolecules*, 1991, **24**, 6816–6822.
264 J. F. Matthews, M. E. Himmel and M. F. Crowley, *Cellulose*, 2012, **19**, 297–306.
265 J. A. Sirviö and M. Lakovaara, *Biomacromolecules*, 2021, **22**, 3366–3376.
266 Q. Wu, J. Xu, S. Zhu, Y. Kuang, B. Wang and W. Gao, *Carbohydr. Polym.*, 2020, **249**, 116827.
267 M. Wada, H. Chanzy, Y. Nishiyama and P. Langan, *Macromolecules*, 2004, **37**, 8548–8555.
268 P. H. Hermans and A. Weidinger, *J. Colloid Sci.*, 1946, **1**, 495–504.
269 A. Okiyama, M. Motoki and S. Yamanaka, *Food Hydrocolloids*, 1993, **6**, 503–511.
270 R. N. Goldberg, J. Schliesser, A. Mittal, S. R. Decker, A. F. L. O. M. Santos, V. L. S. Freitas, A. Urbas, B. E. Lang, C. Heiss, M. D. M. C. Ribeiro Da Silva, B. F. Woodfield, R. Katahira, W. Wang and D. K. Johnson, *J. Chem. Thermodyn.*, 2015, **81**, 184–226.
271 Y. Nishiyama, J. Sugiyama, H. Chanzy and P. Langan, *J. Am. Chem. Soc.*, 2003, **125**, 14300–14306.
272 P. Samyn and A. Osorio-Madrazo, in *Handbook of Nanofibers*, ed. A. Barhoum, M. Bechelany and A. S. H. Makhlouf, Springer International Publishing, Cham, 2019, pp. 287–321.
273 S. Park, R. A. Venditti, D. G. Abrecht, H. Jameel, J. J. Pawlak and J. M. Lee, *J. Appl. Polym. Sci.*, 2007, **103**, 3833–3839.
274 A. Kafy, H. C. Kim, L. Zhai, J. W. Kim, L. V. Hai, T. J. Kang and J. Kim, *Sci. Rep.*, 2017, **7**, 17683.
275 Y. Wang, P. Zhang, J. Guo, Z. Zhong, W. Li and X. Liu, *BioResources*, 2023, **18**, 5813–5837.
276 Y. Liu, B. Li, W. Mao, W. Hu, G. Chen, Y. Liu and Z. Fang, *ACS Omega*, 2019, **4**, 7861–7865.
277 J. Wang, Q. Gao, Y. Wang, X. Liu and S. Nie, *Ind. Crops Prod.*, 2022, **178**, 114599.
278 M. Pääkkö, M. Ankerfors, H. Kosonen, A. Nykänen, S. Ahola, M. Österberg, J. Ruokolainen, J. Laine, P. T. Larsson, O. Ikkala and T. Lindström, *Biomacromolecules*, 2007, **8**, 1934–1941.
279 M. R. K. Sofla, R. J. Brown, T. Tsuzuki and T. J. Rainey, *Adv. Nat. Sci.:Nanosci. Nanotechnol.*, 2016, **7**, 035004.
280 S. Eyley, C. Schütz and W. Thielemans, in *Cellulose Science and Technology*, ed. T. Rosenau, A. Potthast and J. Hell, Wiley, 1st edn, 2018, pp. 223–252.
281 A. H. Nordin, S. Wong, N. Ngadi, M. Mohammad Zainol, N. A. F. Abd Latif and W. Nabgan, *J. Environ. Chem. Eng.*, 2021, **9**, 104639.
282 J. M. Antoniw, V. A. Gabriel, M. V. Kiriakou, M. A. Dubé, M. F. Cunningham and E. D. Cranston, *RSC Appl. Polym.*, 2024, **2**, 262–274.
283 S. Amine, A. Montembault, M. Fumagalli, A. Osorio-Madrazo and L. David, *Polymers*, 2021, **13**, 2023.
284 A. Kondor, A. Santmarti, A. Mautner, D. Williams, A. Bismarck and K.-Y. Lee, *Front. Chem. Eng.*, 2021, **3**, 738995.
285 A. Mautner, M. Hakalahti, V. Rissanen and T. Tammelin, in *Nanocellulose and Sustainability*, ed. K.-Y. Lee, Series: Sustainability contributions through science and technology, CRC Press, Boca Raton, 1st edn, 2018, pp. 87–128.
286 B. B. Hallac and A. J. Ragauskas, *Biofuels, Bioprod. Biorefin.*, 2011, **5**, 215–225.
287 T. V. Patil, D. K. Patel, S. D. Dutta, K. Ganguly, T. S. Santra and K.-T. Lim, *Bioact. Mater.*, 2022, **9**, 566–589.
288 P. A. R. Pires, N. I. Malek, T. C. Teixeira, T. A. Bioni, H. Nawaz and O. A. E. Seoud, *Ind. Crops Prod.*, 2015, **77**, 180–189.
289 R. Alimohammadzadeh, A. A. Rafi, L. Goclik, C.-W. Tai and A. Cordova, *Carbohydr. Polym. Technol. Appl.*, 2022, **3**, 100205.
290 Z. Yao, S. Mi, B. Chen, F. Liu, H. Na and J. Zhu, *ACS Sustainable Chem. Eng.*, 2022, **10**, 17327–17335.
291 B. V. M. Rodrigues, R. T. Polez, O. A. El Seoud and E. Frollini, *Int. J. Biol. Macromol.*, 2023, **243**, 125256.
292 B. P. Frank, D. P. Durkin, E. R. Caudill, L. Zhu, D. H. White, M. L. Curry, J. A. Pedersen and D. H. Fairbrother, *ACS Appl. Nano Mater.*, 2018, **1**, 7025–7038.
293 G. Siqueira, J. Bras and A. Dufresne, *Langmuir*, 2010, **26**, 402–411.
294 M. Lalanne-Tisné, S. Eyley, J. De Winter, A. Favrelle-Huret, W. Thielemans and P. Zinck, *Carbohydr. Polym.*, 2022, **295**, 119840.
295 D. Roy, J. T. Guthrie and S. Perrier, *Macromolecules*, 2005, **38**, 10363–10372.
296 Z. Zhang, X. Wang, K. C. Tam and G. Sèbe, *Carbohydr. Polym.*, 2019, **205**, 322–329.
297 Z. Zhang, G. Sèbe, Y. Hou, J. Wang, J. Huang and G. Zhou, *J. Appl. Polym. Sci.*, 2021, **138**, 51458.
298 M. Stepanova and E. Korzhikova-Vlakh, *Polymers*, 2022, **14**, 1477.
299 G. Conzatti, S. Cavalie, C. Combes, J. Torrisani, N. Carrere and A. Tourrette, *Colloids Surf., B*, 2017, **151**, 143–155.
300 M. Krouit, J. Bras and M. N. Belgacem, *Eur. Polym. J.*, 2008, **44**, 4074–4081.
301 R. Mincheva, L. Jasmani, T. Josse, Y. Paint, J.-M. Raquez, P. Gerbaux, S. Eyley, W. Thielemans and P. Dubois, *Biomacromolecules*, 2016, **17**, 3048–3059.
302 K. Neubauerova, M. C. C. G. Carneiro, L. R. Rodrigues, F. T. C. Moreira and M. G. F. Sales, *Sens. Biosens. Res.*, 2020, **29**, 100368.
303 J. Fan, M. Xu, Y.-T. Xu, W. Y. Hamad, Z. Meng and M. J. MacLachlan, *Chem. Eng. J.*, 2023, **457**, 141175.
304 Z. Deng, Z. Wu, M. Alizadeh, H. Zhang, Y. Chen and C. Karaman, *Environ. Res.*, 2023, **219**, 114995.
305 S. A. Al Kiey, A. M. Khalil and S. Kamel, *Int. J. Biol. Macromol.*, 2023, **239**, 124302.
306 R. H. Althomali, K. A. Alamry, M. A. Hussein and R. M. Guedes, *Diamond Relat. Mater.*, 2022, **122**, 108803.

307 J. Ji, L. Qu, Z. Wang, G. Li, W. Feng and G. Yang, *Microchem. J.*, 2022, **175**, 107133.
308 M. A. Khalilzadeh, S. Tajik, H. Beitollahi and R. A. Venditti, *Ind. Eng. Chem. Res.*, 2020, **59**, 4219–4228.
309 H. N. Abdelhamid, D. Georgouvelas, U. Edlund and A. P. Mathew, *Chem. Eng. J.*, 2022, **446**, 136614.
310 V. Gautam, K. P. Singh and V. L. Yadav, *Carbohydr. Polym.*, 2018, **189**, 218–228.
311 H.-A. S. Tohamy and H. S. Magar, *ECS J. Solid State Sci. Technol.*, 2022, **11**, 127003.
312 Q. Bi, S. Dong, Y. Sun, X. Lu and L. Zhao, *Anal. Biochem.*, 2016, **508**, 50–57.
313 X. Wang, C. Karaman, Y. Zhang and C. Xia, *Chemosphere*, 2023, **331**, 138813.
314 A. S. Santhosh, S. Sandeep, D. James Bound, S. Nandini, S. Nalini, G. S. Suresh, N. K. Swamy, J. R. Rajabathar and A. Selvaraj, *Surf. Interfaces*, 2021, **26**, 101377.
315 V. Velusamy, S. Palanisamy, S.-W. Chen, S. Balu, T. C. K. Yang and C. E. Banks, *Talanta*, 2019, **192**, 471–477.
316 Y. Zhang, G. Liu, X. Yao, S. Gao, J. Xie, H. Xu and N. Lin, *Cellulose*, 2018, **25**, 3861–3871.
317 S. Ummartyotin and H. Manuspiya, *Renewable Sustainable Energy Rev.*, 2015, **41**, 402–412.
318 J. Moon, J.-A. Park, S.-J. Lee, T. Zyung and I.-D. Kim, *Sens. Actuators, B*, 2010, **149**, 301–305.
319 P. Sun, W. Wang, Y. Liu, Y. Sun, J. Ma and G. Lu, *Sens. Actuators, B*, 2012, **173**, 52–57.
320 M. Zhang, Z. Yuan, J. Song and C. Zheng, *Sens. Actuators, B*, 2010, **148**, 87–92.
321 L. Zhao, L. Zhao, Y. Xu, T. Qiu, L. Zhi and G. Shi, *Electrochim. Acta*, 2009, **55**, 491–497.
322 Y. Liao, C. Wang, Y. Dong, Z. Miao, H. Yu, G. Chen, J. Yao, Y. Zhou and Y. Liu, *Adv. Funct. Mater.*, 2024, **34**, 2409813.
323 P. Tayeb and A. H. Tayeb, *Carbohydr. Polym.*, 2019, **224**, 115149.
324 Z. Pang, Z. Yang, Y. Chen, J. Zhang, Q. Wang, F. Huang and Q. Wei, *Colloids Surf., A*, 2016, **494**, 248–255.
325 N. S. Abdel Rahman, Y. E. Greish, S. T. Mahmoud, N. N. Qamhieh, H. F. El-Maghraby and D. Zeze, *Carbohydr. Polym.*, 2021, **258**, 117643.
326 J. Hur, S. Park, J. H. Kim, J. Y. Cho, B. Kwon, J. H. Lee, G. Y. Bae, H. Kim, J. T. Han and W. H. Lee, *ACS Sustainable Chem. Eng.*, 2022, **10**, 3227–3235.
327 S. Yun and J. Kim, *Sens. Actuators, B*, 2010, **150**, 308–313.
328 J. Im, E. Sterner and T. Swager, *Sensors*, 2016, **16**, 183.
329 J. Zhang, X. Maimaitiyiming and A. Obolda, *Sens. Actuators, B*, 2024, **418**, 136199.
330 H. Nawaz, W. Tian, J. Zhang, R. Jia, Z. Chen and J. Zhang, *ACS Appl. Mater. Interfaces*, 2018, **10**, 2114–2121.
331 M. Wang, I. V. Anoshkin, A. G. Nasibulin, J. T. Korhonen, J. Seitsonen, J. Pere, E. I. Kauppinen, R. H. A. Ras and O. Ikkala, *Adv. Mater.*, 2013, **25**, 2428–2432.
332 J. Huang, Y. Yang, L. Chao, W. Liu, H. Li, L. Zhao and X. Zhang, *Cellulose*, 2025, **32**, 2289–2301.
333 H. Zhong, S. Wang, Z. Wang and J. Jiang, *Chem. Eng. J.*, 2024, **486**, 150203.
334 Q. Xiang, H. Zhang, Z. Liu, Y. Zhao and H. Tan, *Chem. Eng. J.*, 2024, **480**, 147825.
335 J. Liu, P. Li, W. Wang, L. Bai, H. Chen, L. Yang, K. Yin, H. Yang and D. Wei, *Ind. Crops Prod.*, 2024, **216**, 118728.
336 T. Zhou, P. Li, Y. Sun, W. Wang, L. Bai, H. Chen, H. Yang, L. Yang and D. Wei, *J. Mater. Chem. B*, 2025, **13**, 2705–2716.
337 L. Wang, J. Wei, M. You, Y. Jin, D. Li, Z. Xu, A. Yu, J. Li and C. Chen, *Carbohydr. Polym.*, 2025, **354**, 123345.
338 M. L. Soriano and M. J. Dueñas-Mas, in *Carbon-Based Nanosensor Technology*, ed. C. Kranz, Springer International Publishing, Cham, 2018, vol. 17, pp. 273–301.
339 J. Yao, P. Ji, B. Wang, H. Wang and S. Chen, *Sens. Actuators, B*, 2018, **254**, 110–119.
340 K. B. R. Teodoro, F. L. Migliorini, W. A. Christinelli and D. S. Correa, *Carbohydr. Polym.*, 2019, **212**, 235–241.
341 H. Orelma, A. Hokkanen, I. Leppänen, K. Kammiovirta, M. Kapulainen and A. Harlin, *Cellulose*, 2020, **27**, 1543–1553.
342 S. Kumari and G. S. Chauhan, *ACS Appl. Mater. Interfaces*, 2014, **6**, 5908–5917.
343 J. Fu, Z. Pang, J. Yang, F. Huang, Y. Cai and Q. Wei, *Appl. Surf. Sci.*, 2015, **349**, 35–42.
344 B. W. Davis, N. Niamnont, C. D. Hare, M. Sukwattanasinitt and Q. Cheng, *ACS Appl. Mater. Interfaces*, 2010, **2**, 1798–1803.
345 D. Chauhan and P. R. Solanki, *ACS Appl. Polym. Mater.*, 2019, **1**, 1613–1623.
346 C. Esmaeili, M. Abdi, A. Mathew, M. Jonoobi, K. Oksman and M. Rezayi, *Sensors*, 2015, **15**, 24681–24697.
347 H. Qi, E. Mäder and J. Liu, *Sens. Actuators, B*, 2013, **185**, 225–230.
348 X. Xu, J. Zhou, Y. Xin, G. Lubineau, Q. Ma and L. Jiang, *Sci. Rep.*, 2017, **7**, 4317.
349 S. Veeralingam, P. Sahatiya, A. Kadu, V. Mattela and S. Badhulika, *ACS Appl. Electron. Mater.*, 2019, **1**, 558–568.
350 E. Morales-Narváez, H. Golmohammadi, T. Naghdi, H. Yousefi, U. Kostiv, D. Horák, N. Pourreza and A. Merkoçi, *ACS Nano*, 2015, **9**, 7296–7305.
351 N. Morimoto, F. M. Winnik and K. Akiyoshi, *Langmuir*, 2007, **23**, 217–223.
352 C. Ruiz-Palomero, M. L. Soriano and M. Valcárcel, *Sens. Actuators, B*, 2016, **229**, 31–37.
353 C. Ruiz-Palomero, M. L. Soriano and M. Valcárcel, *TrAC, Trends Anal. Chem.*, 2017, **87**, 1–18.
354 L.-Z. Huang, M.-G. Ma, X.-X. Ji, S.-E. Choi and C. Si, *Front. Bioeng. Biotechnol.*, 2021, **9**, 690773.
355 H. Østby and A. Várnai, *Essays Biochem.*, 2023, **67**, 533–550.
356 N. Zhang, S. Li, L. Xiong, Y. Hong and Y. Chen, *Modell. Simul. Mater. Sci. Eng.*, 2015, **23**, 085010.
357 H. V. Scheller and P. Ulvskov, *Annu. Rev. Plant Biol.*, 2010, **61**, 263–289.
358 X. Jin, Z. Hu, S. Wu, T. Song, F. Yue and Z. Xiang, *Carbohydr. Polym.*, 2019, **215**, 235–245.
359 C. Chen, W. Yin, G. Chen, G. Sun and G. Wang, *Materials*, 2017, **10**, 514.
360 Y. Zheng, J. Shi, M. Tu and Y.-S. Cheng, in *Advances in Bioenergy*, Elsevier, 2017, vol. 2, pp. 1–68.

361 Y. Lu, Q. He, G. Fan, Q. Cheng and G. Song, *Green Process. Synth.*, 2021, **10**, 779–804.
362 Z. Yan, M. A. Alam, J. Li, W. Xiong, S. Zhang, Z. Zhan and J. Xu, *Bioenergy Res.*, 2024, **17**, 1469–1480.
363 Y. Zeng, M. E. Himmel and S.-Y. Ding, *Biotechnol. Biofuels*, 2017, **10**, 263.
364 I. Gabrielii, P. Gatenholm, W. G. Glasser, R. K. Jain and L. Kenne, *Carbohydr. Polym.*, 2000, **43**, 367–374.
365 E. M. Jincy and K. S. Femina, in *Handbook of Biomass*, eds. S. Thomas, M. Hosur, D. Pasquini and C. Jose Chirayil, Springer Nature Singapore, Singapore, 2023, pp. 1–32.
366 L.-P. Xiao, G.-Y. Song and R.-C. Sun, in *Hydrothermal Processing in Biorefineries*, ed. H. A. Ruiz, M. Hedegaard Thomsen and H. L. Trajano, Springer International Publishing, Cham, 2017, pp. 45–94.
367 F. Delbecq, Y. Wang, A. Muralidhara, K. El Ouardi, G. Marlair and C. Len, *Front. Chem.*, 2018, **6**, 146.
368 A. Ebringerová, *Macromol. Symp.*, 2005, **232**, 1–12.
369 W. Duan, A. González, M. Gich and C. Fernández-Sánchez, *ACS Sustainable Chem. Eng.*, 2024, **12**, 4386–4397.
370 W. Zhang, J.-Y. Wen, M.-G. Ma, M.-F. Li, F. Peng and J. Bian, *J. Mater. Res. Technol.*, 2021, **14**, 555–566.
371 Y. Li, M. Yao, Y. Luo, J. Li, Z. Wang, C. Liang, C. Qin, C. Huang and S. Yao, *ACS Appl. Mater. Interfaces*, 2023, **15**, 5883–5896.
372 X. Gong, C. Fu, N. Alam, Y. Ni, L. Chen, L. Huang and H. Hu, *Biomacromolecules*, 2022, **23**, 2272–2279.
373 Y. Xu, K. Liu, Y. Yang, M.-S. Kim, C.-H. Lee, R. Zhang, T. Xu, S.-E. Choi and C. Si, *Front. Bioeng. Biotechnol.*, 2023, **10**, 1110004.
374 L. Zhao, B. Luo, S. Gao, Y. Liu, C. Lai, D. Zhang, W. Guan, C. Wang and F. Chu, *Int. J. Biol. Macromol.*, 2024, **282**, 137313.
375 J. Pérez, J. Muñoz-Dorado, T. De La Rubia and J. Martínez, *Int. Microbiol.*, 2002, **5**, 53–63.
376 M. M. Abe, M. C. Branciforti and M. Brienzo, *Recycling*, 2021, **6**, 22.
377 H.-A. S. Tohamy, *Sci. Rep.*, 2025, **15**, 741.
378 T.-A. Le and T.-P. Huynh, *ACS Sens.*, 2024, **9**, 4975–5001.
379 W. Zhang, J. Wen, J. Yang, M. Li, F. Peng, M. Ma and J. Bian, *Int. J. Biol. Macromol.*, 2022, **223**, 1–10.
380 K. Sharma, M. Kaur, P. Tewatia, V. Kumar, C. Paulik, H. Yoshitake, M. Sharma, G. Rattan, S. Singhal and A. Kaushik, *Bioresour. Technol.*, 2023, **389**, 129825.
381 L. Hu, Y. Xie, S. Gao, X. Shi, C. Lai, D. Zhang, C. Lu, Y. Liu, L. Du, X. Fang, F. Xu, C. Wang and F. Chu, *Carbohydr. Polym.*, 2023, **312**, 120827.
382 R. Helim, A. Zazoua, N. Jaffrezic-Renault and H. Korri-Youssoufi, *Talanta*, 2023, **265**, 124784.
383 X. Jiang, J. Huang, T. Chen, Q. Zhao, F. Xu and X. Zhang, *Int. J. Biol. Macromol.*, 2020, **153**, 412–420.
384 P. Yang, Z. Zhu, M. Chen, W. Chen and X. Zhou, *Opt. Mater.*, 2018, **85**, 329–336.
385 P. Yang, Z. Zhu, M. Chen, X. Zhou and W. Chen, *Spectrochim. Acta, Part A*, 2019, **213**, 301–308.
386 A. Dammak, C. Moreau, N. Beury, K. Schwikal, H. T. Winter, E. Bonnin, B. Saake and B. Cathala, *Holzforschung*, 2013, **67**, 579–586.
387 P. T. Martone, J. M. Estevez, F. Lu, K. Ruel, M. W. Denny, C. Somerville and J. Ralph, *Curr. Biol.*, 2009, **19**, 169–175.
388 Z. Mahmood, M. Yameen, M. Jahangeer, M. Riaz, A. Ghaffar and I. Javid, in *Lignin – Trends and Applications*, ed. M. Poletto, InTech, 2018.
389 Q. Liu, L. Luo and L. Zheng, *Int. J. Mol. Sci.*, 2018, **19**, 335.
390 Y. Lu, Y.-C. Lu, H.-Q. Hu, F.-J. Xie, X.-Y. Wei and X. Fan, *J. Spectrosc.*, 2017, **2017**, 1–15.
391 E. M. Anderson, M. L. Stone, R. Katahira, M. Reed, W. Muchero, K. J. Ramirez, G. T. Beckham and Y. Román-Leshkov, *Nat. Commun.*, 2019, **10**, 2033.
392 X. Chen, H. Li, S. Sun, X. Cao and R. Sun, *Sci. Rep.*, 2016, **6**, 39354.
393 J. Zheng, L. Chen, Z. Huang and X. Qiu, *Green Chem.*, 2024, **26**, 2783–2792.
394 M. Parot, D. Rodrigue and T. Stevanovic, *Bioresour. Technol. Rep.*, 2022, **17**, 100880.
395 T. Rashid, N. Gnanasundaram, A. Appusamy, C. F. Kait and M. Thanabalan, *Ind. Crops Prod.*, 2018, **116**, 122–136.
396 D. Watkins, Md. Nuruddin, M. Hosur, A. Tcherbi-Narteh and S. Jeelani, *J. Mater. Res. Technol.*, 2015, **4**, 26–32.
397 S. Angelini, D. Ingles, M. Gelosia, P. Cerruti, E. Pompili, G. Scarinzi, G. Cavalaglio, F. Cotana and M. Malinconico, *J. Cleaner Prod.*, 2017, **151**, 152–162.
398 S. Laurichesse and L. Avérous, *Prog. Polym. Sci.*, 2014, **39**, 1266–1290.
399 D. Saha, Y. Li, Z. Bi, J. Chen, J. K. Keum, D. K. Hensley, H. A. Grappe, H. M. Meyer, S. Dai, M. P. Paranthaman and A. K. Naskar, *Langmuir*, 2014, **30**, 900–910.
400 F. A. Faria, D. V. Evtuguin, A. Rudnitskaya, M. T. Gomes, J. A. Oliveira, M. P. F. Graça and L. C. Costa, *Polym. Int.*, 2012, **61**, 788–794.
401 D. Gnana Prakash, K. P. Gopinath, S. M. Prasanth, S. Harish, M. Rishikesh, R. Sivaramakrishnan and A. Pugazhendhi, *Chemosphere*, 2022, **293**, 133473.
402 R. Y. Nsimba, C. A. Mullen, N. M. West and A. A. Boateng, *ACS Sustainable Chem. Eng.*, 2013, **1**, 260–267.
403 E. O. Owhe, N. Kumar and J. G. Lynam, *Biocatal. Agric. Biotechnol.*, 2021, **32**, 101949.
404 N. Muhammad, Z. Man, M. A. Bustam, M. I. A. Mutalib and S. Rafiq, *J. Ind. Eng. Chem.*, 2013, **19**, 207–214.
405 H. Luo and M. M. Abu-Omar, *Green Chem.*, 2018, **20**, 745–753.
406 A. Meraj, M. Jawaid, S. P. Singh, M. M. Nasef, H. Ariffin, H. Fouad and B. Abu-Jdayil, *Sci. Rep.*, 2024, **14**, 8672.
407 V. Provost, S. Dumarcay, I. Ziegler-Devin, M. Boltoeva, D. Trébouet and M. Villain-Gambier, *Bioresour. Technol.*, 2022, **349**, 126837.
408 E. García-Cisneros, F. S. Mederos-Nieto, R. Hernández-Altamirano, M. A. González-Espinosa and V. Castillejos-Torres, *Biofuels*, 2024, **15**, 793–800.
409 G. Kabir and B. H. Hameed, *Renewable Sustainable Energy Rev.*, 2017, **70**, 945–967.

410 C. Xu and F. Ferdosian, *Conversion of Lignin into Bio-Based Chemicals and Materials*, Springer Berlin Heidelberg, Berlin, Heidelberg, 2017.
411 M. S. Ganewatta, H. N. Lokupitiya and C. Tang, *Polymers*, 2019, **11**, 1176.
412 C. Welker, V. Balasubramanian, C. Petti, K. Rai, S. DeBolt and V. Mendu, *Energies*, 2015, **8**, 7654–7676.
413 A. Tolbert, H. Akinosho, R. Khunsupat, A. K. Naskar and A. J. Ragauskas, *Biofuels, Bioprod. Biorefin.*, 2014, **8**, 836–856.
414 S. Sugiarto, Y. Leow, C. L. Tan, G. Wang and D. Kai, *Bioact. Mater.*, 2022, **8**, 71–94.
415 D. Wang, Y. Gu, S. Feng, W. Yang, H. Dai, H. Xiao and J. Han, *Green Chem.*, 2023, **25**, 9020–9044.
416 S. Sen, S. Patil and D. S. Argyropoulos, *Green Chem.*, 2015, **17**, 4862–4887.
417 B. Yu, Z. Chang and C. Wang, *Mater. Chem. Phys.*, 2016, **181**, 187–193.
418 I. Spiridon, *Environ. Chem. Lett.*, 2020, **18**, 771–785.
419 J. Y. Ryu and E. J. Na, *Biomed. Dermatol.*, 2018, **2**, 15.
420 A. P. Richter, J. S. Brown, B. Bharti, A. Wang, S. Gangwal, K. Houck, E. A. Cohen Hubal, V. N. Paunov, S. D. Stoyanov and O. D. Velev, *Nat. Nanotechnol.*, 2015, **10**, 817–823.
421 M. Özparpucu, N. Gierlinger, I. Cesarino, I. Burgert, W. Boerjan and M. Rüggeberg, *J. Exp. Bot.*, 2019, **70**, 4039–4047.
422 W. J. Cousins, *Wood Sci. Technol.*, 1976, **10**, 9–17.
423 A. Emonet and A. Hay, *Plant Physiol.*, 2022, **190**, 31–43.
424 M. Schwaighofer, L. Zelaya-Lainez, M. Königsberger, M. Lukacevic, S. Serna-Loaiza, M. Harasek, O. Lahayne, V. Senk and J. Füssl, *Mater. Des.*, 2023, **227**, 111765.
425 S. Sahoo, M. Misra and A. K. Mohanty, *Composites, Part A*, 2011, **42**, 1710–1718.
426 A. Shakoor Shar, N. Wang, T. Chen, X. Zhao and Y. Weng, *Polymers*, 2023, **15**, 4049.
427 D. Zappi, G. Varani, E. Cozzoni, I. Iatsunskyi, S. Laschi and M. T. Giardi, *Nanomaterials*, 2021, **11**, 3428.
428 J. S. Rodrigues, A. De, S. M. De Freitas, L. F. De Lima, H. S. M. Lopes, C. C. Maciel, L. V. B. V. Fré, A. A. F. Pires, V. H. De Lima, V. J. R. Oliveira, C. De A. Olivati, M. Ferreira, A. Riul and V. R. Botaro, *Int. J. Biol. Macromol.*, 2024, **268**, 131883.
429 A. Antonacci, V. Frisulli, L. B. Carvalho, L. F. Fraceto, B. Miranda, L. De Stefano, U. Johanningmeier, M. T. Giardi and V. Scognamiglio, *Int. J. Mol. Sci.*, 2023, **24**, 10088.
430 H. Liu, Y. Guan, L. Yan, Y. Zheng, C. Si and L. Dai, *Green Chem.*, 2024, **26**, 9281–9294.
431 S. Paul, N. S. Thakur, S. Chandna, V. Sagar and J. Bhaumik, *ACS Appl. Nano Mater.*, 2022, **5**, 2748–2761.
432 S. Wang, M. T. Innocent, Q. Wang, H. Xiang, J. Tang and M. Zhu, *Int. J. Biol. Macromol.*, 2020, **151**, 730–739.
433 M. Vasudevan, S. Remesh, V. Perumal, P. B. Raja, M. N. M. Ibrahim, S. C. B. Gopinath, S. Karuppanan and M. Ovinis, *Chem. Eng. J.*, 2023, **468**, 143613.
434 T. Bao, Q. Wang, Y. Jiang, X. Zhao, Y. Cao, J. Cao, Q. Li and W. Si, *Crystals*, 2024, **14**, 506.
435 S. S. L. Gonçalves, A. Rudnitskaya, A. J. M. Sales, L. M. C. Costa and D. V. Evtuguin, *Materials*, 2020, **13**, 1637.
436 A. Duval and M. Lawoko, *React. Funct. Polym.*, 2014, **85**, 78–96.
437 R. Chokkareddy, G. G. Redhi and T. Karthick, *Heliyon*, 2019, **5**, e01457.
438 D. V. Stergiou, P. G. Veltsistas and M. I. Prodromidis, *Sens. Actuators, B*, 2008, **129**, 903–908.
439 A. Jędrzak, T. Rębiś, M. Kuznowicz and T. Jesionowski, *Int. J. Biol. Macromol.*, 2019, **127**, 677–682.
440 A. Beaucamp, M. Culebras and M. N. Collins, *Green Chem.*, 2021, **23**, 5696–5705.
441 C. Tortolini, E. Capecchi, F. Tasca, R. Pofi, M. A. Venneri, R. Saladino and R. Antiochia, *Nanomaterials*, 2021, **11**, 718.
442 L. Xu, W. Mao, J. Huang, S. Li, K. Huang, M. Li, J. Xia and Q. Chen, *Sens. Actuators, B*, 2016, **230**, 54–60.
443 O.-N. Hur, S. Park, S. Park, B.-H. Kang, C.-S. Lee, J.-Y. Hong, S.-H. Park and J. Bae, *Mater. Chem. Phys.*, 2022, **285**, 126166.
444 S. Rai, B. K. Singh, P. Bhartiya, A. Singh, H. Kumar, P. K. Dutta and G. K. Mehrotra, *J. Lumin.*, 2017, **190**, 492–503.
445 M. M. Pillai, K. R. Karpagam, R. Begam, R. Selvakumar and A. Bhattacharyya, *Mater. Lett.*, 2018, **212**, 78–81.
446 N. A. Nguyen, K. M. Meek, C. C. Bowland, S. H. Barnes and A. K. Naskar, *Macromolecules*, 2018, **51**, 115–127.
447 J. Yang, K. Yang, X. An, Z. Fan, Y. Li, L. Yin, Y. Long, G. Pan, H. Liu and Y. Ni, *Adv. Funct. Mater.*, 2025, 2416916.
448 Q. Zhou, M. Sun, J. Hu, Y. Wu, Q. Yang, L. Hui, Z. Liu and D. Ding, *Int. J. Biol. Macromol.*, 2025, **300**, 140322.
449 C. Chen, X. Wang, M. Li, Y. Fan and R. Sun, *Sens. Actuators, B*, 2018, **255**, 1569–1576.
450 V. Gigli, E. Capecchi, C. Tortolini, A. Isidori, R. Antiochia and R. Saladino, *ACS Biomater. Sci. Eng.*, 2023, **9**, 3597–3605.
451 X. Fu, H. Ji, X. Liu and W. Zhu, *Ind. Crops Prod.*, 2021, **173**, 114112.
452 A. Jędrzak, T. Rębiś, Ł. Klapiszewski, J. Zdarta, G. Milczarek and T. Jesionowski, *Sens. Actuators, B*, 2018, **256**, 176–185.
453 L. Meng, S. Chirtes, X. Liu, M. Eriksson and W. C. Mak, *Biosens. Bioelectron.*, 2022, **218**, 114742.
454 Y. Lei, A. H. Alshareef, W. Zhao and S. Inal, *ACS Appl. Nano Mater.*, 2020, **3**, 1166–1174.
455 Y. Fei, Z. Jiang, D. Zhou, F. Meng, Y. Wu, Y. Xiong, Y. Ye, T. Liu, Z. Fei, T. Kuang, M. Zhong, Y. Li and F. Chen, *J. Energy Storage*, 2023, **73**, 108978.
456 X. Gao, Y. Wang, J. Wu, Z. Xue, C. Yan, H. Zhang, Y. Wang, Y. Zhang, M. Jiang and Y. Zhao, *ACS Sustainable Chem. Eng.*, 2024, **12**, 15159–15172.
457 D. Yang, J. Wang, Y. Cao, X. Tong, T. Hua, R. Qin and Y. Shao, *ACS Appl. Electron. Mater.*, 2023, **5**, 593–611.
458 J. Wen, S. Wang, J. Feng, J. Ma, H. Zhang, P. Wu, G. Li, Z. Wu, F. Meng, L. Li and Y. Tian, *J. Mater. Chem. A*, 2024, **12**, 6190–6210.